Eur. Phys. J. A (2017) **53**: 79
DOI 10.1140/epja/i2017-12262-1

THE EUROPEAN PHYSICAL JOURNAL A

Review

Fission fragment distributions within dynamical approach

K. Mazurek[1,a], P.N. Nadtochy[2], E.G. Ryabov[3], and G.D. Adeev[3]

[1] Institute of Nuclear Physics Polish Academy of Sciences, PL-31342 Krakow, Poland
[2] Omsk State Technical University, Mira prospekt 11, Omsk, 644050, Russia
[3] Omsk State University, Physics department, Mira prospekt 55-A, Omsk, 644077, Russia

Received: 2 December 2016 / Revised: 6 March 2017
Published online: 27 April 2017

Communicated by N. Alamanos

Abstract. The review covers recent developments and achievements in the dynamical description of fission process at high excitation energy. It is shown that the dynamical approach based on multidimensional Langevin equations combined with the statistical description of nuclear decay by particles evaporation is capable of fairly well describing the formation of fission fragment mass-energy, charge, and angular distributions of fission fragments in coincidence with the pre- and post-scission particle emission. The final yields of fission and evaporation residues channels products could be obtained. The detailed description of fission dynamics allows studying different stages of fission process, indicating the most important ingredients governing fission process and studying in detail such fundamental nuclear properties as nuclear viscosity and fission timescale. The tasks and perspectives of multidimensional dynamical approach are also discussed.

1 Introduction

The nuclear fission is a magnificent phenomenon of a quantal large-scale collective motion during which the substantial rearrangement of initial compound nucleus results in its splitting on two or more parts. However, the character of the compound nucleus evolution is still not well established, and it is not yet understood in detail how the original compound nucleus is transformed into a variety of fission products. Just after the discovery of induced-fission of uranium by Hahn, Meitner and co-authors [1,2], the substantial efforts in the experimental and theoretical studies of this process were undertaken. The spontaneous fission of the uranium was discovered in 1940 by Flerov and Petrzhak. Since then the fission phenomenon is widely investigated because of the military and the power plant applications.

In given conditions almost every nucleus can split into two or more fragments. However, in the present paper we will mainly focus on the discussion of the fusion-fission process. The compound nucleus (CN) is created in the collision of two ions at moderate energies. Ordinarily, this kind of reaction can provide even exotic systems, which are far from the stability line. The energy of the collision is transformed into excitation energy of the created nucleus. The hot system is unstable, thus the internal energy could be changed into the deformation energy, rotational energy and/or energy of emitted particles and γ-rays. The sharp limits of beam energies and angular momenta which define the fusion-fission process are difficult to give but in general, this reaction can occur for excitation energies $E^\star = 0$–$250\,\mathrm{MeV}$ and angular momenta 0–$100\,\hbar$. There are obviously reactions which compete with fusion-fission such as the quasi-fission, fusion-evaporation, nucleon transfer or in extreme- deep-inelastic or multifragmentation. However the most dominant in this range of excitation energies and angular momenta are the fusion-fission and fusion-evaporation and quasi-fission channels. The quasi-fission channel becomes important at high angular momenta.

Soon after the discovery of fission, Bohr and Wheeler suggested to describe the fissioning nucleus [3] using the macroscopic analogy of a charged liquid drop. Within this picture, fission results from the competition between disrupting Coulomb repulsion and stabilizing surface tension effects. Following the ideas of Bohr and Wheeler, fission models based on the level densities of the nucleus at the ground state and at the transition state were developed. The transition state may be assumed as the fission saddle or scission point [4]. Different variants of the transition-state model emerged in the mean time. The ideas developed in the scission-point model of Wilkins *et al.* [5] were particularly successful in explaining fragment formation in low-energy fission. However, the aforementioned models based on statistical considerations, only, do not include the dynamics of the fission process that starts from the ground

[a] e-mail: katarzyna.mazurek@ifj.edu.pl

state, passes through the saddle point and finally reaches the scission point. Along this shape evolution, light particles (hereafter called pre-scission) may be emitted, modifying the excitation energy and potential-energy surface of the system in the course of its decay. Additionally, inertia and friction forces may be exerted on the system. In order to account for the dynamics, an original idea was given by Kramers [6], which considers fission as a dissipative diffusion process. Indeed, the discrepancy between experimental results and predictions by Bohr and Wheeler transition-state model were interpreted as an indication of the non-equilibrium dynamical nature of the fission process. Following the Kramers idea [6], most recent dynamical models of fission are transport theories. Inclusion of dynamical effects removes uncertain assumptions, like establishment of statistical equilibrium at a specific transition state, the fact that the nucleus trajectory faithfully follows the bottom of the fission valley, etc.

Since the mid-1980s, when deep inelastic transfer reactions were first discovered [7], stochastic methods have also been widely used in nuclear physics. Using an approach that he named the diffusion model, Kramers proposed describing nuclear fission with a small number of degrees of freedom, which would then interact with a thermostat formed by all the other single-particle degrees of freedom. Under these circumstances, the collective-variable dynamics becomes similar to Brownian-particle dynamics, since the collective subsystem energy varies only slightly during one act of interaction with a single-particle subsystem. The motion in such a physical model is adequately described by the set of the Langevin equations or by the physically equivalent Fokker-Planck equation (FPE), introduced for the description of the distribution function of collective coordinates and their conjugate momenta.

Using the analogy between nuclear-fission dynamics and Brownian-particle motion, Kramers calculated the diffusion rate of Brownian particles, which are initially located in a potential well, through a potential barrier separating the initial and final states of a system. With this approach, Kramers refined the Bohr and Wheeler equation [3] for fission width obtained one year earlier. The Kramers refining factor takes into account the influence of nuclear viscosity on the fission rate (the fission width).

The stochastic approach has been successfully applied to many problems related to collective nuclear dynamics: theories of deep inelastic transfers [8], induced fission [9–12], and description of prescission neutron multiplicity [13, 14]. The Langevin approach was firstly applied to fusion process [15] followed by description of deep inelastic collisions in [16] as it is more convinient than Fokker-Planck equations. In recent years, preference also in fission desciption has been given to the Langevin equations, since an exact solution of the FPE is substantially more difficult and generally requires the use of various approximations, in comparison with solution of the corresponding Langevin equations. However, even using the Langevin equations involves serious difficulties at the current level of computer engineering. In order to describe a large number of experimentally observed fission characteristics, it is necessary to introduce large number of collective variables (coordinates). The introduction of each new coordinate considerably increases the amount of calculations. Therefore, it is natural that one-dimensional Langevin calculations are performed first and, only after that, two-dimensional calculations. One-dimensional models, combined with some particle evaporation code, make it possible to calculate the fission probability and multiplicities of evaporating prescission particles. Two-dimensional models provide the additional possibility of calculating either the fragment-mass distribution corresponding to the most probable kinetic energy of fragments or the energy distribution corresponding to a fixed ratio between fragment masses.

The experimentally observed two-dimensional mass-energy distribution cannot be obtained in terms of either one-dimensional or two-dimensional Langevin calculations. In this case, it is necessary to have at least three collective coordinates. For a simultaneous description of the angular and charge distributions, it is inevitably necessary to introduce the fourth and fifth collective coordinates, which will determine the formation of the angular distribution of fission fragments and the charge distribution between fragments.

Results from the first estimative three-dimensional calculations of the parameters of the distribution of fission fragments over kinetic energy and the mean prescission neutron multiplicity [17] were published only in 1995. Since 2000–2001, the results of systematic four-dimensional [18] and three-dimensional [19–27] Langevin calculations began to appear regularly in publications.

At the present time, the theoretical basis of the stochastic approach to collective nuclear dynamics based on the Langevin equations and the results of calculations are adequately described in the published reviews of Abe *et al.* [28] and Fröbrich [29], and in the book by Fröbrich and Lipperheide [30]. Some recent results and developments could be found also in the book of Krappe and Pomorski [31]. For this reason, we mostly omit the fundamentals of the stochastic approach in this review and focus our attention on clarification and discussion of the most important results obtained in last years within the multidimensional stochastic approach applied to the fission process of the highly excited nuclei. We place particular emphasis on the specific problems and difficulties resulting from the multidimensionality of the approach developed and used in the calculations.

The main observables, which could be obtained within the stochastic approach and compared with experimental measurements are: the mass, charge and total kinetic energy distributions (MED) of the fission fragments (FF) or evaporation residue (ER), their isotopic/isobaric/isotonic distributions (ID) and light particles multiplicities and its energy spectra. According to the theoretical model applied to description of the reaction, there are several phenomena which are studied. The most important is a collective energy dissipation during the time evolution of the system from two colliding ions through a compact shape to scission into fragments. Usually an assumption is made that the energy is lost for friction or/and inertia during

the shape evolution, thus the transport coefficients govern the splitting of the CN into fragments.

The fission observables could be studied fully stochastically or using the thermodynamic properties. The dinuclear system model based on the thermodynamics with Boltzmann factor included [32–35] allows to calculate cross-section of fusion, fission and also evaporation or quasi-fission. The potential energy surface is obtained with two-center shell model (TCSM) and the emission barriers for particles, clusters is obtained with Skyrme-type nucleon-nucleon interaction. The evaporation and binary decay are treated on the same footing as a collective motion of complex system in the mass asymmetry coordinate. The dinuclear system model is applied already for various reactions, starting with medium mass region [35–37], by actinides [38–40] up to super-heavy nuclei [41].

There are two main directions in which stochastic models describing fission reactions are going: the statistical approach, based on well-defined physical theories and formulas, fitted to measured data, and the dynamical treatment of the shape evolution of excited nuclei. The Monte Carlo method is applied to vary the initial condition such as the angular momenta or sort of emitted particles and its energy. The outcome of the statistical approach is very effective in the regions where the experimental data are well known and in many cases it provides interesting information about measured data. The newest and probably the most efficient statistical-like code describing the observables for spontaneous fission, neutron-induced fission and, more generally, for fission of a compound nucleus from any other entrance channels, with given excitation energy and angular momentum is the GEF (GEneral description of Fission observables) [42]. The GEF model is very powerful as it is used for a wide range of heavy and super-heavy isotopes from $Z = 80$ to $Z = 112$ and beyond, up to excitation energies of about 100 MeV. The outcomes from this models are: fission barriers, fission probabilities, fission fragment mass and charge distributions, isomeric ratios, total kinetic energies, and prompt-neutron and prompt-gamma yields and energy spectra from neutron-induced and spontaneous fission. The fission fragment distributions and deformations at scission is described by a statistical approach based on the estimation of the depths and the widths of the fission valleys within localization of nucleonic wave functions in a necked-in shape. Many well-known theories and formulas are applied in this model and fitted to known experimental observables. Thus, the GEF code does not need any additional empirical data as many of abstract theoretical systems important for fundamental and applied science will never be measured.

The fully statistical code, which is used widely, from fusion-evaporation up to spallation reaction is GEMINI++. First code was dedicated to a binary decay as it was presented in [43]. Statistical model calculations were applied to the Nb+Be and C reactions at bombarding energies of $E/A = 11.4$, 14.7 and 18.0 MeV. The charge distributions were estimated with the conditional barriers predicted with the rotating Finite-Range Liquid Drop model (FRLDM) [44]. The GEMINI code was developed over the years and in [45] for the first time the results with the improved version called "GEMINI++" appeared. The charge distribution is based on fission barriers for various rotational liquid drop models. The first assumption was to reproduce systematically the wide range of the evaporation spectra for light and heavy compound nuclei excited in a broad energy range. The transmission coefficient are calculated within the global optical-model potentials in place of global fits to elastic-scattering data. Also the level-density parameter was changed from the constant $A/8$ or $A/10$ prescription by including the dependence on an excitation-energy of the system. The third important change was the reduction of the macroscopic rotational energy of the nucleus predicted with the FRLDM model by the relation of the angular momentum with the level density in light nuclei at large spins. Lately the GEMINI++ has been ameliorated by adding the emission of collective excitation such as Giant Dipole Resonances [46] or possibility to describe the multifragmentation reactions or even a spallation processes [47]. As GEMINI++ code uses the Monte Carlo method for choosing the sort and energy of emitted particles, there is possibility to get the FF mass/charge distributions, and after tuning some parameters the experimental data are reproduced correctly.

There are other statistically-based codes on the market such as THALYS, PACE, Monte Carlo Cascade, but their descriptions of the fission reaction are focused mainly on applications. These computer programs are still used as they give good predictions in the region of the energies/masses/reaction for which they are dedicated. The results are obtained quite fast and they obey wide range of the estimated observables. Special attention should be put on the possibility to calculate the angular distribution of the fission fragments or evaporated particles. The codes as GEMINI++ or PACE are easily connected to the filters used directly in the data analysis and this facilitate the comparison between theory and experiment. As the standard phenomena are included in these models, all the inconsistencies which could appear, are the potentially interesting cases for further, more time-consuming studies.

The second kind of approaches is a dynamical evolution of the compound nucleus in time. Such a method uses also the Monte Carlo method for taking a decision not only about the initial angular momentum or evaporation conditions, but also the determination of the shape change is taken into account in each time step. This kind of treatment is more sophisticated and more time-consuming than the statistical estimations but the main profit is controlling each constituent of the reaction on this same footing. There are at least two procedures (classical and quantal) to describe theoretically the fission process. The most frequent is the solving of the set of stochastic equations such as Smoluchowski, Langevin, or Master type in the collective coordinate space with dissipation energy included by friction and inertia tensors. This method is combined with the model responsible for the emission of the light particles such as neutrons, protons, α, γ-rays and others. The main ingredients which will be described later in this article are the potential energy approaches, dissipation models and various nuclear shape parameterizations.

The fission dynamics of the medium mass nucleus at low excitation energy has been investigated in [21, 22]. The set of Langevin equations has been solved in two-dimensional deformation plane and the evaporation channel has been taken as a Master equation. The Strutinsky shell correction with the BCS (Bardeen-Cooper-Schrieffer) pairing model added to Liquid Drop macroscopic energy allowed to describe an influence of the quantal effects, friction and scission condition on the shape of the mass distribution.

The set of Langevin equations in three-dimensional collective coordinate space has been applied for the description of binary decay firstly in the heavy nuclei (^{244}Cm, ^{184}Pt, ^{162}Yb) [19, 48] and later for rare-earth nuclei [49, 50]. The authors compared the fission fragment distributions, angular momentum dependence, fission barriers and pre-scission neutron multiplicities calculated with the FRLDM model to experimental data. Later on the fission fragments angular anisotropy was also investigated for series of nuclei at excitation energy $E^\star = 85$–$148\,\mathrm{MeV}$ [51]. As the potential energy has been obtained with the macroscopic approach, the physics of moderate excitation energy was mainly discussed.

The low excitation energy reactions are also inquired within a fully stochastic way by solving the set of Langevin equations in a multidimensional collective coordinates space. In the papers [52–54], a method is presented to dynamically study the fission process, including the shell effects, pairing effects, dissipation and fluctuation. The choice of five deformation parameters, with three free degrees of freedom and an application of the two-center shell model for receiving the single-particle energy spectra, allows to investigate the shape of each fragment separately. The liquid drop formula together with Strutinsky shell corrections assures the proper treatment of the potential energy. The dissipation is taken as the wall-and-window formula [55–58] for friction tensor and hydrodynamical inertia tensor is applied as the Werner-Wheeler approximation. The mass distributions for U and Pu isotopes are used for investigation of the shell effects damping with an increasing the excitation energy of the system [52]. The importance of the scission point for the shape of the MED is discussed in [54] and a new way to define nuclear deformation with the optimal shape parametrization to study the form of the nucleus before and after splitting is given in [53].

The calculation in four-dimensional collective coordinate space are done by three independent groups: the authors of [59, 60] focused efforts on investigation of the low-energy processes and in [61–66] the moderate excitation energies are discussed. The collective coordinate space contains three deformation parameters and a variable responsible for the space orientation of the fissioning system. The details will be discussed in next chapters.

A similar methodology is widely used to estimate the survival probability of the super-heavy nuclei. As the production of super-heavy species is one of the most crucial topics nowadays, the most efficient modes to create heavier and heavier nuclei are the huge interest. The Langevin transport equations based on two-center shell model PES are used to estimate not only fission but also the fusion probability. Obviously, super-heavy species deexcite by α emission in the first stage, but later the fission is probable [67, 68]. The ternary fission of the super-heavy nuclei into three similar fragments was studied as a new, competitive channel to the binary decay [69].

The progress in describing the fusion-fission is done by the group of Kosenko and collaborators [25, 70–72]. They describe the motion of two nuclei toward each other and the state of the interacting nuclei is defined in terms of three collective coordinates. These parameters are the distance between the centers of mass of the nuclei and the deformation parameter for each of them. Only the nose-to-nose orientation of the nuclei is assumed. The set of Langevin equations in three collective degrees of freedom are solved to depict the evolution of the nucleus from contact point to scission. The new and interesting idea is to use as a nuclear interactions the Gross-Kalinovsky or even Woods-Saxon potential which together with Coulomb energy gives the potential energy of the system. The shell and pairing energies obtained within Strutinsky method allow to treat low energy fission. In [72] the shell structure of colliding ions, their orientation in the space, and the effect of tunneling of ions through the Coulomb barrier are taken into account as well as the shell structure of the compact system. Such a procedure estimates the compound nucleus and evaporation residue formation cross sections and the impact of the tunneling effect in the entrance channel on the fusion and evaporation residue cross sections.

Randrup and Möller with coworkers in a series of articles show the evolution of the methodology based on Brownian motion and performing random walks on five-dimensional fission potential-energy surfaces [73–80]. The potential energy space is obtained within finite-range liquid drop model (FRLDM) [81] for the macroscopic part and folded-Yukawa for the single-particle energy spectra. The Strutinsky shell corrections with BCS+Lipkin-Nogami method [82–84] responsible for pairing parts combined with macroscopic energy permit to reproduce the known fission barriers. The Metropolis walk used here as a way to obtain the random character of the description is based on the assumption that inertial effects and the MED are insensitive of the dissipation tensors. Despite this simplification the wide range of the actinide nuclei has been studied [78–80] and its charge/mass distributions of the fission fragments estimate fit well quantitatively and qualitatively the experimental data, not only for spontaneous fission but also for the neutron induced reactions [80]. The self-consistent approach are also used to investigated the fission dynamics. The Time-Dependent Hartree-Fock (TDHF) with BCS pairing [85, 86] was used firstly for the description of the fusion reactions but later also for studies the nucleon transfer in symmetric heavy-ion reactions at energies below the Coulomb barrier. The self-consistent calculation of isotopic distribution have been also compared to the phenomenological mean-field potential [87].

The new methodology has been proposed by Sadhukhan, Nazarewicz and Schunck [88], where they obtained

microscopically the mass and charge distributions of spontaneous fission yields. The Langevin dynamics has been combined with a nuclear density functional theory used to calculate the potential energy and also the inertia tensors in collective coordinate space. The collective coordinate space contains not only the deformation but also the pairing parameters. The method allows to track the fission trajectories from ground state to the scission. The results reproduce with good accuracy the experimental charge and mass distributions in the spontaneous fission of ^{240}Pu.

The step forward is done by an American-Polish collaboration of Bulgac and Magierski [89], where the fission dynamics of ^{240}Pu has been investigated as a configuration in the proximity of the outer fission barrier to full scission. They extended nuclear density functional theory to superfluid systems and real-time dynamics. Also the formation of the fission fragments is done microscopically. All collective degrees of freedom are included in this fully nonadiabatic approach of nuclear dynamics. The complicity of the calculation is such that only mean values of mass/charge/TKE of the fission fragments is obtained but it permits to trace dynamically the influence of various pairing forces during the way of the compound nucleus to the separation into two daughter nuclei. The methodologies proposed in [88] or [89] are big steps in direction of fully microscopic description of the processes in hot nuclei. However still some work has to be done to correctly describe the ion-induced fission.

The statistical and dynamical models are complementary and very important. The main advantage of the statistical codes is treating all well-known physical phenomena and giving the results for many observables in reasonably fast time. The discrepancies between experimental data and statistical estimations are hints for the new physical effects [90, 91]. These exotic cases are frequently investigated by dynamical calculations as they are usually more time-consuming and there is no reason to employ them for every reactions. From other side the physics studied by the dynamical approach, for instance charge variation, energy dissipation effects, brings the extra-push for the development or a justification of the phenomenology in the statistical models.

The present review demonstrates mainly the results obtained at high energy fission and contains six sections. Section 2 describes the models used to obtain the fission dynamics and, as main results, the fission fragments mass/charge and total kinetic distributions. These observables and their sensitivity on potential energy models, level-density parameters, viscosity and other model constituents are discussed in sect. 3. Section 4 is dedicated to the angular distribution of the fission fragments as it facilitates the comparison with a measurement. The present developments in the detection techniques allow to obtain not only full charge and mass distributions but also the detailed isotopic/isobaric/isotonic distributions of the fission fragments and evaporation residues, which is a step forward in comparison to the MED, thus in sect. 5 a short presentation of various calculations is done. The last part consists of a brief summary and perspectives.

2 The model and basic equations

2.1 Parametrization of nuclear surface and collective coordinates

One of the main ingredient of the dynamical fission model is the nuclear shape parametrization. From one side it should be flexible enough in order to generate all possible shapes, which could be realized during the fission process, and from the other side it should not be complicated in order to avoid unnecessary difficulties during the numerical solution of the Langevin equations. An axially symmetric nuclear shape can be described in cylindrical coordinates by the profile function $\rho_s(z)$, whose rotation around the symmetry axis determines the nuclear surface. The most frequently used parameterizations are the $\{c, h, \alpha\}$ [92], three-quadratic surface [93], Trentalange [94], Brosa [95], Cassini ovaloids [96–98], and two-center parametrization [99, 100]. A comprehensive collection of formulas and relevant comments are given in monographs [31, 101].

The use of a particular nuclear-shape parametrization is closely connected to the problem of choosing collective coordinates. All the possible collective coordinates can be conditionally divided into coordinates describing a nuclear shape and coordinates not associated with nuclear shape degrees of freedom. The chosen parametrization should involve at least three parameters for an adequate description of nuclear shape evolution in fission process and allow introduction of the following shape coordinates: nuclear elongation, a coordinate determining neck evolution in a nuclear shape, and a mirror-asymmetry coordinate. Such a minimal set of collective coordinates permits the calculation of the two-dimensional mass-energy distributions (MEDs) of fission fragments. All relevant collective coordinate should be related directly with the experimental observables. The mass-asymmetry collective coordinate determines the mass distribution of fission fragments. The elongation parameter determines the relative distance of the future fragments, and, as a result, influence on the total kinetic energy of fission fragments, as well as the prescission particles multiplicities and fission width. The coordinate determining neck evolution in a nuclear shape for given elongation influence the total kinetic energy of fission fragments. Among the collective coordinates not associated with nuclear shape, we mention, for example, the charge-asymmetry coordinate specifying the charge distribution between formed fragments. In general, the fission model should contain the dynamic coordinate - charge asymmetry, as it is done, for example, in refs. [69,102–104]. However, these theoretical calculations show that charge coordinate has quite small relaxation time, thus, it very fast reaches the statistical equilibration, and, therefore, this coordinate could be considered using statistical approximation. The calculations [103, 104] show that such consideration gives quite close results to the pure dynamical modeling.

A successful choice of collective coordinates could provide substantial simplification of the dynamical calculation procedure. In this context, we now discuss the in-

troduction of collective shape coordinates using the well-known $\{c, h, \alpha\}$ parametrization [92]. In refs. [92, 105], it was shown that, in terms of this parametrization, it is possible to reproduce accurately different characteristics of nuclear saddle point configurations obtained on the basis of variational calculations [106].

This parametrization has been also used for static calculations performed with the Strutinsky shell correction method [92], dynamic calculations of MEDs in the diffusion model [12], and for calculating a large number of different fission characteristics in the Langevin approach [19, 20, 107–109]. The parameter c describes nuclear elongation (the nuclear length, in units of the initial-sphere radius R_0, is equal to $2c$), the parameter h defines neck-thickness variation for a given elongation, and the coordinate α sets the ratio between the masses of future fragments. The nuclear-surface equation in the $\{c, h, \alpha\}$ parametrization is written as

$$\rho_s^2(z) = \begin{cases} \left(c^2 - z^2\right)\left(A_s c^2 + \frac{Bz^2}{c^2} + \frac{\alpha' z}{c}\right), & B \geq 0; \\ \left(c^2 - z^2\right)\left(A_s + \frac{\alpha' z}{c}\right)\exp(Bcz^2), & B < 0, \end{cases} \tag{1}$$

where z is the coordinate along the symmetry axis and ρ_s is the radial coordinate of the nuclear surface. In eq. (1) the quantities A_s and B are defined as

$$B = 2h + \frac{c-1}{2};$$

$$A_s = \begin{cases} c^{-3} - \frac{B}{5}, & B \geq 0; \\ -\frac{4}{3}\frac{B}{\exp(Bc^3) + (1 + \frac{1}{2Bc^3})\sqrt{-\pi Bc^3}\,\mathrm{erf}(\sqrt{-Bc^3})}, & B < 0. \end{cases} \tag{2}$$

Nuclear shapes in the $\{c, h, \alpha\}$ parametrization are enclosed within $z_{\min} = -c$ and $z_{\max} = c$. If the function $\rho_s(z)$ vanishes within these limits only at $z = \pm c$, we have continuous nuclear shapes. If there are two more roots at the interval $[z_{\min}, z_{\max}]$, such shapes are interpreted as being discontinuous. Other cases (with an odd number of roots within $[z_{\min}, z_{\max}]$) cannot be considered as nuclear shapes and are frequently referred as forbidden or "non-physical" shapes (for a more detailed discussion of such shapes, see [110]).

It is useful to determine the neck condition for the $\{c, h, \alpha\}$ parametrization. The coordinate z for which the function $\rho_s(z)$ reaches a minimum is defined as the neck coordinate z_N. The neck coordinate is determined from the condition

$$\frac{\partial \rho_s^2(z)}{\partial z} = 0, \tag{3}$$

which results in an algebraic equation. If there are three real roots lying within $[z_{\min}, z_{\max}]$, one of them (a minimum) is the neck coordinate z_N and other two (maxima) are coordinates of the thickest positions of the nascent fission fragments. These maxima determine the coordinates of formed fragments.

The following conditions should be taken into account, when choosing the collective shape coordinates: i) Collective coordinates are functions of the nuclear-shape parameters. Therefore, the simpler the form of these functions, the easier to use these coordinates. By simplicity, we also refer to the possibility of finding analytical inverse functions for the dependence of the shape parameters on the collective coordinates. ii) The mesh for dynamic calculations should involve the largest possible variety of nuclear shapes that can be given by the chosen parametrization and no forbidden shapes. iii) The choice of collective coordinates is closely related to boundary conditions at the mesh edges. One boundary condition can be extracted from the scission criteria, which determines the rupture of the neck connecting nascent fragments. The remaining limits for the collective coordinates should be chosen in such a way that their values do not affect the calculated results. It could be guaranteed by the large values of potential energy at the limits of the mesh. The potential energy should be larger than excitation energy of the fissioning compound nuclei. Therefore, Langevin trajectory will not have opportunity to reach the limits of the grid. The substantial uncertainty to the calculated results could be brought in this case.

Usually, collective coordinates are chosen by two methods. First, physical values describing nuclear shape are chosen as collective coordinates, for example, the distance between the mass centers of nascent fragments R (elongation coordinate), neck thickness r_N, ratio of the difference between the masses of formed fission fragments and the total nuclear mass η_A (the mass-asymmetry coordinate)

$$\eta_A = \frac{A_R - A_L}{A_R + A_L} = \frac{3}{4R_0^3}\left(\int_{z_N}^{z_{\max}} \rho_s^2(z)\mathrm{d}z - \int_{z_{\min}}^{z_N} \rho_s^2(z)\mathrm{d}z\right), \tag{4}$$

where A_R and A_L are the mass numbers of the formed fragments (here and below, the subscripts R and L marks right-hand and left-hand fragments, respectively). However, such definition of collective coordinates is not simple, as it works for the nuclear shapes, which have well defined neck. In case of the mononuclear shapes, featuring no neck, it could be difficult to introduce degrees of freedom connected with nascent fragments. Thus, second possibility is to use shape parameters as a collective coordinates. This way is convenient from the first condition mentioned above and frequently extremely inconvenient according to the second and third conditions. Therefore, in the case of the $\{c, h, \alpha\}$ parametrization we perform transformation of the shape parameters c, h and α to the collective coordinates q_1, q_2, and q_3, as described below.

First of all, we discuss the problem of forbidden shapes. It should be noted that forbidden shapes exist only for $\alpha \neq 0$. In addition, for each c and h, it is possible to find $\alpha_{\max}$ such that nuclear shapes are within $|\alpha| \leq \alpha_{\max}$ and forbidden shapes lie in the remaining region. We note that the ultimate values of the parameter η_A (± 1) are attained when the mass of one of the fragments is equal to zero. This condition can be written as

$$\left(\frac{\partial \rho_s^2(z)}{\partial z}\right)_{z = z_{\min}(z_{\max})} = 0. \tag{5}$$

Condition (5) means that the minimum (the neck) is at one of the extreme points ($z_{\min}$ or $z_{\max}$) of a nuclear shape. Using eq. (5) and taking into account that the function $\rho_s(z)$ vanishes at the extreme points, we obtain, for the $\{c, h, \alpha\}$ parametrization,

$$\alpha_{\max} = \begin{cases} (A_s + B)\,, & B \geq 0; \\ A_s, & B < 0. \end{cases} \tag{6}$$

Thus, $\alpha_{\max}$ essentially depends on c and h. This dependence creates the problem of constructing a mesh with the use of the shape parameter α as the mass-asymmetry coordinate. It is impossible to construct a rectangular mesh with respect to c, h, and α collective coordinates excluding forbidden shapes. In order to avoid this we proposed [27] a method of introducing the mass-asymmetry coordinate,

$$q_3 = \frac{\alpha}{\alpha_{\max}} = \begin{cases} \alpha/\,(A_s + B)\,, & B \geq 0; \\ \alpha/A_s, & B < 0. \end{cases} \tag{7}$$

For such a choice, the problem of forbidden shapes is completely solved: all the possible asymmetric nuclear shapes (for given c and h) are enclosed within $|q_3| \leq 1$.

It is convenient to choose the collective parameter responsible for formation of the neck in a nuclear shape in such a way that the condition of zero neck thickness is satisfied for the same (or nearly the same) value of this parameter. In the case of $\alpha = 0$, zero neck thickness is attained for

$$h = h_{\rm sc} = \frac{5}{2c^3} + \frac{1-c}{4}\,. \tag{8}$$

From eq. (8), it follows that the value $h_{\rm sc}$ depends strongly on c. Therefore, we introduce the collective neck coordinate as follows:

$$q_2 = \frac{h + 3/2}{h_{\rm sc} + 3/2}\,. \tag{9}$$

The coordinate q_2 has the following properties: if $q_2 = 0$, $h = -3/2$ which guarantees reasonably high values of potential energy, inaccessible for Langevin trajectory; if $q_2 = 1$, the neck thickness is equal to zero for symmetric shapes. For asymmetric nuclear shapes, the neck thickness vanishes for somewhat smaller, but close to unity, values of q_2.

Thus, in our opinion, the collective coordinates $\mathbf{q} = (q_1 = c, q_2, q_3)$ are optimal for dynamical modeling at rectangular mesh of collective coordinates in case of the $\{c, h, \alpha\}$ parametrization. We use these coordinates with the following limits: $q_1 \in [0.5, 4.5]$, $q_2 \in [0, 1]$ and $q_3 \in [-1, 1]$. When studying the charge mode, it is convenient to additionally introduce [102–104] a charge-asymmetry coordinate in the form of $q_4 = \eta_Z = (Z_R - Z_L)/(Z_R + Z_L)$, where Z_R and Z_L are the charges of the formed right-hand and left-hand fragments. The nuclear forms (fig. 1) are calculated by eq. (1) for a combination of collective coordinates (q_1, q_2) and $q_3 = 0$ in some cases to visualize the influence of variables. Unrealistic spindle-like shapes are obtained for small values of q_2 and increasing this values the neck formation is visible. The curves mark the scission lines for several values of mass asymmetry coordinates $q_3 = 0.5$, 0.75 and 1.0. The left top corner of the plane (q_1, q_2) contains values of the deformation papameters provided to the shapes, which are already separated into two parts and the limits of creation compound shapes depend mainly on the asymmetry parameter.

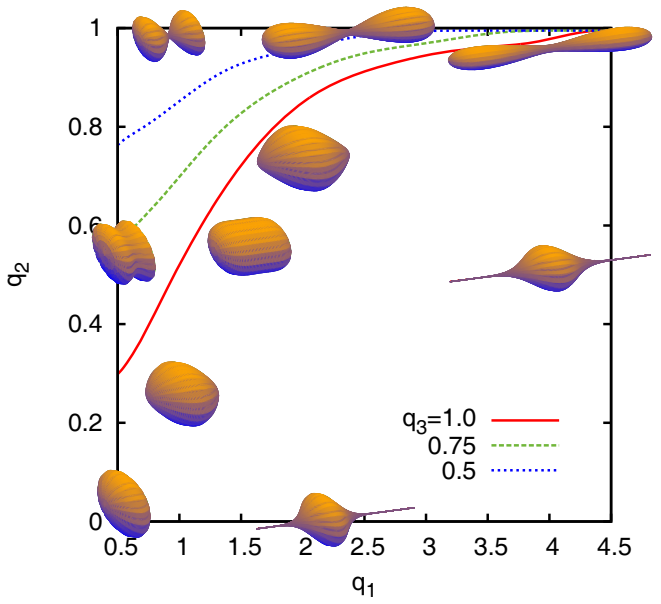

Fig. 1. (Color online) The nuclear shapes are calculated within eq. (1) for several sets of variables (q_1, q_2) and $q_3 = 0$. The full, dashed and dotted lines mark the scission lines calculated for asymmetry coordinates $q_3 = 0.5$, 0.75 and 1.0.

2.2 Equations of motion

In the stochastic approach [6, 28, 29, 31], evolution of the collective coordinates is considered as motion of Brownian particles which interact stochastically with a large number of internal degrees of freedom, constituting the surrounding "heat bath". The hydrodynamical friction force is assumed to be derived from the random force averaged over a time larger than the collision time scale between collective and internal degrees of freedom. The random part is modeled as a Gaussian white noise which causes fluctuations of the collective variables resulting in fluctuations of the physical observables in fission process. The coupled Langevin equations describing this process have the form:

$$\begin{aligned} \frac{{\rm d}q_i}{{\rm d}t} &= \mu_{ij} p_j, \\ \frac{{\rm d}p_i}{{\rm d}t} &= -\frac{1}{2} p_j p_k \frac{\partial \mu_{jk}}{\partial q_i} - \left(\frac{\partial F}{\partial q_i}\right)_T - \gamma_{ij}\mu_{jk} p_k + \theta_{ij}\xi_j(t), \end{aligned} \tag{10}$$

where $\mathbf{q}$ is the vector of collective coordinates, $\mathbf{p}$ is the vector of conjugate momenta, $F(\mathbf{q}, K) = V(\mathbf{q}, K) - a(\mathbf{q})T^2$ is the Helmholtz free energy, $V(\mathbf{q})$ is the potential energy, $m_{ij}(\mathbf{q})$ ($\|\mu_{ij}\| = \|m_{ij}\|^{-1}$) is the tensor of inertia, and

$\gamma_{ij}(\mathbf{q})$ is the friction tensor. The $\xi_j(t)$ is a random variable satisfying the relations

$$\langle \xi_i \rangle = 0,$$
$$\langle \xi_i(t_1)\xi_j(t_2)\rangle = 2\delta_{ij}\delta(t_1 - t_2). \tag{11}$$

Thus, the Markovian approximation is assumed to be valid. The strength of the random force θ_{ij} is given by Einstein relation $\sum \theta_{ik}\theta_{kj} = T\gamma_{ij}$. The temperature of the "heat bath" T has been determined by the Fermi-gas model formula $T = (E_{\rm int}/a)^{1/2}$, where $E_{\rm int}$ is the internal excitation energy of the nucleus and $a(\mathbf{q})$ is the level-density parameter. It should be stressed that the driving force in an excited system is not simply the negative gradient of the conservative potential $V(\mathbf{q})$, but should contain a thermodynamical correction. It can be derived from the well-known thermodynamical relations [29]

$$Q_i = -\left(\frac{\partial F}{\partial q_i}\right)_T = T\left(\frac{\partial S}{\partial q_i}\right)_E. \tag{12}$$

Thus, the conservative driving force for the Fermi-gas model can be expressed in the form

$$Q_i = -\frac{\partial V(\mathbf{q})}{\partial q_i} + \frac{\partial a(\mathbf{q})}{\partial q_i}T^2. \tag{13}$$

During a random walk along the Langevin trajectory in the space of the collective coordinates, the energy conservation law is used in the form $E^\star = E_{\rm int} + E_{\rm coll} + V + E_{\rm evap}(t)$. Here $E^\star$ is the total excitation energy of the nucleus, $E_{\rm coll} = 0.5\sum \mu_{ij}p_ip_j$ is the kinetic energy of the collective degrees of freedom. The value $E_{\rm evap}(t)$ is the energy carried away by the evaporated particles by the time t. The potential energy of the nucleus, as well as level-density parameter could be calculated within different models, allowing to probe in the numerical modeling of fission process the influence of various parameters on the calculated observables, comparable with experimental data. As will be shown later the use of the level-density parameter calculated with the coefficients taken from the work of Ignatyuk and coauthors [111] and the potential energy calculated within the framework of a macroscopic model with finite range of the nuclear forces [112] provide good qualitative and quantitative description of experimental data in multidimensional Langevin calculations.

In fig. 1 of article [63], we present the potential energy in the coordinates q_1 and q_2 at $q_3 = 0$ for the ^{224}Th compound nucleus. The dashed line in this figure represents the mean trajectory calculated under the assumption of a one-body mechanism of nuclear viscosity with $k_s = 0.25$, and the crosses mark the saddle point and nuclear ground state. In addition, this figure shows examples of nuclear shapes for the given q_1 and q_2 values.

Quite often the applications of Langevin dynamics to fission process imply zero spin about symmetry axis of the fissioning compound nucleus, in other words it was always assumed that angular momentum is not only perpendicular to the reaction plane, but also to the fission direction. As first pointed out by Lestone in ref. [113], this assumption is not consistent with statistical model as well as with dynamical treatment of the orientation degree of freedom [114]. Subsequently, Lestone and McCalla introduced the overdamped Langevin equation to describe the dynamical evolution of orientation degree of freedom (K coordinate) and stressed that a large volume of heavy-ion induced fission data needs to be reanalyzed with dynamical treatment of the orientation degree of freedom [115]. Clearly, consideration of K coordinate as an independent collective coordinate in multidimensional Langevin dynamics is necessary for dynamical treatment of the fission fragment angular distribution. Yet, in almost all cases, the analysis of the latter is restricted only by the framework of statistical transition-state model. An alternative dynamical description of the evolution of the orientation degree of freedom on the basis of a Metropolis algorithm and an algorithm of Kubo-Anderson process was previously developed in refs. [51,116–118]. This approach was successfully applied to describe the fission fragment angular distribution obtained in fission of highly excited compound nuclei.

However, the description of evolution of the K collective coordinate using the Langevin equation for overdamped motion is more consistent than the application of Metropolis algorithm [51, 118]. The Langevin equation for K coordinate allows to model the relaxation process of K states depending on the instantaneous physical properties of fissioning system like temperature, moment of inertia instead of treating the corresponding relaxation time τ_K as a free parameter [51,116,118]. The overdamped Langevin equation for the K coordinate has the form

$$\mathrm{d}K = -\frac{\gamma_K^2 I^2}{2}\frac{\partial V}{\partial K} + \gamma_K I\sqrt{\mathrm{d}t\frac{T}{2}}\xi(t), \tag{14}$$

where $\xi(t)$ has the same meaning as in (10) and γ_K is a parameter controlling the coupling between the orientation degree of freedom K and the "heat bath". As the level density parameter $a(\mathbf{q})$ does not depend on K, the conservative force in the Langevin equation (14) is calculated as a derivative of the potential energy.

The Langevin equations for the shape parameters (10) and Langevin equation for the K coordinate (14) are connected through the potential energy. The Langevin dynamics of K coordinate is influenced by the actual value of potential energy $V(\mathbf{q}, I, K)$. At the same time, the rotational part of the potential energy is dependent on the actual K value at time t, and this way it influences the dynamical evolution of shape parameters.

The rotational part of the potential energy is determined by the expression

$$E_{\rm rot}(\mathbf{q}, I, K) = \frac{\hbar^2 K^2}{2J_\parallel(\mathbf{q})} + \frac{\hbar^2[I(I+1) - K^2]}{2J_\perp(\mathbf{q})}$$
$$= \frac{\hbar^2 I(I+1)}{2J_\perp(\mathbf{q})} + \frac{\hbar^2 K^2}{2J_{\rm eff}(\mathbf{q})}. \tag{15}$$

The functionals $J_\parallel$ and $J_\perp$ are the rigid body moments of inertia, about and perpendicular to, the symmetry axis. The effective moment of inertia is $J_{\rm eff}^{-1} = J_\parallel^{-1} - J_\perp^{-1}$.

2.3 Initial and final conditions

In the most general case, the initial values of collective coordinates $\mathbf{q}_0$, momenta $\mathbf{p}_0$, and total compound-nucleus momentum I can be sampled by the Neumann method using the generating function

$$P(\mathbf{q}_0, \mathbf{p}_0, I, t=0) \sim P(\mathbf{q}_0, \mathbf{p}_0)\sigma_{\rm fus}(I)P(K, t=0). \quad (16)$$

The function $\sigma_{\rm fus}(I)$ describes the initial momentum distribution of compound nuclei and is frequently approximated by the expression

$$\sigma_{\rm fus}(I) = \frac{2\pi}{k^2}(2I+1)T(I), \quad (17)$$

where $k^2 = 2\mu E_{\rm lab}/\hbar^2$, μ is the reduced mass of the projectile-target system, and $T(I)$ is the penetrability coefficient, which is defined within a model reproducing experimental fusion cross sections. When performing Langevin calculations, the difference between the total nuclear spin $I = |\mathbf{l}+\mathbf{s}_{\rm t}+\mathbf{s}_{\rm p}|$ ($\mathbf{s}_{\rm p}$ and $\mathbf{s}_{\rm t}$ are the spin of the projectile and target nuclei, respectively) and the angular momentum l is usually disregarded.

In our calculations, the following form of the function $T(I)$ was used:

$$T(I) = \frac{1}{1+\exp[(I-I_c)/\delta I]}\,. \quad (18)$$

In the first approximation, I_c and δI values were defined according to the scaled prescription [29], which reproduces to a certain extent the dynamical results of the surface friction model [119] for the fusion of two heavy ions. Finally, the quantities I_c and δI were constrained from the experimental fusion cross section and $\langle I^2\rangle$.

When studying the fission of excited compound nuclei, the initial values of the collective coordinates are frequently chosen for use as the compound-nucleus ground state. In this case, the initial momentum distribution is chosen as the equilibrium value. Then,

$$P(\mathbf{q}_0, \mathbf{p}_0) \sim \exp\left\{-\frac{V(\mathbf{q}_0, l)+E_{\rm coll}(\mathbf{q}_0, \mathbf{p}_0)}{T}\right\}\delta(\mathbf{q}_0-\mathbf{q}_{\rm gs}), \quad (19)$$

where $\mathbf{q}_{\rm gs}$ are the coordinates of the nuclear ground state. For spinless ions participating in fusion reactions and projectile energies substantially exceeding the fusion barrier, states with different values of $K(t=0)$ must be populated with nearly equal probabilities. Bearing this in mind, we took the initial distribution $P(K,0)$ to be uniform over the interval $[-I; I]$ in just the same way as in [115,116]. In case of subbarrier energies or compound nucleus with nonzero spin the above-mentioned assertion about uniformity is not valid, and more detail complicated analysis of the entrance channel should be considered [120].

The choice of initial conditions in the form of eqs. (16)–(19) means that we begin the Langevin calculations with a completely statistically equilibrium state of a compound nucleus with a fixed initial excitation energy. It should be noted that such a choice of initial conditions can be considered only as an approximation of a real complicated situation. Different reaction mechanisms including fast-fission, quasi-fission reactions are possible in case of heavy colliding ions at high excitation energies and angular momenta. These reaction mechanisms not necessary lead to formation of statistically equilibrated compound nucleus at ground state. Moreover, in case of light compound nuclei fission near the Businaro–Gallone point it is difficult to distinguish fission fragments from the products of the deep-inelastic scattering. Therefore, the most natural choice of initial conditions can be obtained from consideration of the nuclear reaction entrance channel.

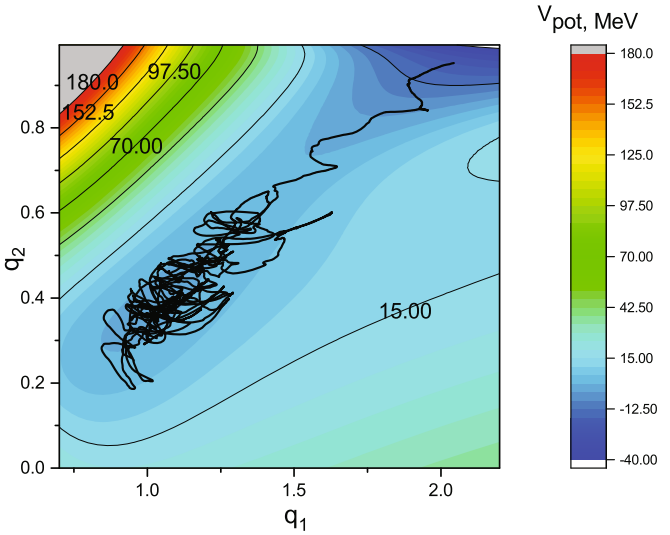

Fig. 2. (Color online) The Langevin trajectory for the fissioning ^{248}Cf.

As a final condition of the compound nucleus evolution we consider the formation of an evaporation residue nucleus and fission of compound nucleus into two fragments. Evaporation residue is formed, as a result of light-particle and γ-quanta emission, if the sum $E_{\rm int} + E_{\rm coll}(\mathbf{q}, \mathbf{p})$ becomes lower than $\min(B_f, B_n)$, where B_f and B_n are the fission barrier and the neutron binding energy, respectively. We assume that the fissioning compound nucleus disintegrates into fission fragments after crossing the scission surface by the Langevin trajectory in space of collective coordinates. The scission surface is determined on the basis of some scission criteria. At present, there is no unambiguous approach to the choice of the scission criterion. However, the most frequently used criterion is imposing conditions to the equality of the neck thickness radius to some constant value, which is determined by the implementation of some instability criteria (see for example refs. [92,95,121]). In view of the above discussion, we consider that the fission of a nucleus into fragments occurs for a neck radius equal to $0.3R_0$, since this condition is in good agreement with the instability criterion of a nucleus with respect to the variations of the neck thickness [92]. The equation for the scission surface can be written as

$$\rho_s(z_N) = r_N, \quad (20)$$

where r_N is the neck radius corresponding to the prescission shapes. Example of Langevin trajectory is shown in

fig. 2. A spherical nuclear shape is chosen as the initial deformation $q_1 = 1$ and $q_2 = 0.375$, and numerical integration of the Langevin equations stops when a nucleus reaches the scission configuration around $q_1 \simeq 2$ and $q_2 \simeq 0.98$. Different fission observables were calculated by simulating the ensemble of Langevin trajectories, which represents the ensemble of fissioning nuclei.

2.4 Transport tensors

The so-called transport coefficients, *i.e.*, the mass (inertia) and friction parameters, are important components of dynamical models. As numerous calculations have shown, they generally define the character of the motion of a fissile system and directly influence both the fission fragment MED parameters and the fission timescale, as well as the multiplicities of prescission and postscission particles. Thus, calculation of the transport coefficients is extremely important.

The inertia and friction tensors are frequently calculated within the hydrodynamic approximation for incompressible irrotational flow. In this case, the mechanism of nuclear viscosity is a two-body one. In the hydrodynamic approximation, the Navier-Stokes equations for a viscous medium are usually solved on the basis of the Werner-Wheeler approximation [122,123], which makes it possible to obtain reasonably simple expressions for the inertia and friction tensors. When calculating the mass tensor, it was found that the Werner-Wheeler approximation provides very high accuracy for the elongation degree of freedom. For example, when describing the nuclear shape using the Lawrence parametrization [124], mass tensor components calculated from the elongation coordinate in the Werner-Wheeler approximation coincide with the exact solution of the corresponding hydrodynamic Neumann problem [125], which was obtained by a method based on potential theory [126]. In ref. [122], it was shown that the difference between mass parameters determined by solving the corresponding Neumann problem and with the Werner-Wheeler method increased proportionally to the multipolarity of the vibrations near a spherical shape.

For the friction tensor, the Werner-Wheeler approximation of the collective coordinate associated with elongation is in good agreement with the result obtained for the exact solution of the corresponding Neumann problem [125], as in the case of the mass tensor. At the same time, for the coordinate related to the neck evolution, the Werner-Wheeler approximation for the Lawrence parametrization results in a 30–40% overestimation of the corresponding friction tensor components.

In addition to the two-body mechanism of nuclear viscosity, the one-body mechanism [55,127] is more widely used in calculations of the friction tensor. In this mechanism of nuclear viscosity, the Pauli blocking principle, which forbids nucleon scattering into occupied states, is taken into account in calculation of dissipation strength. The Pauli blocking principle imposes restrictions on the mean free path of particles (it increases up to the size of the system itself); therefore, the role of two-particle collisions decreases, *i.e.*, particles move almost freely inside the nuclear shape and elastically hit only a moving "wall" simulating the nuclear surface.

In refs. [55,127,128], two formulas were presented for calculations of the one-body friction strength: The first, named the "wall" formula, describes the dissipation of nuclear shapes without a neck, and the second, called the "wall-plus-window" formula, was introduced for strongly necked-in nuclear shapes featuring two formed fragments. A quantum consideration of one-body dissipation showed [129] that the nuclear viscosity amounts to only about 10% of the values calculated using the wall formula [55,128], although the functional dependence of viscosity on nuclear shape is adequately reproduced by this formula. In this context, Nix and Sierk [130] proposed a modified variant of the one-body dissipation that led to the surface-plus-window formula. In this case, the contribution from the wall formula to the dissipation is reduced by almost four times. The reduction coefficient $k_s = 0.27$ was found from an analysis of the experimental width of giant resonances. From a comparison of the calculated average values of the kinetic energy of fission fragments with the experimental data, it was found [57] that k_s is in the range $0.2 < k_s < 0.5$. The friction tensor corresponding to the surface-plus-window formula can be written in cylindrical coordinates as [20]

$$\begin{aligned}\gamma_{ij} = \frac{1}{2}\rho_m \bar{v}\Bigg\{ & \frac{\partial R}{\partial q_i}\frac{\partial R}{\partial q_j}\Delta\sigma + \frac{32}{9}\frac{1}{\Delta\sigma}\frac{\partial V_1}{\partial q_i}\frac{\partial V_1}{\partial q_j} + \\ & + k_s\pi\Bigg[\int_{z_{\min}}^{z_N}\left(\frac{\partial \rho_s^2}{\partial q_i} + \frac{\partial \rho_s^2}{\partial z}\frac{\partial D_1}{\partial q_i}\right)\left(\frac{\partial \rho_s^2}{\partial q_j} + \frac{\partial \rho_s^2}{\partial z}\frac{\partial D_1}{\partial q_j}\right) \\ & \times\left(\rho_s^2 + \left(\frac{1}{2}\frac{\partial \rho_s^2}{\partial z}\right)^2\right)^{-\frac{1}{2}}\mathrm{d}z + \\ & + \int_{z_N}^{z_{\max}}\left(\frac{\partial \rho_s^2}{\partial q_i} + \frac{\partial \rho_s^2}{\partial z}\frac{\partial D_2}{\partial q_i}\right)\left(\frac{\partial \rho_s^2}{\partial q_j} + \frac{\partial \rho_s^2}{\partial z}\frac{\partial D_2}{\partial q_j}\right) \\ & \times\left(\rho_s^2 + \left(\frac{1}{2}\frac{\partial \rho_s^2}{\partial z}\right)^2\right)^{-\frac{1}{2}}\mathrm{d}z\Bigg]\Bigg\}, \end{aligned} \tag{21}$$

where ρ_m is the mass density of the nucleus, $\bar{v}$ is the average nucleon speed inside the nucleus, $\Delta\sigma$ is the area of window between two parts of the system, D_1, D_2 are the positions of mass centers of two parts of the fissioning system relative to the center of mass of the whole system, $z_{\min}$ and $z_{\max}$ are the left and right ends of the nuclear shape, z_N is the position of the neck plane which divides the nucleus into two parts.

We have chosen the position of the z_N at minimum of $\rho_s^2(z)$. The case $k_s = 1$ corresponds to the total one-body viscosity, then eq. (21) corresponds to the "wall-plus-window" formula. The two terms in square brackets in eq. (21) correspond to the "wall" formula for the left-hand and right-hand fragments. For compact nuclear shapes, featuring no neck, the friction tensor is usually calculated from the "wall" formula multiplied by the k_s coefficient, the "surface-plus-window" formula is applied

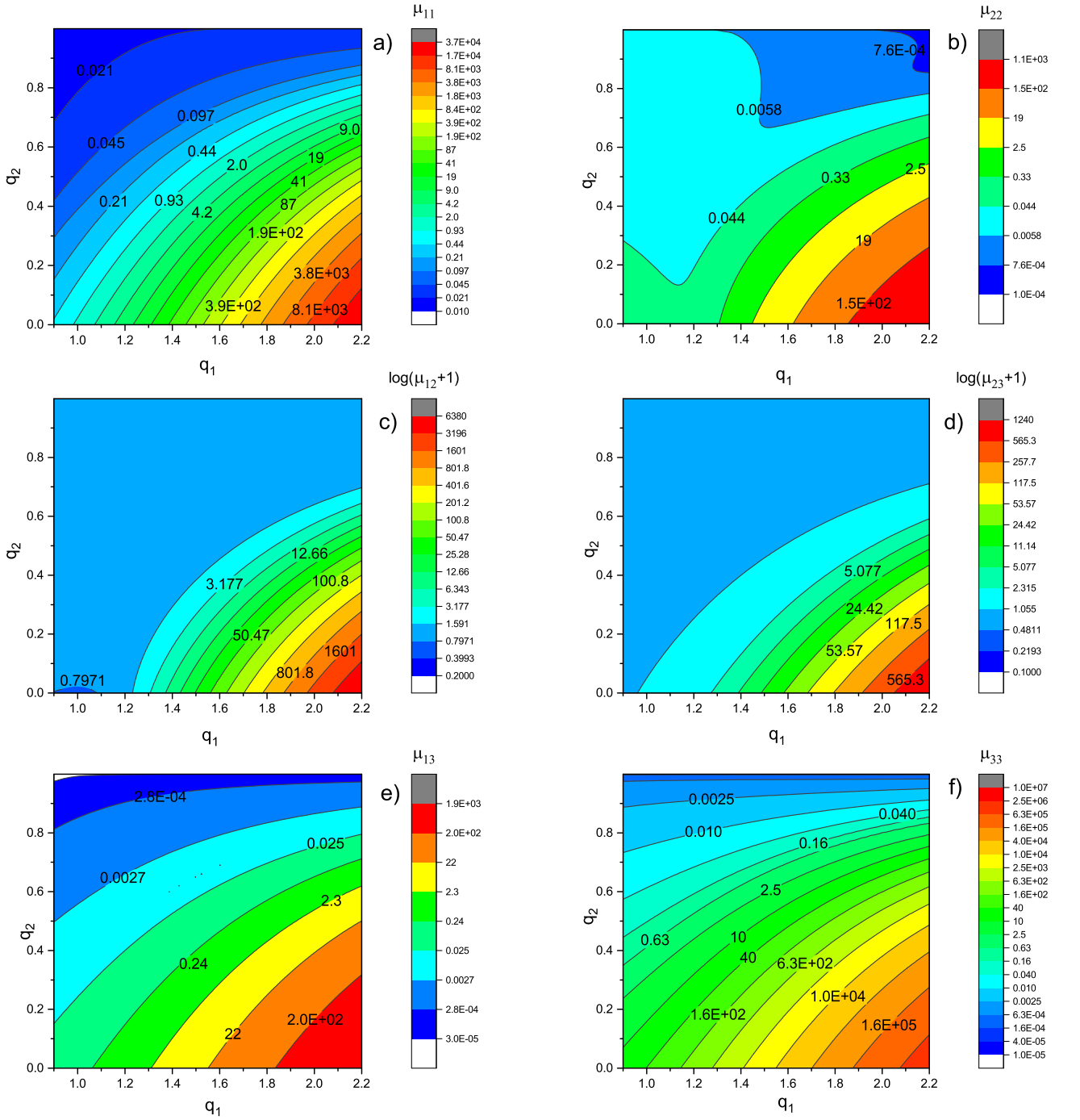

Fig. 3. (Color online) The components of the mass tensor for the ^{224}Th in collective coordinates (q_1, q_2) at $q_3 = 0$. The unit for the components of the mass tensor is 10^{-42} MeV s^2.

to strongly necked-in shapes. In order to describe the dissipation in an intermediate case, expressions of the type $\gamma_{ij} = k_s\gamma_{ij}^w f(R_N) + \gamma_{ij}^{sw}(1 - f(R_N))$ are usually used. The choice of the function $f(R_N)$ is quite arbitrary. As a rule, it is chosen to satisfy the conditions $f(0) = 0$ to $f(1) = 1$. However, this choice is ambiguous [8,131–133] and can affect the calculated characteristics [128]. In our model we usually choose $f(R_N) = \sin^2(\pi R_N/(2R_L))$, where R_L is the maximum value of $\rho_s(z)$ for lighter fragment.

The components of the inertia and friction tensors calculated on two dimensional mesh in collective coordinates q_1 and q_2 $(q_3 = 0)$ under the assumption of the one-body mechanism of nuclear viscosity are displayed in figs. 3 and 4. As can be seen from last figure, the deformation dependence of various components of the friction tensor is substantially different and strongly dependent on the values of collective coordinates. It should be emphasized that it is difficult to compare these components of the inertia

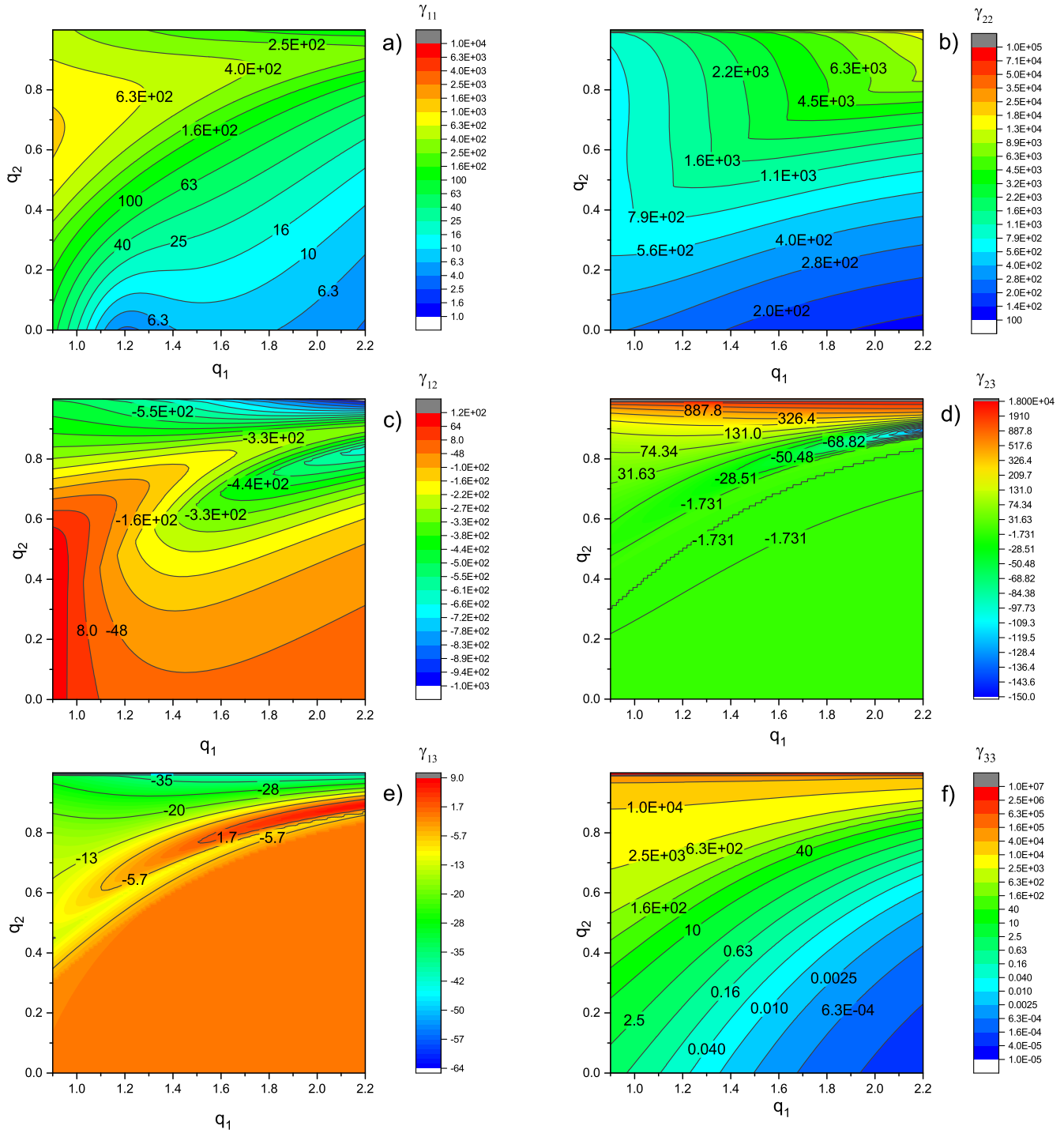

Fig. 4. (Color online) The components of the friction tensor for the ^{224}Th calculated with the one-body dissipation mechanism in collective coordinates (q_1, q_2) at $q_3 = 0$ for $k_s = 1$. The unit for the components of the friction tensor is 10^{-21} MeV s.

and friction tensors with the results of other studies. Even in case of using the same parametrization to describe nuclear shape, the qualitative behavior of the components depends on the chosen collective coordinates.

The assumptions used in derivation of the "wall" formula do not apply under certain conditions as it was shown in refs. [55, 134–136]. For example, the assumption of the randomness of the particle motion inside a nuclear shape cannot be applied to the motion of particles in integrable potentials such as spherical or ellipsoidal sharp edged potentials. In this case, the particle motion inside the nuclear shape is ordered. For this reason, the dissipation predicted by the wall formula is considerably overestimated. In this context, the authors of [137] proposed a deformation-dependent reduction coefficient in the wall formula reflecting the degree of particle motion

randomization. However, it had already been shown in [55] that, even in integrable potentials, it is possible to obtain values close to those given by the wall formula if the particle motion is randomized. In refs. [25, 138], it was also shown that collisions between particles could result in randomization of the particle motion, whose degree depends on the temperature and density of states near the Fermi energy.

In [139], the reduction coefficient of the contribution from the "wall" formula was defined through the measure of chaos in the single-particle motion of nucleons inside a nuclear shape. The measure of chaos (the randomness of nucleon motion) depends on the nuclear shape, *i.e.*, on the collective coordinates. The degree of randomness was found to vary from zero to one during the evolution of a nucleus from the spherical to scission configurations. Thus, the reduction coefficient explicitly depends on deformation, and this dependence is calculated on the basis of the general principles of the chaos theory [140] instead of being introduced as an adjusting constant parameter to reproduce experimental data. The first application of such an approach to describing fission widths, prescission neutron multiplicities, and cross sections for evaporation residues appeared to be reasonably successful, although the calculations were carried out in the one-dimensional model [141].

The systematics of the parameters of fission fragment kinetic energy (mean value of the kinetic energy and its variance) were fairly well reproduced [28, 55, 128] using both the two-body and the one-body mechanisms of nuclear viscosity. However, it was shown [28, 142] that one-body dissipation is preferable in order to describe the prescission neutron multiplicity data. The assumption that the mechanism of nuclear viscosity has the nature of one-body dissipation is physically better justified.

In the present paper we do not consider the results of calculations with two-body viscosity. Our calculations [143, 144] with analysis of intermediate fissility system ^{132}Ce have shown that in case of two-body dissipation one needs to use $\nu_0 0.15 \times 10^{-21}\,\mathrm{MeV\,s\,fm^{-3}}$ to get the best description of experimental data on fission fragment MED parameters, fusion-fission and evaporation residue cross sections, and prescission particles multiplicities. This value is in agreement with previous findings in ref. [145], where the value $\nu_0 0.125 \times 10^{-21}\,\mathrm{MeV\,s\,fm^{-3}}$ has been found to be more suitable for the description of experimental values of n_{pre}, as well as fusion-fission and evaporation residue cross sections. We have to mention here that in ref. [145] this value of ν_0 is considered to give rise to an unrealistically strong two-body viscosity (close to infinite viscosity) and a smaller fission fragment kinetic energy. This latter point occurs also in our study and constitutes an additional reason why we continue our analysis only with the one-body dissipation model.

The reduced friction coefficient $\beta_{q_2q_2} = \gamma_{q_2q_2}/m_{q_2q_2}$ is an important characteristic of the fission process and is frequently used during its analysis. In fig. 5, we show the component $\beta_{q_2q_2}$ calculated using the one-body mechanisms of nuclear viscosity. As our calculations show, this component generally defines the timescale and character of the motion of a fissile nucleus to scission, although the coordinate q_2 is not the pure elongation coordinate. From this figure, it can be seen that the constant values of the k_s coefficient and one obtained from the chaos theory deformation-dependent $k_s(\mathbf{q})$ generate a substantially different behavior of the $\beta_{q_2q_2}$ component. In case of constant k_s the $\beta_{q_2q_2}$ has a decreasing behavior from the local maxima for compact shapes around the ground state to the scission direction. The deformation-dependent $k_s(\mathbf{q})$ on the contrary generate the local minima for the ground state region and demonstrate increase to the scission direction. The similar qualitative behavior was proposed in ref. [146] in order to reproduce a large amount of fission observables in one-dimensional Langevin calculations.

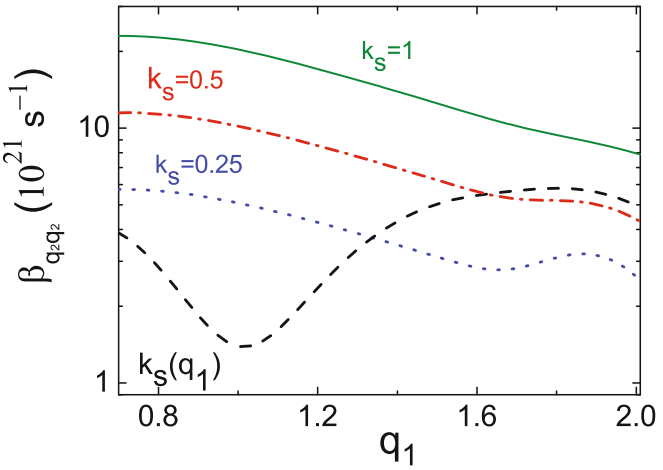

Fig. 5. (Color online) The component $\beta_{q_2q_2} = \gamma_{q_2q_2}/m_{q_2q_2}$ at different k_s options.

An important aspect of studying fusion-fission reactions in terms of the stochastic approach is consideration of the temperature dependence of kinetic coefficients [147]. The different theoretical approaches used to calculate kinetic coefficients apply various approximations and parameters, which, however, are determined with insufficient accuracy. For this reason, the obtained temperature dependencies of the friction tensor differ dramatically. For example, when the wall formula is derived with the approximations used in [55], it predicts a friction coefficient that is almost temperature independent. The expression for the wall formula also can be derived within linear-response theory [25, 134, 138], but, in this case, the temperature dependence of the friction coefficient is such that the friction increases with temperature proportionally to T^2. In turn, the two-body viscosity decreases with temperature in accordance with $1/T^2$ [148]. Experimental studies of the temperature dependence of the friction was performed in refs. [149–151] and it was found that the friction coefficient increases with temperature. A different result was found for the ^{220}Th system by Rubchenya *et al.* [152], on the basis of pre-scission neutron multiplicities: the effective average value of nuclear viscosity decreases with increasing excitation energy, similar to the temperature dependence of the two-body friction. A systematic study

was also carried out by Bhattacharya *et al.* [153]: the values of viscosity coefficient used to reproduce the observed neutron multiplicities should increase with the mass and the excitation energy per nucleon of the composite system.

Different studies both from statistical and dynamical models, provide a contradictory picture of the values of β, which range over an order of magnitude, and rather controversial conclusions on the nature of nuclear dissipation and its dependence on the shape and temperature. Therefore, nuclear studies should analyze more observables in order to impose severe constraints on the model parameters, which can help better understand the physics of the fission process.

The transport coefficients can also be calculated within microscopic approaches [25, 135, 138, 154, 155]. This can help to remove many of the approximations that are inevitably applied in calculations of the transport coefficients within macroscopic models. Nevertheless, performing these calculations within microscopic approaches is complicated. In addition, the transport coefficients obtained in these calculations and their temperature and deformation dependencies hinge on the method used, the set of constants, etc., and tend to differ considerably. Therefore, the transport coefficients most frequently used in dynamic simulation of reactions involving heavy ions are calculated within macroscopic models. Moreover, recently in ref. [156] it was shown that under certain conditions the predictions of Langevin calculations performed with the transport coefficient obtained from microscopic approach and from macroscopic considerations are almost the same.

The friction component for the K coordinate could be determined based on the works of Døssing and Randrup [157, 158]. Later on Lestone and McCalla [114, 115] have shown that in the case of a dinucleus γ_K can be expressed as

$$\gamma_K = \frac{1}{R_N R_{\rm cm}\sqrt{2\pi^3 n_0}}\sqrt{\frac{J_\parallel |J_{\rm eff}| J_R}{J_\perp^3}}\,, \qquad (22)$$

where R_N is the neck radius, $R_{\rm cm}$ is the distance between the centers of mass of the nascent fragments, n_0 is the bulk flux in standard nuclear matter ($0.0263\ \mathrm{MeV\,zs\,fm^{-4}}$) [158], and $J_R = M_0 R_{\rm cm}^2/4$ for a reflection-symmetric shape. In a limiting case $\gamma_K \to 0$ and with an initial K value equal to zero, the present 4D Langevin model is reduced to 3D model [19, 20, 27].

The deformation dependence of the dissipation coefficient γ_K given by (22) should be used with caution, as stated in [115], because eq. (22) was obtained by assuming the nuclear shapes featuring a well-defined neck.

The eq. (22) predicts the values of γ_K quite low, in average around $0.0077\,(\mathrm{MeV\,zs})^{-1/2}$, which is 10 times less than the constant $\gamma_K = 0.077\,(\mathrm{MeV\,zs})^{-1/2}$ value found from the fit of experimental data. Moreover, our recent results [63] demonstrate that constant $\gamma_K \simeq 0.077\,(\mathrm{MeV\,zs})^{-1/2}$ is suitable for heavy nuclei and a larger value of $\gamma_K \simeq 0.2\,(\mathrm{MeV\,zs})^{-1/2}$ is needed for the nuclei with mass $A_{\rm CN} \simeq 200$. This inconsistency of the model from the theoretical point of view and inability of the constant γ_K coefficient to reproduce anisotropy of the fission fragment angular distribution for fissioning nuclei in a wide mass range motivated us to investigate the possible deformation dependence of the γ_K coefficient. The outcome of this investigation is presented in ref. [159].

Using such a different value of γ_K for deformations before the saddle and deformations along the saddle-scission descent the dynamics of the K coordinate tends to the predictions of the transition-state model at the saddle point. As the large values of γ_K at the region of compact shapes assume quick equilibration of the K coordinate to the moment when saddle point shapes will be reached by the fissioning system.

2.5 Statistical description of the compound nucleus decay

When performing dynamic calculations, the statistical model is usually used for description of the light-particle emission, which accompanies fission and competes with it. A combination of the dynamical and statistical models makes it possible to describe theoretically the nuclear decay process, where fission fragments or evaporation residues formed. Such a combination was used for the first time in [13, 14], where the standard Fokker-Planck equation was supplemented with a term describing the continuous-mode emission of light particles. In spite of the fact that, in this study, the authors restricted the analysis to only one collective coordinate and continuous-mode particle emission, they succeeded in reproducing the principal effects produced by the influence of particle emission on the nuclear fission dynamics. Later, discrete particle emission scheme was used in dynamical calculations [160]. Both the continuous [28] and the discrete [19, 20, 29] methods of taking into account particle emission are now widely used.

Within the statistical model, the probability of emission of a certain particle is specified by the nuclear decay width in the corresponding channel. The decay widths are expressed according to the density of nuclear excited states, which, in turn, depends on the excitation energy, angular momentum, compound nucleus deformation, and its nucleonic composition.

As a rule, the expression for the nuclear level density is chosen within the Fermi-gas model and has the following form [161]:

$$\rho(E_{\rm int}, I) = \frac{(2I+1)a(\mathbf{q})}{12}\left(\frac{\hbar^2}{2J_\perp}\right)^{3/2}\frac{\exp\left(2\sqrt{aE_{\rm int}}\right)}{E_{\rm int}^2} \times K_{\rm vib}K_{\rm rot}. \qquad (23)$$

Here, A is the mass number, T is the temperature, $E_{\rm int}$ is the excitation energy, and I is the spin. The values of $K_{\rm vib}$ and $K_{\rm rot}$ (the collective and rotational enhancements

of the level density) are given by the expressions [162]

$$K_{\rm vib} = \exp(0.0555A^{2/3}T^{4/3}),$$
$$K_{\rm rot} = \begin{cases} 1, & \text{for spherical shape,} \\ J_\perp T, & \text{for deformed shape.} \end{cases} \quad (24)$$

The importance of including collective enhancements when calculating the level density, as well as their damping with the increase of the temperature, was noted, for example, in [162–164]. Nevertheless, collective enhancements were seldom taken into account in the Langevin models. In ref. [165], it was shown that the inclusion of collective corrections produces a substantial effect on the calculated observables such as the mean prescission neutron multiplicity and the fission probability. Therefore, it is necessary to pay special emphasis on the accuracy of the level-density calculation when performing such an analysis, as these characteristics are frequently used to obtain information about, for example, nuclear viscosity.

It is well known that, for small nuclear deformations, it is possible to introduce only a vibrational enhancement of the level density, while rotational mode is small due to the symmetry effects. In contrast, for strongly deformed nuclei, it is possible to take into account only a rotational enhancement of the level density, while the vibrational term proves to be 10–100 times lower and is usually disregarded. However, for the intermediate region of deformations, it still remains unclear how to pass from vibrational to rotational enhancements as the deformation increases [162]. In this context, an estimation was made in [162] showed that, for quadrupole deformations with $\beta_2 < 0.15$, it is possible to consider a nucleus to be reasonably close to a spherical deformation and that, correspondingly, there is only vibrational enhancement of the level density in this deformation region. The rotational term sharply increases to the values given by eq. (24) and becomes predominant for the more deformed shapes.

The partial widths of nuclear decay with the emission of a particle j ($j = \mathrm{n, p, d, t,}$ ^{3}He, and α particles) can be expressed [161] through the single-particle level density ρ_j of a residual nucleus and the cross section $\sigma_{\rm inv}^{(j)}$ for the absorption of this particle by the residual nucleus:

$$\Gamma_j = \frac{g_j m_j}{(\pi\hbar)^2} \frac{1}{\rho_0(E_{\rm int}^{(0)})} \int_{V_j}^{E_{\rm int}^{(j)}-B_j} \sigma_{\rm inv}^{(j)}(E)\rho_j \times \left(E_{\rm int}^{(j)} - B_j - E\right) E\mathrm{d}E, \quad (25)$$

where g_j, m_j, V_j, B_j are the spin factor, the mass, the Coulomb barrier, and the binding energy of the j-particle, respectively, and $E_{\rm int}^{(0)}$, $E_{\rm int}^{(j)}$ are the internal excitation energy of the initial and residual nuclei.

The radiation widths of γ-quanta emission are calculated from the equation

$$\Gamma_\gamma = \frac{1}{(\pi\hbar c)^2} \frac{1}{\rho_0(E_{\rm int}^{(0)})} \int_0^{E_{\rm int}^{(0)}} \sigma_\gamma(E)\rho_\gamma \left(E_{\rm int}^{(0)} - E\right) E^2\mathrm{d}E, \quad (26)$$

where $\sigma_\gamma(E)$ is the inverse cross section for absorption of the j-particle or γ-quanta with kinetic energy E by the residual nucleus. However, it should be noted that, for a correct description of the particle emission when numerically simulating fission within the Langevin models, it is necessary to take into account the deformation dependence of statistical-model parameters such as the emission barriers, binding energies of particles, and cross sections for inverse processes [21,22,166]. This necessity is caused by the fact that a compound nucleus goes through ground state to strongly necked in shapes, substantially different from spherical.

The statistical model can be used in dynamic calculations related to description of not only light-particle emission but also nuclear fission. With a decrease in the fissility parameter and/or the excitation energy of a compound nucleus, the mean fission time very quickly increases and the fissility decreases. Therefore, due to the long calculation time needed, the use of a purely dynamic approach becomes impossible for fissile systems with low fissility. We instead switch to the statistical branch, where not only light-particle evaporation but also fission width is calculated. This approach was proposed for the first time in [160]. Such an approach can be used if the following conditions are met: i) a system is in the ground-state region before the ridge, ii) the time of calculations exceeds a certain time $t > t_{\rm stat}$, and iii) the ratio between the nuclear temperature and a fission barrier is $T/B_f < 0.2$. The parameter $t_{\rm stat}$ is selected so that it is certain to satisfy the condition that the particle flux through the fission barrier attains its quasisteady value.

Within the statistical branch of calculations, the fission width can be found in the multidimensional case [9]. Because, as was mentioned above, a nucleus is a thermodynamic system, the quasistationary fission width should be calculated using thermodynamic potentials. Below, we give an expression for the quasistationary value of the fission width in the case of the Helmholtz free-energy potential

$$\Gamma_f = \omega_K \left(\frac{\det \Omega_{ij}^2(\mathbf{q}_{\rm gs})}{\det|\Omega_{ij}^2(\mathbf{q}_{\rm sd})|}\right)^{\frac{1}{2}} \exp\left(-\left(F(\mathbf{q}_{\rm sd}) - F(\mathbf{q}_{\rm gs})\right)/T\right). \quad (27)$$

Here

$$\Omega_{ij}^2(\mathbf{q}_{\rm gs}) = \mu_{ik}(\mathbf{q}_{\rm gs}) \left(\frac{\partial^2 F(\mathbf{q})}{\partial q_k \partial q_j}\right)_{\mathbf{q}=\mathbf{q}_{\rm gs}}, \quad (28)$$

$$\Omega_{ij}^2(\mathbf{q}_{\rm sd}) = \mu_{ik}(\mathbf{q}_{\rm sd}) \left(\frac{\partial^2 F(\mathbf{q})}{\partial q_k \partial q_j}\right)_{\mathbf{q}=\mathbf{q}_{\rm sd}} \quad (29)$$

and ω_K is the Kramers frequency, which is a unique positive root of the equation

$$\det\left(E\left(\frac{2\pi\omega_K}{\hbar}\right)^2 + \frac{2\pi\omega_K}{\hbar}\mu_{ik}(\mathbf{q}_{\rm sd})\gamma_{kj}(\mathbf{q}_{\rm sd}) + \Omega_{ij}^2(\mathbf{q}_{\rm sd})\right) = 0. \quad (30)$$

Here, E is the unit matrix, and the coordinates $\mathbf{q}_{\rm sd}$ and $\mathbf{q}_{\rm gs}$ determine the saddle-point and ground-state positions, respectively. In the statistical branch of the model, the probability of the fissioning system deexcitation by the emission of particles or fission is calculated using the Monte Carlo method, with the decay probabilities proportional to the partial decay widths Γ_j and Γ_f. If the system has to go to fission, we switch back from the statistical branch to the dynamic simulation, but, in this case, the calculation proceeds from the ridge surface and the return of a nucleus to the ground-state region is blocked.

It is necessary to note that the choice of the Helmholtz free-energy potential $F(\mathbf{q})$ for calculating the quasistationary fission width is ambiguous, because entropy could be used instead of $F(\mathbf{q})$ and eq. (27) could have a different form. Further discussion of this question and results of dynamic calculations using the entropy can be found, for example, in [29]. However, in our opinion, the use of the entropy for calculating the fission width is not the best solution, since only the behavior of the potential energy near the ground state and at the saddle point is taken into account in eq. (27) and not the potential-energy landscape. In this sense, a more consistent method of fission-width calculation is based on the concept of a mean first passage time [167,168] or the alternative concept of mean last passage time [169]. Such a method has been successfully applied for a long time in other fields of physics [170]. Nevertheless, until now, it has been developed only for the non general case of system motion in an overdamped mode. Therefore, the development and improvement of this method is currently one of the important problems to be solved in fission physics.

3 Mass, charge and TKE distributions

3.1 Two-dimensional MEDs of fission fragments

The mass, charge and total kinetic energy (TKE) distributions of the fission fragments, prescission and post scission particle multiplicities together with the evaporation residues (ER) and fusion-fission (FF) cross sections has been widely investigated in the theoretical and experimental studies.

Mass-energy distributions (MEDs) of fission fragments are usually used as a source of information about fission dynamics. They were fully investigated for the first time by Nix and Swiatecki in their zero-viscosity dynamic model [93, 171]. Within the framework of this model, the authors succeeded in describing MED parameters for fission fragments of light fissile nuclei with fissility $Z^2/A \leq 31$. The zero-viscosity model [93, 171] predicts the values of the variances of mass and energy distributions lower than experimental data for heavier fissioning nuclei.

Considerable success was attained in relation to description of the MED characteristics of fission fragments and understanding of the role of nuclear dissipation within the diffusion model based on the multidimensional Fokker-Planck equation for the distribution function of collective variables [11, 12, 172]. The important achievement of the diffusion model is the possibility to explain the strong increase in the variances of mass and energy distributions that is observed experimentally with increase of the Z^2/A parameter. However, the model still has a number of deficiencies. Its main drawback consists in the fact that it uses approximate methods for solving the Fokker-Planck equation. In ref. [173], the variances of energy distributions calculated from the diffusion and two-dimensional Langevin models were compared. As a result, the uncertainty, which is due to the approximate nature of the methods used for solving the Fokker-Planck equation, was estimated as being equal to about 30%. Another important characteristic of the fission process, which was not taken into account, is the emission of prescission light particles. The evaporation of prescission particles not only changes the A and Z of the compound nucleus, but also significantly decreases the excitation energy of the fissioning nucleus. In turn, this strongly affects the evolution of the collective degrees of freedom, and finally influences the calculated observables.

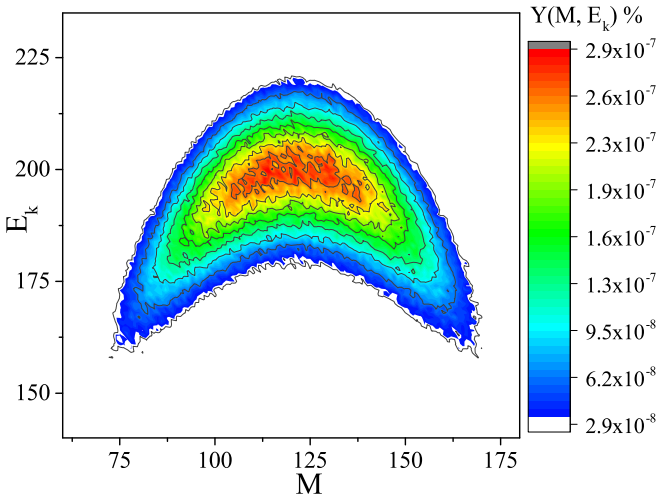

Fig. 6. (Color online) Fission fragment mass-energy distribution for the reaction ^{16}O(128 MeV) + ^{232}Th $\rightarrow$ ^{248}Cf ($E^* = 83$ MeV).

The stochastic approach based on the set of 4D Langevin equations enables to study the process of formation of the fission fragment MEDs in detail, presenting at every time step the exact value for each physical quantity. The method used for the calculation of the observed characteristics applies the concept of a rupture surface. It is assumed that the distribution of the collective variables and their conjugate momenta are formed during the whole evolution of the fissioning system from a ground state to a certain scission configuration at which an instantaneous rupture of the nuclear neck takes place without any change in elongation. The further evolution of the collective variables produces only a minor effect on the formed mass and kinetic energy distributions of the reaction products. In the present calculation it was considered that the total kinetic energy E_K of fission fragments is the sum of the Coulomb repulsion energy V_C, the nuclear attraction energy V_n of the fission fragments, the rotational energy $V_{\rm rot}$, and the kinetic energy of their relative motion (the prescission kinetic energy $E_{\rm ps}$).

All the terms in this sum ($E_K = V_C + V_n + E_{\rm ps} + V_{\rm rot}$) were calculated at the scission surface. The calculated formulas for the V_C and V_n in the FRLDM could be found in ref. [174], while exact relations for $V_{\rm rot}$ are discussed, for example, in [49]. The calculated fission fragment MED for the ^{248}Cf compound nucleus is shown in fig. 6. It can be seen that the shape of the fission fragment MED qualitatively corresponds to the experimentally observed results. Usually the quantitative comparison between the calculated results and experimental data are performed in terms of the parameters of one-dimensional mass (or charge) and kinetic energy distributions of fission fragments.

3.2 Mass distribution of fission fragments

One-dimensional mass and kinetic energy distributions can be obtained by integration of the two-dimensional MED over the corresponding parameter. In case of heavy fission nuclei at high excitation energy the mass and energy distributions are characterized by single-peak curves which are usually approximated by Gaussian curves with average values and variances, which are the principal characteristics of these distributions. In case of light fissioning nuclei which are below the Businaro-Gallone (BG) point the mass distribution is characterized by the U-like shape of the mass distribution. The Bussinaro-Gallone point [175] indicates the transition between the mass distributions for nuclei which prefarably fission in mass symmetric fragments ("W" shape) and those which nascent fragments differ in mass ("U" shape). The BG point depends on the fissility of the compound nucleus but in second order also on its spin and excitation energy. The discussion of the details are presented in [176].

The lowering of excitation energy will result in manifestation of shell effects in the potential energy surface, which finally could be seen in structured mass distribution of fission fragments.

A very important parameter which influence the shape of the mass/charge distribution is the viscosity reduction factor k_s appeared in eq. (21). Its influence on the friction tensor is shown in fig. 5. In the present 4D Langevin code there is possibility to use one-body or two-body dissipation models with constant reduction coefficient k_s and also the chaos weighted viscosity parameters described in details in [61]. The dissimilarity between two treatments of the dissipation reduction parameters for the compound nucleus ^{250}Cf at $E^\star = 45$ MeV is shown in fig. 7. The saddle point for heavy nuclei ^{250}Cf is for rather small elongation and the path from saddle to scission is quite long, thus for $k_s = 0.5$ the FF charge distribution is almost identical for the chaos-weighted ($k_s(q_1)$) reduction factor. This is a consequence of the mass tensor behavior presented in fig. 5 where curves for $\beta_{q_2q_2}$ ($k_s = 0.5$) cover with $\beta_{q_2q_2}$ ($k_s(q_1)$) for elongation $q_1 \geq 1.6$ when for full viscosity there is substantial difference. Similar behavior is observed in other mass regions.

As is shown by the performed calculations, the variances of the mass and energy distributions are sensitive

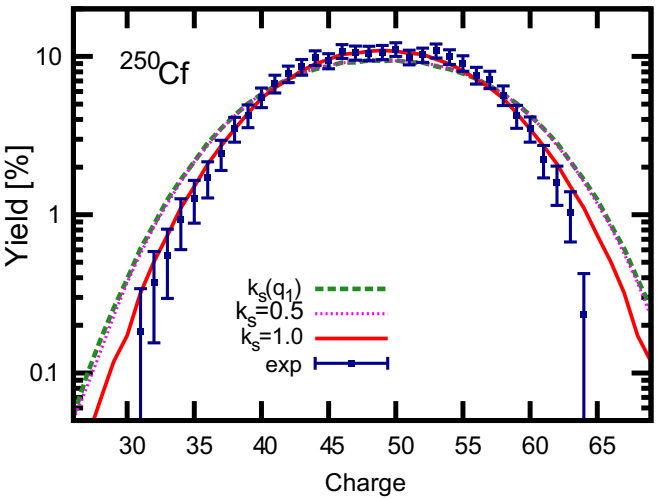

Fig. 7. (Color online) Fission Fragment charge distribution for binary decay of ^{250}Cf at $E^\star = 45$ MeV produced in reaction ^{238}U(6.1 AMeV) + ^{12}C: experimental data [177] (full squares) are compared to calculations obtained with the "wall-and-window" ($k_s = 1$) (full red line), reduced "wall-and-window" ($k_s = 0.5$) (dotted pink line) and the chaos-weighted ($k_s(q_1)$) (dashed green line) friction.

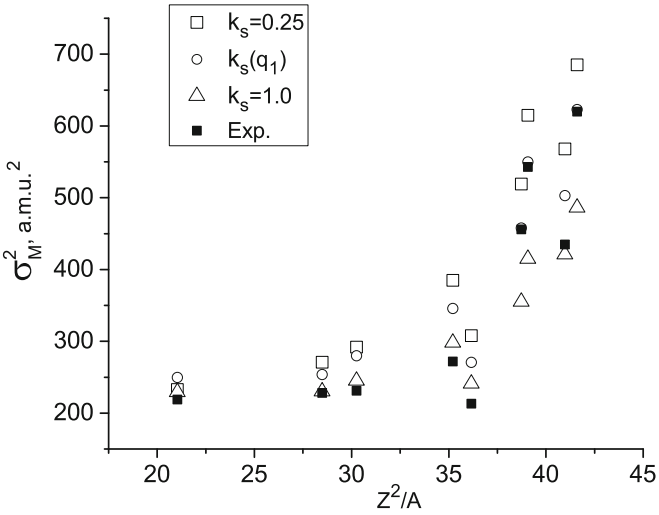

Fig. 8. Variance of the fission fragment mass distribution for different fissioning heavy nuclei at different k_s values. The results for the following reactions are presented: ^{93}Nb + ^{12}C → ^{105}Ag ($E_{\rm lab}$ = 1060 MeV); ^{18}O + ^{144}Sm → ^{162}Yb ($E_{\rm lab}$ = 158.8 MeV); ^{18}O + ^{154}Sm → ^{172}Yb ($E_{\rm lab}$ = 158.8 MeV); ^{18}O+^{197}Au → ^{215}Fr ($E_{\rm lab}$ = 158.4 MeV); ^{16}O+^{208}Pb → ^{224}Th ($E_{\rm lab}$ = 108 MeV); ^{16}O + ^{232}Th → ^{248}Cf ($E_{\rm lab}$ = 128 MeV); ^{18}O + ^{238}U → ^{256}Fm ($E_{\rm lab}$ = 159 MeV); ^{20}Ne^{240}Pu → ^{260}Rf ($E_{\rm lab}$ = 174 MeV); ^{18}O + ^{246}Cm → ^{264}Rf ($E_{\rm lab}$ = 102.5 MeV).

to the viscosity used in the theoretical calculations, details of PES calculations, parameters taken for description of particles emission and the character of the descent of trajectories from the saddle to the scission surface. In fig. 8, we show the variance of the mass distribution as a function of the parameter Z^2/A. Following this figure, it is possible to reproduce the sharp increase observed in the

experimental values in the heavy-nuclei range within the stochastic approach and using the modified variant of the one-body viscosity. The explanation for the increase of the fission fragment mass distribution widths as k_s decreases is as follows: on the one hand, the rigidity of the potential energy with respect to the mass-asymmetry coordinate during the descent from the saddle to the scission steadily increases; correspondingly, the mass distribution also narrows. On the other hand, the system keeps a "memory" of the former wider mass distribution because the descent process takes a finite time, which is lower than the relaxation time of the mass mode. Thus, the faster the descent, the larger the "stored" variance. The rate of descent generally depends on the viscosity, whose value depends on the coefficient k_s. A detailed discussion of this mechanism of formation of the mass distribution can be found in [11].

The results of the dynamical calculations based on the 4D Langevin model demonstrate the advantage of such approach, because the 4D dynamical model allows consistent calculations of fission fragments MED, angular distribution of fission fragments, and prescission particle multiplicities. The calculations performed in refs. [61,63] have shown that the 4D model could describe the fission fragment MED parameters and prescission particles multiplicities for heavy nuclei using almost the same dissipation strength, which is not possible within the 3D calculations [27]. We performed calculations for several heavy fissioning systems, where the 3D Langevin calculations [19,20] fail to reproduce simultaneously the prescission neutron multiplicities and the width of fission fragments mass and kinetic energy distributions. Reproduction of MED parameters in the 3D calculations required small values of $k_s \simeq 0.1$, whereas $k_s \geq 1$ values are needed to reproduce prescission neutron multiplicities [19]. In the 4D calculations the consistent description of MED parameters and the $\langle n_{\rm pre}\rangle$ could be obtained with much closer k_s values. In fig. 9 we present the prescission neutron multiplicity of the fissioning compound nuclei obtained in 4D Langevin calculations, for the same nuclei as in fig. 8. As x-axis we choose initial temperature multiplied by squared isospin in order to present the $n_{\rm pre}$ values in a more systematized way, as the $n_{\rm pre}$ increases with the increase of initial temperature and isospin of the fissioning compound nucleus.

We obtain around 10% increase of $\langle n_{\rm pre}\rangle$ and at the same time around 80% increase of σ_M^2 in comparison with 3D, as a result of the dynamical calculations with non-zero K values, which increase fission barrier heights, and decrease the stiffness of the nucleus with respect to mass-asymmetry deformations. Thus, for very heavy nuclei $Z^2/A > 38$ the experimental $\langle n_{\rm pre}\rangle$ values could be reproduced with k_s around 1.0, or with deformation dependent $k_s(q_1)$. At the same time these large k_s values also allow to have a wide mass distribution. For lighter nuclei $35 < Z^2/A < 38$ the experimental $\langle n_{\rm pre}\rangle$ values could already be reproduced with $k_s(q_1)$. Such k_s values allow to obtain the variance of mass distribution σ_M^2 in the calculations, which is close to the experimental one (the difference between experimental and calculated σ_M^2 values does not exceed 30%). Considering the deformation-dependent $k_s(q_1)$ obtained from the chaos-weighted wall formula one can see that these calculations predict larger $\langle n_{\rm pre}\rangle$ values compared to that with $k_s = 0.25$. This is due to the enhanced emission during the descend from saddle to scission point, where $k_s(q_1) > 0.25$.

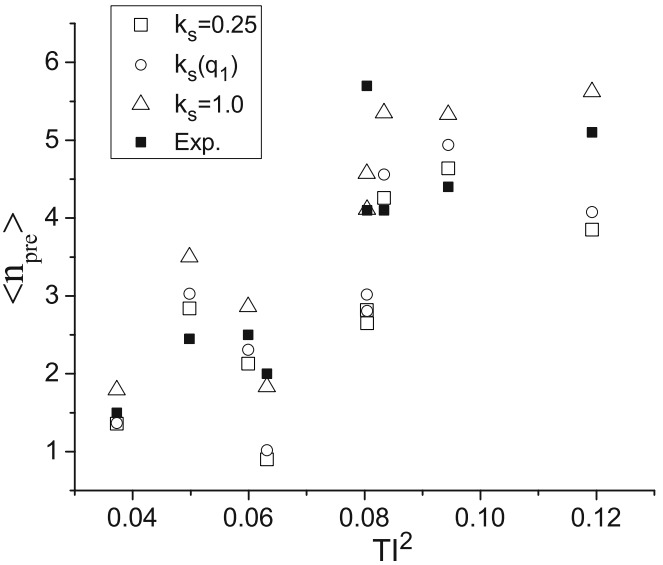

Fig. 9. Prescission neutron multiplicity for different fissioning heavy nuclei at different k_s values as a function of initial temperature T multiplied by squared isospin ($I = (N - Z)/A$). The reactions are the same as in fig. 8.

For the lighter systems the mean prescission neutron multiplicity could be reproduced with lower k_s values. The calculations with $k_s = 0.25$ are already very close to the experimental data. At the same time the calculated σ_M^2 values exceed the experimental data by about 20%, and the best reproduction of σ_M^2 could be obtained with $k_s = 1$. Thus, the calculations with $k_s(q_1)$ provide a reasonable balance ensuring satisfactory reproduction of both σ_M^2 and $\langle n_{\rm pre}\rangle$ experimental values with a reasonable quality. A detailed investigation of this effect from static and dynamical point of view is presented in refs. [61,63]. More subtle tuning of the parameters of the statistical model [144] that governs the particle evaporation, for example, the level-density parameter a, could also provide a better reproduction of prescission particle multiplicities.

Powerful microscopic calculations of fission dynamics became possible during the last decade [178,179]. Nevertheless, a fully microscopic model is still challenging to implement. Huge computational resources are required, and existing models do not reach the potential of systematic and widespread comparison with experiment yet. Even current large-scale shell-model studies are not able to provide a fully-microscopic and global description of nuclear structure in heavy/deformed nuclei, due to the dimension of the Hamiltonian matrix. Also, the extension and application of microscopic models becomes difficult with increasing excitation energy. On the contrary, classical approaches based on the macroscopic diffusion equation can readily be implemented, and provide a large variety of observables for comparison with experiment. In

this context, the combination of macroscopic and microscopic methods developed by Strutinsky [92] showed to be both pertinent and powerful; it attracted much attention during the last decades, being rapidly growing field of research, as it allows to avoid computer-consuming fully microscopic calculations. At the same time, calculations within the shell correction method are rather simple, in contrast to pure microscopic calculations. Recent elaborate dynamical investigations demonstrated that the macroscopic-microscopic method provides the possibility to consider a large variety of nuclear shapes and predict many experimental observables [73,180,181].

The fission fragment mass distribution has been calculated at low excitation energies in the framework of Langevin dynamics. In refs. [21, 22], the results of two-dimensional Langevin calculations of the mass distribution were presented for the ^{227}Pa compound nucleus at low excitation energies. Moreover, the shell corrections were taken into account when calculating the potential energy, level-density parameter, and the deformation dependence of the penetrability coefficient in determining the particle-emission widths. In these studies, multimodal fission was obtained in theoretical calculations. In addition, the mass-distribution shape appeared to be very sensitive to the nuclear viscosity (to the value of the coefficient k_s). Therefore, the authors of [21, 22] concluded that the mass-distribution parameters are more sensitive to viscosity at low excitation energies than to prescission particle multiplicity. In addition, the authors of [21, 22] stressed the importance of taking into account the temperature dependence of the nuclear viscosity.

3.3 Energy distribution of fission fragments

The total kinetic energy-distribution parameters have been investigated for various nuclei in a large number of experimental [182–184] and theoretical [107,173,185,186] studies. From an analysis of the available experimental data, it was found that $\langle E_K \rangle$ is virtually independent of both angular momentum and an excitation energy [182]. In addition, it was shown in [182, 183] that $\langle E_K \rangle$ is not a linear function of the parameter $Z^2/A^{1/3}$, as follows from the Viola systematics [187], and has a break at $Z^2/A^{1/3} \simeq 900$. It was proven that $\langle E_K \rangle$ could be approximated by the two different linear functions. The fracture is observed if only the results on strongly heated nuclei are selected from the experimental data and low-energy and spontaneous fission strongly influenced by shell effects, as well as quasi-fission reactions, are excluded. The systematics proposed in [182, 183] has the form

$$\langle E_K \rangle = \begin{cases} 0.104 Z^2/A^{1/3} + 24.3\,\mathrm{MeV} & (Z^2/A^{1/3} > 900); \\ 0.131 Z^2/A^{1/3}\,\mathrm{MeV} & (Z^2/A^{1/3} \leq 900). \end{cases} \quad (31)$$

According to the Viola systematics [187], $\langle E_K \rangle$ is given by the expression

$$\langle E_K \rangle = 0.1189 Z^2/A^{1/3} + 7.3\,\mathrm{MeV}. \quad (32)$$

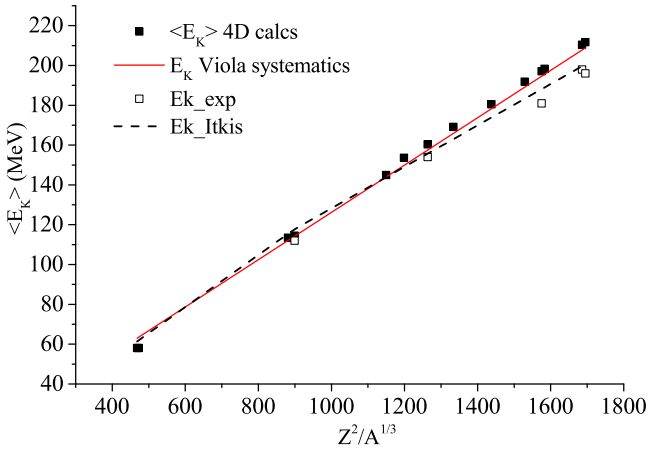

Fig. 10. (Color online) The fission fragment mean kinetic energy $\langle E_K \rangle$ as a function of $Z^2/A^{1/3}$. The closed squares are the results of the 4D calculation obtained with $k_s = 0.25$ and $\gamma_K = 0.077\,(\mathrm{MeV\,zs})^{-1/2}$. The solid red line is the Viola systematics [187]. The black dashed curve is the systematics from [182, 183]. The reactions are the same as in fig. 8.

The mean kinetic energy of fission fragments obtained in 4D Langevin calculations with the one-body viscosity as a function of the fissility parameter Z^2/A is presented in fig. 10. From fig. 10, it can be seen that the calculated values of $\langle E_K \rangle$ agree well with the experimental data and lie closer to the Viola systematics. It is necessary to emphasize that the calculated $\langle E_K \rangle$ values [20,188] decrease with the reduction coefficient k_s, as the mean scission deformation of the fissioning compound nuclei increases a little bit with decrease of the k_s. A similar result was obtained in two-dimensional calculations [56] with a neck radius equal to zero taken as the rupture condition. In [56], the best description of the experimental data was attained with k_s approximately equal to 0.3. The values obtained in 3D and 4D calculations of $\langle E_K \rangle$ do not appear to be as sensitive to k_s; therefore, it is difficult to make conclusions about the value of viscosity based on them. The fact that $\langle E_K \rangle$ actually ceases to depend on k_s is associated with the inclusion of the evolution of a nucleus in the mass asymmetry coordinate of the three-dimensional calculations, in contrast to that of the two-dimensional calculations [56]. Indeed, in paper [28] the influence of the mass-asymmetry coordinate on the $\langle E_K \rangle$ is quantitatively demonstrated.

The results [189] of dynamical calculations of $\langle E_K \rangle$ show that the mean distance between the centers of mass of nascent fragments at the scission configuration increases linearly with the parameter $Z^2/A^{1/3}$. This distance changes approximately from 2.35 R_0 for ^{119}Xe to 2.6 R_0 for ^{256}Fm. In spite of this increase in mean distance between future fragments at scission, the linear dependence of $\langle E_K \rangle$ on the parameter $Z^2/A^{1/3}$ remains approximately valid over a wide range of the Coulomb parameter $Z^2/A^{1/3}$.

Calculated values of $\sigma^2_{E_K}$ for different k_s are shown in fig. 11. It can be seen that the calculations in the 4D Langevin dynamics with $k_s \simeq 0.25$ or $k_s(q_1)$ make it possible to reproduce qualitatively the increase of the variances

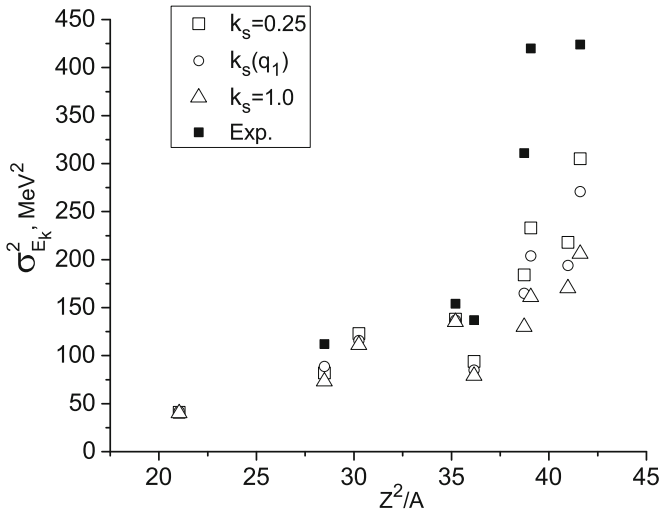

Fig. 11. Variance of the fission fragment kinetic energy distribution for different fissioning heavy nuclei at different k_s values. The reactions are the same as in fig. 8.

$\sigma^2_{E_K}$ with Z^2/A, as it is obtained in experimental studies. The inclusion of the mass-asymmetry collective coordinate results in an increase of the calculated $\sigma^2_{E_K}$ values in comparison with the calculations performed in 2D Langevin models [185] for symmetric fission. However, the 4D calculations fails to reproduce quantitatively the slope of the increase of experimental data, especially for very heavy fissioning nuclei.

The present 4D calculations as well as previous calculations in 3D model [19,20] substantially underestimate the experimental $\sigma^2_{E_K}$ values. As we discussed [27,61,121], the main reason of this underestimation is the insufficient flexibility of the (c, h, α)-parametrization, which cannot generate the elongated shapes with a thick and long cylindrical neck. The inclusion of the K coordinate can only a little improve theoretical description of $\sigma^2_{E_K}$ in 4D calculations in comparison with 3D one. As examples of the nuclear shape parameterizations, which can improve the description of the $\sigma^2_{E_K}$ in multidimensional Langevin calculations, we can mention the ones used in refs. [73, 95, 190, 191]. The consideration of post-scission dynamic can also influence on the parameters of kinetic energy distribution.

3.4 MED dependent on the PES choice

The estimation of the shape evolution of the hot, rotating nucleus in its path to fission allows accurate studies of the potential energy approaches as the fission fragment mass/charge distribution are very sensitive on the choice of the potential energy (PES) model used in calculation. The final MED is governed by the energy space in which the nucleus is moving. Each macroscopic model has the parameters fitted to known observables. Part of them are fitted to the ground state energies, means measured nuclear masses, others are adjusted also to the experimentally extracted fission barrier heights. The statistical codes take into account usually this two observables thus the choice of the potential energy landscape model is not so crucial. The dynamical approaches are the best choice to verify the ability of the phenomenological models to describe the reaction phenomena such as fission or evaporation.

The move of the nucleus through the PES space as it was described in sect. 2, allows to trace step by step the fine details of the energy space generated by various models. As the Monte Carlo method is applied to randomize trajectories, not only ground-state and saddle points plays a role but also all saddles and scission points are studied. As it was already mentioned the choice of the collective coordinates is crucial to correctly describe the reality. This is not only the problem of computing time but also compatibility between the nuclear shape parametrization and the energy model. The stiffness of the landscapes obtained with two various energy formulas in this same deformation plane could differ dramatically and this is visible in the MED shape.

The influence of the potential energy surface on the fission dynamics has been investigated in few articles, see for example refs. [62, 192] and references therein. The potential energy surface determines the fission barrier height, and, as a result, the fission rate. The sensitivity of the potential energy on the collective coordinates like neck and mass-asymmetry of compound nucleus is reflected in the mass and energy distributions of fission fragments. In the present study the two widely used models for potential energy are investigated. There are finite range liquid drop model (FRLDM) [44,112] with a recent modifications (FRLDM+W) [73, 81] and Lublin-Strasbourg drop (LSD) approach [193] with congruence energy (LSD+C.) [194].

The FRLDM takes into account the diffusive density profile of nuclear surface and includes the deformation-dependent nuclear, rotational and Coulomb parts [112, 195]. The inclusion of the deformation dependent Wigner plus A^0 macroscopic energies in the FRLDM [73] allows to decrease substantially the large discontinuities that appears in the potential energy at the transition point between single and separated systems [81]. The parameters of FRLDM with deformation-dependent Wigner plus A^0 terms obtained in ref. [81] have been found from the fit of 1989 nuclear masses and 31 fission barriers for the nuclei with $16.5 < Z^2/A < 38.1$.

The LSD model is one of the newest versions of the drop formula which takes into account the deformation dependence of the surface, curvature, rotational and Coulomb parts. The parameters of this approach have been fitted to 2766 nuclear masses with the rms deviation of the binding energies $\langle \delta B \rangle = 0.698\,\mathrm{MeV}$ and it reproduced the fission barrier heights with the rms deviation $\langle \delta V_B \rangle = 3.56\,\mathrm{MeV}$ [193] for the nuclei with $15 < Z^2/A < 38$.

The existing expressions for the shape-dependent Wigner plus A^0 terms in FRLDM and the congruence energy in LSD model, are widely used in calculations of static properties of nuclei [81, 190, 193] and dynamical modeling [73, 80, 192]. They are the subject of the [62] where apart of a study the sensitivity of MED parameters on

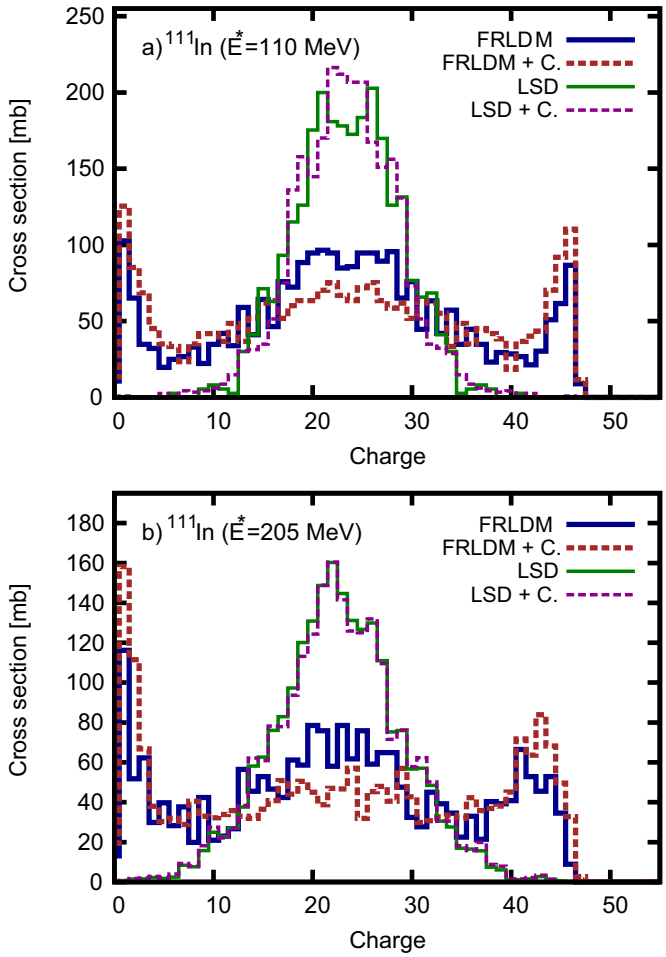

Fig. 12. (Color online) Calculated fission fragment charge distribution for the reaction ^{84}Kr + ^{27}Al → ^{111}In at 5.9 MeV/nucleon (a) and 10.6 MeV/nucleon (b) bombarding energy, as obtained for various PES variants: FRLDM without (blue dotted) and with (red dashed) deformation-dependent Wigner term, LSD without (pink full) and with (green dash-dotted) deformation-dependent congruence term.

the choice of the PES model, also multiplicities of prescission light particles, obtained from dynamical calculations with various macroscopic approaches, are discussed.

The phenomenological potential for the rotating nucleus contains also the rotational part. The rigid body model has been applied to calculate the rotational energy with eq. (15). With increasing the angular momentum, the fission barrier lowers, thus the fission is more probable. The K coordinate behaves in the opposite way as it was shown in figs. 1 and 2 of [61]. The lowest barrier is for $K = 0$ and it increases with K value. The rotational energy depends on the nuclear deformation by moments of inertia. The influence of the rotation on PES is well visible in medium mass nuclei, which can sustain up to very high spins (even around 100 $\hbar$). The heavier nuclei undergo fission more easily so the effect of rotation is less pronounced.

The main goal of the PES investigation was a verification of the newest models and its ingredients by applying the full Langevin calculation on top of it for various compound nucleus mass regions and excitation energies. The crucial point was discovering the nuclear mass range and also physical observables sensitive on changing the PES model.

Below there are series of figures obtained for various compound nuclei. The differences between PES models have been shown for few cases in [62, 192, 196]. The influence of the PES on the mean multiplicities of the emitted particles was investigated in [62, 197] for reactions ^{84}Kr + ^{27}Al at beam energy 5.9 and 10.6 MeV/nucleon thus presently the attention will be focused on the MED distributions.

Figure 12 allows to observe the evolution of the mass distribution for various PES models for the reaction ^{84}Kr + ^{27}Al at 5.9 MeV/nucleon, (a) and 10.6 MeV/nucleon (b) beam energies. As it was previously mentioned for the mass distribution of this reactions [62], the shape of the MED distribution is mainly governed by the PES: flat energy maps in case of FRLDM or FRLDM+C. provide mostly asymmetric fission. A steep LSD and LSD+C. energy landscapes dependence on mass-asymmetry coordinate bring the symmetric division of compound nuclei more pronounced. Such a behavior was noticed also earlier in reaction ^{78}Kr + ^{40}Ca → ^{118}Ba [192]. Despite the shape of the PES for different macroscopic approaches, the fission barrier heights for the FRLDM+C. and LSD+C. have similar values thus in the statistical codes, which are based mainly on these variables, the results are very close to each other.

The comparison of the full distribution of the detected species containing the fission fragments is shown in fig. 13. The difference between experimental and theoretical cross section for charges more than 40 is due to evaporation

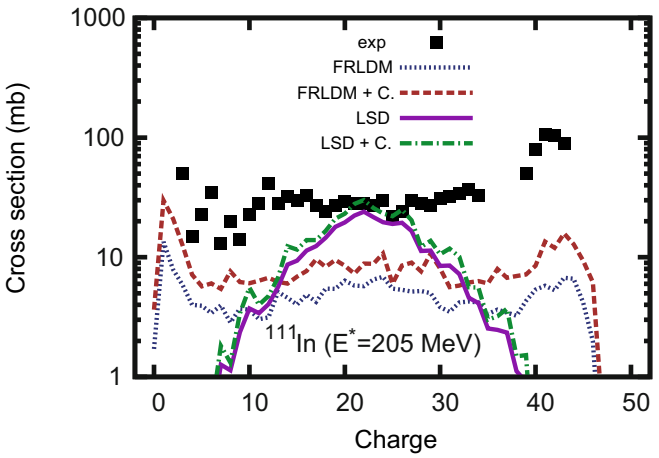

Fig. 13. (Color online) Fission Fragment charge cross-section distribution for the reaction ^{84}Kr + ^{27}Al → ^{111}In at 10.6 MeV/nucleon. The data [198] (black squares) are compared to predictions by various model variants: FRLDM without (blue dotted) and with (red dashed) deformation-dependent Wigner term, LSD without (pink full) and with (green dash-dotted) deformation-dependent congruence term. Experimental error bars are not shown for clarity.

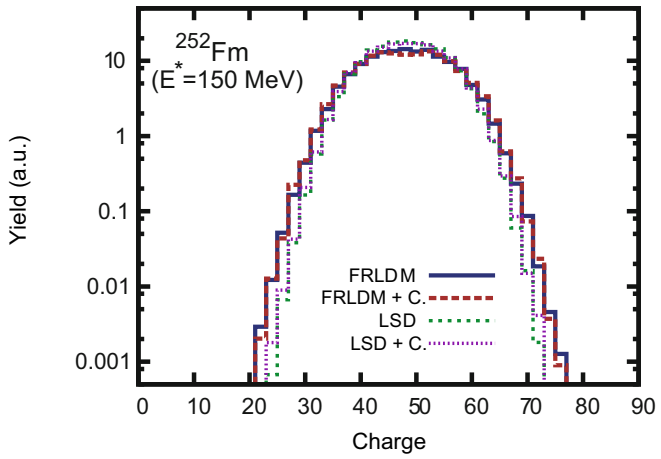

Fig. 14. Fission fragment charge distribution in the reaction $^{20}\mathrm{Ne} + {}^{232}\mathrm{Th} \rightarrow {}^{252}\mathrm{Fm}$ for beam energy 1.25 AMeV.

residues included in measured data as it was shown in [62] fig. 7. Comparison of this two plots brings the conclusion that the PES is more important for the fission channel than in evaporation part.

Figure 14 shows the charge distribution for reaction $^{20}\mathrm{Ne} + {}^{232}\mathrm{Th} \rightarrow {}^{252}\mathrm{Fm}$ with beam energy 1.25 AMeV [199]. The choice of the mass range of the compound nucleus is crucial for effective investigation of the PES dependence of fission-driving observables. The huge difference in the mass/charge distribution noticed in medium mass nuclei such as ^{111}In are almost invisible for heavy and super-heavy systems. The explanation comes directly from the shape of the PES as it was discussed in [196]. The energy maps calculated for heavy and super-heavy nuclei with various macroscopic approaches are much more consistent than for the medium mass compound nuclei.

The excitation energy of the compound nucleus decides mainly about the number of particles evaporated during the motion to fission, thus in fig. 15 for the reaction $^{22}\mathrm{Ne} + {}^{238}\mathrm{U} \rightarrow {}^{260}\mathrm{No}$ for beam energy 6 AMeV and 7.4 AMeV [200] we show a comparison between results obtained with FRLDM and LSD potential energy models. Although the system is very heavy, the difference in the widths of the distribution is slightly visible. This behavior is hardly dependent on the excitation energy of the system.

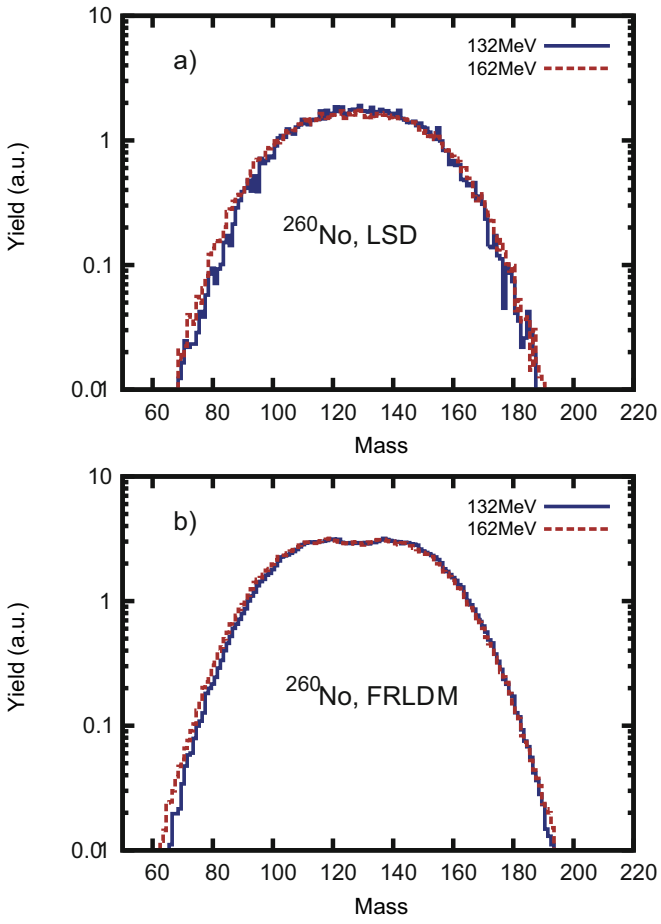

Fig. 15. Fission fragment mass distribution in the reaction $^{22}\mathrm{Ne} + {}^{238}\mathrm{U} \rightarrow {}^{260}\mathrm{No}$ for beam energies: 132 MeV and 162 MeV. The calculation are done with LSD+C. model (a) and FRLDM+C. (b).

4 Angular distribution of fission fragments

4.1 Transition-state model

Until the past decade the standard transition-state model [201,202] is conventionally used in theoretical analysis of the data on angular distribution of fission fragments. The essence of this model consists in the assumption that there is a certain chosen (transition) configuration of a fissile system that determines the angular distribution of the fission fragments. Thus, there are two limiting assumptions on the position of the transition state and, correspondingly two variants of the transition-state model: the saddle-point transition-state (SPTS) model and the scission-point transition-state (SCTS) model.

The SPTS model uses the following assumptions: i) the mean time of stay of a nucleus in the saddle-point region is sufficiently larger than a characteristic time of equilibration of K mode. In other words the time τ_{gs} of the motion of the system from the ground state to the saddle point is much longer than the relaxation time of the K degree of freedom ($\tau_{\mathrm{gs}} \gg \tau_K$). ii) The mean time of descent of a nucleus from the saddle to scission is short in comparison with τ_K. In this case the K distribution is formed at the saddle point and stays approximately the same. iii) The K distribution $P(K)$ is determined by the factor $\exp(-E_{\mathrm{rot}}/T)$ [203], and E_{rot} is given by eq. (15).

Analyzing angular distributions, one usually assumes that fission fragments fly apart along the symmetry axis of the nucleus. In that case the angular distribution is determined by the following three numbers: I, K and M. Here, I is the total angular momentum of the compound nucleus, K is the projection of the total angular momentum onto the symmetry axis of the nucleus and M is the projection of the total angular momentum onto the axis

of the projectile-ion beam. In the case of fusion of spinless ions we have $M = 0$. The angular distribution at fixed values of I and K then has the form

$$W(\theta, I, K) = (I + 1/2)|D^I_{M,K}(\theta)|^2, \tag{33}$$

where the quantum number M is the projection of the total angular momentum I on the space-fixed axis, θ is the angle with respect to the space-fixed axis, and $D^I_{M,K}(\theta)$ is the symmetric-top wave function. In case of zero spin target and projectile nuclei, M is zero. The experimentally observed angular distribution of fission fragments can be obtained upon averaging over the distributions with respect to I and K in the form

$$W(\theta) = \sum_{I=0}^{\infty} \sigma(I) \sum_{K=-I}^{I} P(K) W(\theta, I, K), \tag{34}$$

where $\sigma(I)$ and $P(K)$ are the distributions of compound nuclei with respect to the total angular momentum and its projection, respectively.

A frequently used approximation of the fission fragment angular distribution reads as follows:

$$W(\theta, I) = \frac{(2I + 1) \exp[-p \sin^2 \theta] J_0[-p \sin^2 \theta]}{\mathrm{erf}[\sqrt{2p}]}, \tag{35}$$

where J_0 is the zeroth-order Bessel function, $p = (I + 1/2)^2/(4K_0^2)$, and the variance of the equilibrium K-distribution K_0 is

$$K_0^2 = \frac{T}{\hbar^2} J_{\mathrm{eff}}, \qquad J_{\mathrm{eff}} = \frac{J_\parallel J_\perp}{J_\perp - J_\parallel}. \tag{36}$$

Here T, $J_\parallel$, and $J_\perp$ are the nuclear temperature and the parallel and perpendicular moments of inertia taken at the transition state. Equation (35) is known as the Halpern-Strutinsky formula [201, 203], if one considers the saddle point as a transition state.

An average angular distribution is obtained by averaging the expression (35) over the ensemble of stochastic trajectories The anisotropy of the fission fragment angular distribution is given by

$$A = \frac{\langle W(0^0) \rangle}{\langle W(90^0) \rangle}. \tag{37}$$

There are three factors, which determine the angular distribution: the initial spin distribution of compound nuclei, the effective inertia moments, and the nuclear temperatures at the transition states.

In the case $p \gg 1$ the anisotropy of the angular distribution is given by the approximate relation

$$\frac{\langle W(0^0) \rangle}{\langle W(90^0) \rangle} \simeq 1 + \frac{\langle I^2 \rangle}{4K_0^2}. \tag{38}$$

Equation (38) could be used for qualitative analysis of the anisotropy of angular distribution. Equation (35) is used for quantitative analysis in the present paper.

The expression similar to eq. (35) could be applied in the SCTS model, but factors determined by eqs. (36) should be calculated at the scission point, *i.e.* it is assumed that τ_K is much shorter than the descent time from the saddle to the scission point. In this case the equilibration of the K degree of freedom is supposed to be at the scission point.

4.2 The effect of model dimension on the angular distribution

The set of all the accessible transition states is determined by the potential energy landscape and, hence, by the number of collective coordinates. At the same time, the particular ensemble of transition points strongly depends on the fission dynamics and, consequently, is sensitive to all the components of the model used: the conservative force, the friction and mass tensors, etc. For instance, in the case of the SPTS model in the one-dimensional case there is only one transition state, the saddle point, for each angular momentum, while in the multidimensional case the entire ensemble of conditional saddle points forms the set of transition states. The multidimensional dynamic models, in comparison with the one-dimensional ones, take into account the multidimensional nature of the fission barrier. This circumstance can strongly influence the anisotropy of angular distribution predicted by models with a different number of collective coordinates involved.

In ref. [20], we assumed that the model dimension influences the calculated angular distribution anisotropy. In addition, this influence should be stronger with increase of the nuclear fissility and excitation energy. In fact, under these conditions, the fission barrier becomes lower and a number of transition states accessible for a fissile nucleus becomes larger. An increase of the nuclear excitation energy also results in an increase of the accessible phase space to a nucleus at the ridge.

The one-dimensional Langevin equations was applied to explore the main features of angular distribution [204, 205]. In 2007 Jia and Bao [206] have published the results of the angular distribution calculations within two-dimensional Langevin dynamics. Their results are in a good agreement with the experimental data. The results of the one-dimensional Langevin model are in agreement only at low excitation energies [206].

In order to investigate the dependence of the calculated angular distribution of fission fragments on the number of collective coordinates involved in dynamical consideration in more detail, we calculated the angular distribution anisotropy in the one-dimensional and three-dimensional Langevin models for two reactions: $^{16}\mathrm{O} + {}^{208}\mathrm{Pb} \rightarrow {}^{224}\mathrm{Th}$ and $^{16}\mathrm{O} + {}^{232}\mathrm{Th} \rightarrow {}^{248}\mathrm{Cf}$. We disregarded particle evaporation in order to study only dependence of the anisotropy of the angular distribution on dimensionality. Figure 16 shows that although the anisotropy of the angular distribution almost coincides in the one-dimensional and three-dimensional calculations at low excitation energies, the three-dimensional model predicts considerably higher values than the one-dimensional model at high excitation

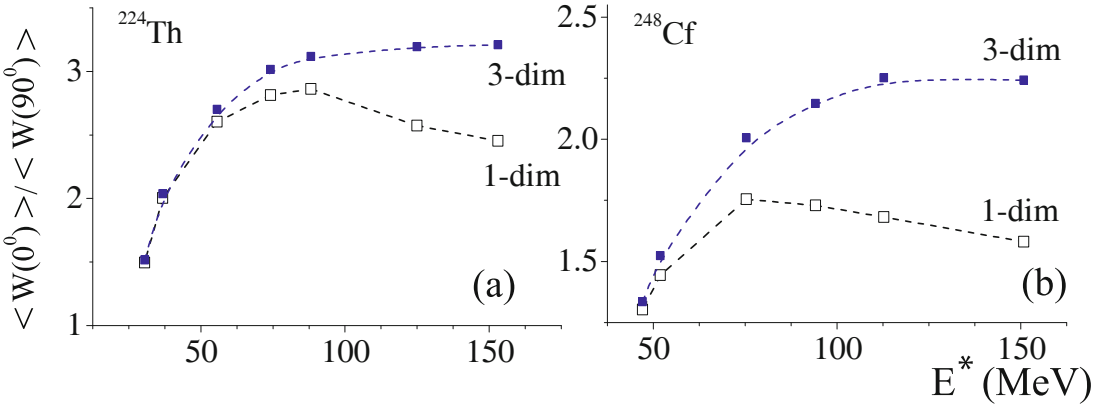

Fig. 16. (Color online) The anisotropy of the angular distribution obtained in one-dimensional (open squares) and three-dimensional (squares) Langevin calculations for the one-body mechanism of nuclear viscosity with the reduction coefficient equal to 0.25 for ^{224}Th (a) and ^{248}Cf (b) nuclei.

energy. It can be seen that the anisotropy of the angular distribution obtained in the three-dimensional calculations for the ^{224}Th nucleus at $E^\star \simeq 150$ MeV is 30% higher than that obtained in the one-dimensional calculations. For the nucleus ^{248}Cf this difference reaches almost 40%. Such dependence agrees with the assumption that the influence of model dimensionality should be stronger for heavier nuclei.

One should consider $J_{\rm eff}$ at the saddle point and its dependence on c, h and α coordinates in order to explain the dependence of A on dimensionality. The saddle point is located at $h \simeq 0$ and $\alpha = 0$. A weak dependence of the effective moment of inertia on the mass-asymmetry parameter and a stronger dependence on the parameter h takes place. In this case, the values of $J_{\rm eff}$ decrease if the parameter h deviates from zero either on the positive or the negative sides. In the multidimensional model the anisotropy of angular distribution is calculated by averaging over the ensemble of transition points, while, in the one-dimensional model, only one transition state (the saddle point) is realized. Therefore, the values of K_0 obtained in the three-dimensional calculations are lower on average than in the one-dimensional case both due to an increase in the effective moment of inertia and a decrease in the transition-state temperature. Lower values of the parameter K_0 correspond to a narrower angular distribution.

4.3 Energy dependence of the anisotropy of the angular distribution

In fig. 17 the calculated results for the anisotropy of the angular distribution are presented for the reactions ^{16}O + ^{208}Pb $\rightarrow$ ^{224}Th, ^{16}O + ^{232}Th $\rightarrow$ ^{248}Cf, ^{16}O + ^{238}U $\rightarrow$ ^{254}Fm and ^{16}O + ^{248}Cf $\rightarrow$ ^{264}Rf. The solid and dashed curves show the results predicted by the SPTS and SCTS models, respectively. The experimental data (open squares) are taken from the work [207]. It is known [201,208,209] that the SPTS model provides good reproduction of the experimental data on the anisotropy of the angular distributions for reactions where ^{3}He, α-particles are used as projectiles. The compound nuclei formed in such reactions have a temperature of about 1 MeV and low angular momenta. It was found that the standard SPTS model regularly predicted low values of the angular distribution anisotropy for reaction with massive ions of carbon, oxygen and heavy ions [208], in comparison with the experimental data, and the values obtained according to the SCTS model.

It is seen from the figure, that the experimental data on the anisotropy of the fission fragment angular distribution can not be reproduced neither of the SPTS or SCTS models especially for compound nuclei heavier than ^{224}Th and for high excitation energies. Experimental data are between the predictions of the both transition-state models. For the case of the light compound nuclei (see results for ^{224}Th), experimental data are reproduced rather well by the SPTS model.

It was assumed that the transition state determining the angular distribution of fission fragments could be located somewhere between the saddle point and the scission point. The existent uncertainty with the position of the transition state indicates that it is necessary to take into account the dynamical features of the angular distribution formation. In this case, the tilting mode could be considered as an independent collective coordinate in the multidimensional Langevin approach. Such completely dynamical approach makes it possible to determine, in the most general form, the non-equilibrium K-mode distribution $P(K,t)$. However, in this case, the problem of calculating the conservative force and the transport parameters (inertial and friction) for the tilting mode arises. At the same time there is no theoretical approach for calculating the transport coefficients for the tilting mode. The calculation of the transport coefficients is one of the involved problems in nuclear dynamics. Therefore, a fully dynamical consideration of the evolution of the K degree of freedom is still difficult.

The dynamical aspects of the angular distribution formation can be evaluated using the relaxation time τ_K for the tilting mode. In refs. [116–118], it was proposed that

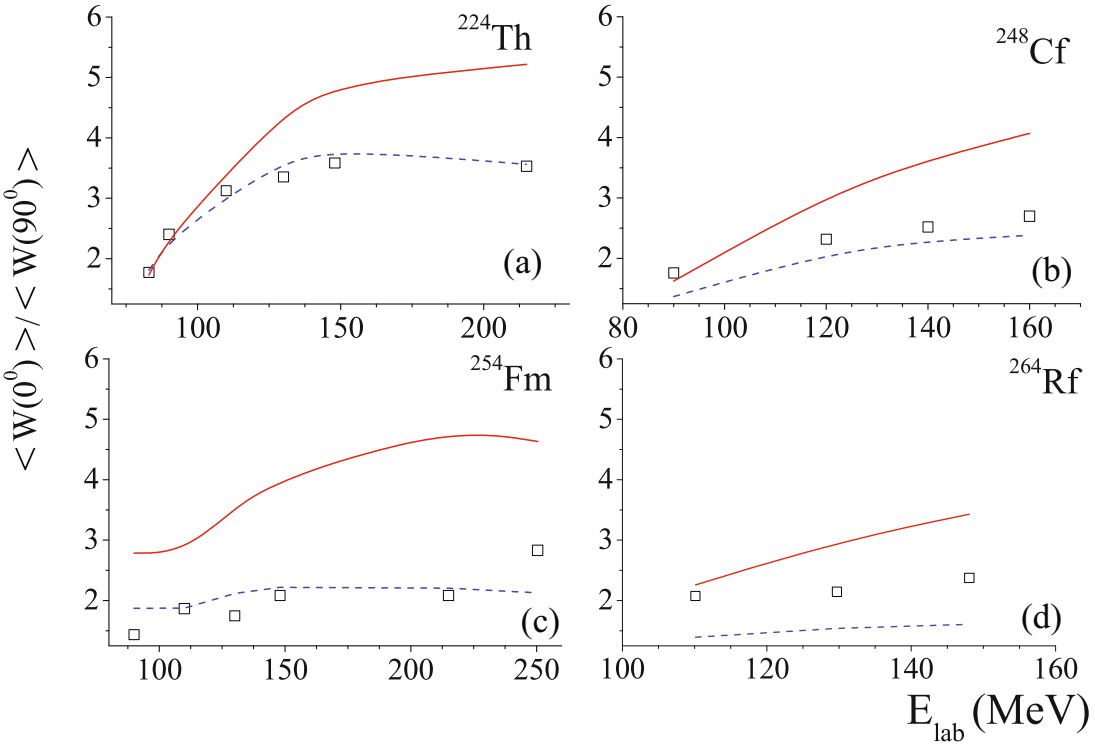

Fig. 17. (Color online) The anisotropy of the angular distribution for the compound systems ^{224}Th (a), ^{248}Cf (b), ^{254}Fm (c), and ^{264}Rf (d). The solid and dashed curves present the results predicted by the SPTS and SCTS models, respectively. The experimental data (open squares) are taken from the work [207].

the evolution of the tilting mode can be considered using the Monte Carlo method. In refs. [116, 117] the dynamical treatment of the tilting mode was joined with one-dimensional Langevin dynamics for shape degree of freedom, while 3-dimensional Langevin equations for shape degree of freedom were employed in refs. [51, 118]. The K equilibration time is deduced to be (20–30) $\times$ 10^{-21} s in refs. [116, 117] and (2–4) $\times$ 10^{-21} s in [51, 118] from fits of the calculated values to experimental data on the anisotropy of the angular distribution for heavy fissioning compound systems.

Theoretical estimates of the relaxation time for the K mode and for other rotational modes in deep-inelastic-transfer reactions were obtained in [157,210], where use of the ideas of nucleon-transport theory in nuclear collisions with allowance for quantum effects [211] was made. In refs. [157,210], the relaxation time τ_K for the tilting mode was estimated in the limits at (2–20) $\times$ 10^{-21} s, the specific value being dependent on the total angular momentum of the system.

The energy dependence of the anisotropy revealed from the developed approach [51,118] was found to be closer to the experimental data than the predictions of the statistical models SPTS and SCTS. Such phenomenologically estimated values for τ_K are comparable with the mean time of the descent from the saddle point to scission [118]. This fact points out that K distribution changes during the descent from the saddle point to scission. These first attempts of using the Langevin dynamics joined with the Monte Carlo algorithm that considers the tilting mode as an independent collective degree of freedom brought a new ideas and understanding about K distribution evolution. It eventually resulted in another step ahead —the pure dynamical consideration of this evolution.

4.4 Angular distribution within 4D Langevin dynamics

Within dynamical consideration of the angular distribution formation, the tilting mode could be considered as an independent collective coordinate in the multidimensional Langevin approach. Such completely dynamical approach makes it possible to determine, in the most general form, the non-equilibrium K-mode distribution $P(K, t)$. However, in this case, the problem of calculating the conservative force and the transport parameters (inertial and friction) for the tilting mode arises. The works of Døssing [157, 210], Randrup [158] and Lestone [115] partially solved those problems, particularly by the use of the overdamped treatment of the K-coordinate dynamic. This assumption took away the open question with inertial tensor for the tilting mode. Anyway, the calculation of the transport coefficients is one of the involved problems in nuclear dynamics, but multidimensional Langevin consideration of the tilting mode relaxation became possible.

Recent theoretical dynamical 4D Langevin calculations [61, 63, 159, 212–214] realized the pure dynamical treatment of the K-mode relaxation process. The investigations were made for light, medium and heavy compound nucleus formed in the heavy ion collisions (from ^{162}Yb to

^{264}Rf). Solved together, Langevin equations for the shape parameters (eq. (10)) and for the K collective coordinate (eq. (14)) made it possible to obtain the new theoretical results on many fission observables within stochastic dynamical approach. Most of them are presented in previous section of our current work and reveal the better agreement with experimental data, than previous 3D, 2D and 1D Langevin calculations.

In case of zero spin target and projectile nuclei, $M=0$, and the angular distribution of fission fragments is determined by averaging the expression (33) over the ensemble of the Langevin trajectories

$$\langle W(\theta)\rangle = \frac{1}{N_f}\sum_{j=1}^{N_f}(I^j+1/2)\left|D^{I^j}_{0,K^j}(\theta)\right|^2, \qquad (39)$$

where upper index j determines the value of the corresponding quantity at the scission surface for the j-th trajectory and N_f is the total number of simulated trajectories which go to fission channel. Applying eq. (39) within the present 4D calculations we determine the fission fragment angular distribution at the scission surface. This procedure does not use the assumptions of the standard transition-state model, as the K distribution is determined at every time step. Thus, there is no need for any assumptions of its distribution at any arbitrary transition point. The qualitative influence of the γ_K parameter on the dynamical evolution of the K coordinate can be found in refs. [61, 63]. The anisotropy of the fission fragment distribution is then given by eq. (38) where the angular distribution $\langle W(\theta)\rangle$ can be found either from the 4D calculations using eq. (39) or from the equilibrium K distribution at the transition-state model [201, 202].

It is worth mentioning, that the most of the analyzed observables, for instance, prescission particle multiplicities and fission fragment MED characteristics do not get the new "physics" or consideration within the 4D dynamics —it is like more evolutionary changes. But much more substantial change we get for the fission fragment angular distribution formation treatment —now we get pure dynamical consideration of the process of its formation, because we get instant K values for any point along the fission trajectory from the dynamical equation (14). Eventually, we get a K-mode distribution for any given moment of time or point along the fission trajectory. So we need no assumption about some special point, where the distribution is formed and does not change anymore. While solving this kind of question, dynamical consideration brings up a new one —the transport coefficients and particularly the viscosity for a new dynamical variable. The friction component for the K coordinate controls the coupling between the orientation degree of freedom and "heat bath". It plays the primary role for the K-mode relaxation process and the angular distribution formation.

Above-mentioned recent works [63, 159, 213, 214] demonstrated that the impact of the dissipation coefficient for shape parameters (k_s) and the one for the K-mode (γ_K) on the calculated observables can be selectively probed. The nuclear viscosity with respect to nuclear shape parameters influences the emitted particle multiplicities ($n_{\rm pre}$), the fission fragment MED parameters, and the angular distribution of fission fragments. At the same time the dissipation coefficient γ_K exerts the angular distribution of fission fragments only. In other words, in order to get close to the experimental values of the angular distribution anisotropy, one could change the γ_K value only, without affecting results for other observables of interest.

The question of value and deformation dependence of γ_K were investigated through several works [63, 159, 213, 214]. Initially deduced by Lestone constant value $\gamma_K = 0.077\,(\mathrm{MeV\,zs})^{-1/2}$ was proved [61, 63] to be a good approximation for fission of heavy compound nucleus with $A_{CN} \simeq 250$.

For lighter fissioning compound nucleus it could be treated as an initial approximation, but substantial scaling (up to several times) of γ_K might be needed in order to get the experimental anisotropy values for each theoretically modeled fission reaction [63, 114, 115, 157, 158]. This fact motivated us to use a deformation-dependent γ_K coefficient calculated following [115] for the shapes featuring a neck, which predicts quite small values of $\gamma_K = 0.0077\,(\mathrm{MeV\,zs})^{-1/2}$. For compact shapes one should use some kind of approximation [63, 214]. Eventually, to reproduce the experimental data on the anisotropy of fission fragment angular distribution the γ_K value for the compact shapes without the neck should be increased up to 0.2–0.4 $(\mathrm{MeV\,zs})^{-1/2}$ for the compound nuclei with $A_{\rm CN} \simeq 200$ and up to 0.1–0.2 $(\mathrm{MeV\,zs})^{-1/2}$ for the heavier nuclei with $A_{\rm CN} \simeq 250$ [159].

An important observation on K-mode dynamical relaxation process could be done based on these results: the dynamics of the K coordinate tends to the predictions of the saddle point transition-state model. Due to the large values of γ_K at the region of compact shapes, one gets the quick equilibration of the K coordinate to the moment when saddle point shapes will be reached by the fissioning system.

5 Isotopic distribution

The fission fragment distribution usually is presented as the charge distribution or the mass distribution of the products. The isotopic distribution of FF produced in the reaction in medium energy excitation is a very rare information. Experimentally it was challenging over the years to have the detectors with good enough resolution to discriminate between different masses and various charges of measured species. In the past the experiment focused on the actinide region because of its application in power plants. The neutron- or proton-induced fission of Th and U isotopes have been discussed for example in [215, 216] showing the isotopic distribution for indium, cesium and rubidium isotopes.

The low energy process as proton- or neutron-induced fission and also high energy reactions providing the nucleon transfer or multifragmentation are very interest-

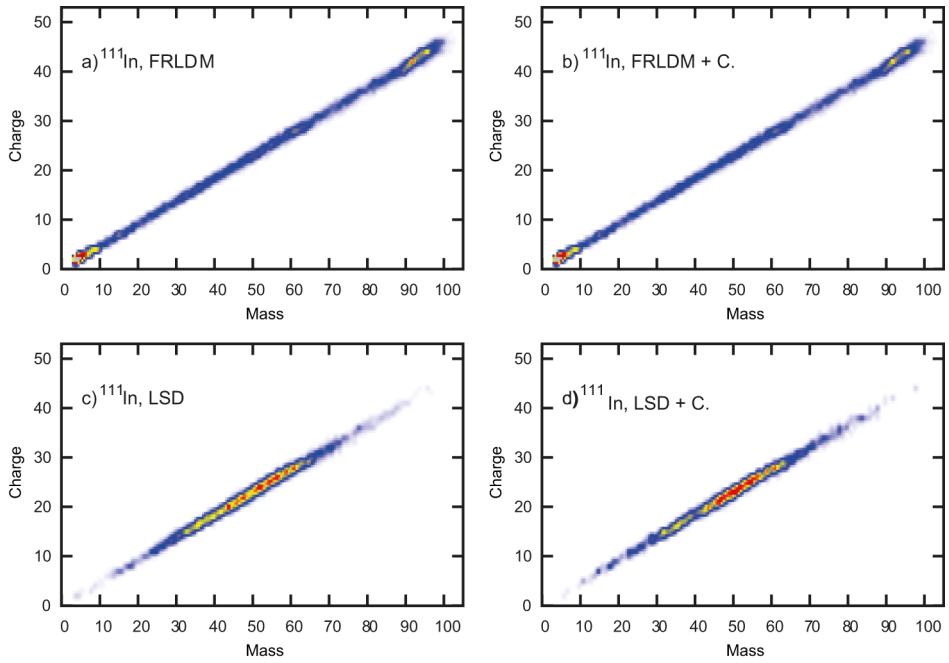

Fig. 18. (Color online) The isotopic distribution of the fission fragments from reaction leading to excited ^{111}In nucleus without (a) and with (b) congruence energy implemented in FRLDM model and for LSD model ((c) and (d)).

ing but they cannot be treated within our stochastic approach. The evolution of the nucleus from its ground state up to the scission point in the four-dimensional space of the deformation degrees of freedom and the projected angular momentum by solving transport equation of the Langevin is well described for the process leading to CN with the medium excitation energy and large spin.

The high energy physics shows also the interest in study of the isotopic distribution. The examination of the isotopic distribution has been done in few cases by the observations of the γ-rays and a deduction of the yield for each isotope separately [217], *i.e.* for the transfer reaction. Also the fragmentation process was more productive to give the isotopic distribution for various fragments. There are attempts to connect the isotopic distribution with the actual temperature of the system [218], which is very important in the multifragmentation reactions.

The experimental data, which contain the isotopic distributions for medium-energy reactions, are rare. One of the examples is the isotopic distribution coming from fusion-fission reaction, where the compound nucleus was ^{111}In [198, 219]. Lately, the isotopic distribution for the fusion-fission reaction of ^{238}U+^{12}C leading to a compound ^{250}Cf with excitation energy of 45 MeV has been measured in GANIL, France with VAMOS spectrometer [177, 220]. As the isotopic distribution is a more detailed observable than the total mass and charge distribution of FF, it should provide the better understanding of dynamic of fission process.

The average neutron excess $\langle N\rangle/Z$ [177], which can be extracted from the isotopic distribution shapes, allows to discuss the equilibration of the neutron-to-proton ratio with an evolution of the nuclear deformation. This observable could discriminate the fusion-fission reaction, where the $\langle N\rangle/Z$ is smooth, on the transfer reaction where it could be approximated by two separate lines, connected with N/Z of projectile and target [64,177].

Another extremely interesting observable, which is extracted from the ID, is the width. The theoretical reproduction of these variables is very difficult, as it demands correct description for all steps of the fission: the emission of the particle before scission, the right treating of the scission point and also an estimation of the postscission emission. A more detailed comparison is provided by the isotopic or isobaric distributions. From the experimental and also from the theoretical point of view such a distribution is quite demanding but also the most sensitive to the model parameter changes.

5.1 Isotopic distribution and PES

The influence of the PES approach on the shape of the isotopic distribution is obvious as it changes dramatically the mass/charge distributions. This conclusion is supported by figs. 18 and 19 for medium mass CN. The isotopic maps (figs. 18) reflect directly the shape of the mass/charge distributions, the PES calculated with FRLDM and also with FRLDM+W. predicts lower barriers for asymmetric shapes and the LSD driven potentials give symmetric partition of the CN.

Figures 18 and 19 display the final fission fragments. In the path from the compound nucleus to the scission point the prescission particles are emitted. After scission, fragments could have still enough excitation energy to deexcite by emission of particles. The isotopic distribution is obviously very sensitive on the multiplicity of emitted particles as the prescission emission changes the N/Z ratio of the scissioning system. The detected particles are

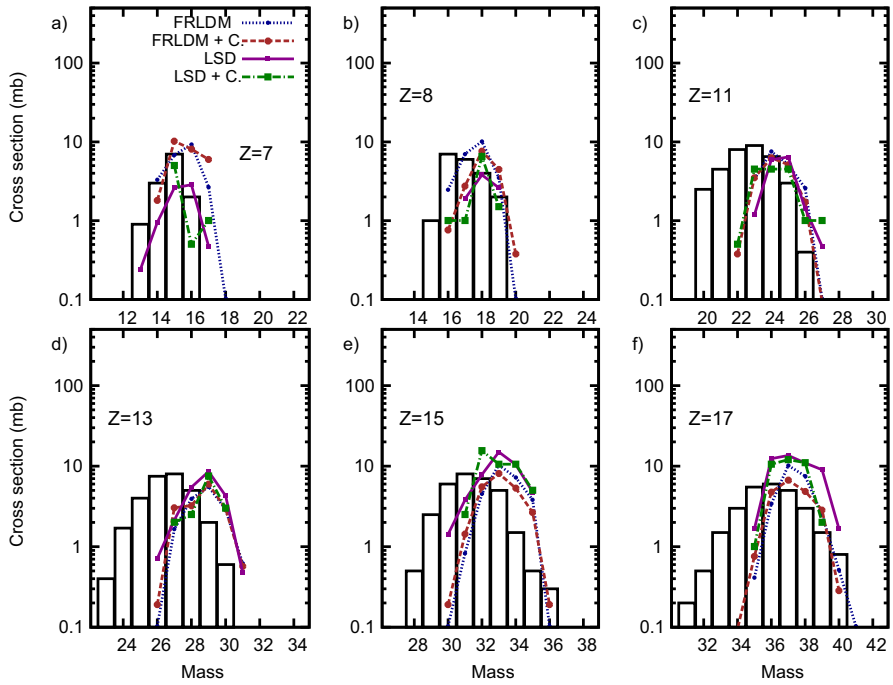

Fig. 19. (Color online) Isotopic cross-section distributions of fission fragments in the reaction ^{84}Kr + ^{27}Al → ^{111}In at 10.6 MeV/nucleon for elements of $Z = 7$, 8, 10, 13, 15, 19 from (a) to (f). The data [198] (gray histograms) are compared to predictions by various model variants: FRLDM without (blue dotted line) and with (red dashed line) deformation-dependent Wigner term, LSD without (pink full line) and with (green dash-dotted line) deformation-dependent congruence term. Experimental error bars are not shown for clarity; they are below 30% in most cases. The isotopic distributions for $Z = 9$, 12, 14, 16, 19, 20 are presented in [62].

cold thus the postscission emission is necessary to compare isotopic distribution with experimental data [197].

The detailed comparison of the isotopic distribution has been shown partially in [62] and supplemented with other charges displayed in fig. 19. As it is seen distributions are too narrow for heavier species for all macroscopic PES. The centroids of the distribution are also shifted, which could be a sign that not enough particles are still evaporated. Plots similar to fig. 18 done for heavy compounds such as ^{250}Cf, ^{252}Fm, ^{260}No and others do not show a visible difference and thus they are not displayed.

5.2 Charge variance

The phenomenological nature of our macroscopic models, which are presented in this paper, permits to reproduce wide range of observables but it includes few presuppositions. As we know the shape of the fissioning nucleus, we can estimate the mass of the fission fragments but its atomic number is unknown.

The assumption of uniformly charged matter and Unchanged Charge Distribution (UCD) allows to divide the charge of the fissioning nucleus into two parts but it is not enough to reproduce the experimental data. One of the first studies of the nuclear charge distribution [221] suggested that fission products of actinides maybe formed predominantly by beta decay processes starting from products of lower Z than expected.

Later on such an idea has been connected with the Equal Charge Displacement (ECD). In the article [222] there is underlined that if the time scale for fission is comparable with time of collision, the polarization is impossible. There is deviation of the FF charge density from expected with assumption of uniformly charged matter.

The division of the nucleus into fragments is usually done with quite low excitation energy after emission prescission particles so the structural effects could play a role. However, our model is fully classical and any quantum effects are negleted. Thus we can only approximately estimate the importance of the charge variation on different fission observables. As we are working in the high excitation energies the influence coming from scission moment is minor but still visible, especially in the isotopic distributions.

The first attempt to include the charge as a collective coordinate was done in [102–104]. The Langevin equations have been solved in three-dimensional collective coordinate space where apart from elongation and neck parameters, the charge asymmetry $\eta_Z = (Z_R - Z_L)/(Z_R + Z_L)$ (Z_L, Z_R are the charges of the left- and right-hand fragments) is taken on this same footing. The PES was a sum of the surface, Coulomb, symmetry and rotational energies, where only the surface part was independent on the charge coordinate. The Werner-Wheeler method has been applied to obtain the mass tensors not only for shape parameters but also the charge one. From the one- and two-body dissipation method also the friction coefficient connected to the η_Z variables was deduced and taken into calculations. The testing reaction was ^{4}He+^{232}Th → ^{236}U

at excitation energies $E^\star = 39$–160 MeV. The influence of the dissipation model was discussed as it changes the behavior of the relaxation time of the charge coordinates from constant (one-body) to more complex (two-body assumption). The widths of the charge distribution is slightly dependent on the friction model, but it increases with enlarging the excitation energy of the system. The comparison of the results with experimental data allowed to deduce that the statistical equilibration of the charge mode is independent on the friction assumption and occurs at each excitation energy.

The calculations have been done assuming the symmetric disintegration of the nucleus but the main outcome permits to approximate the charge mode by statistical limit as it has shorter relaxation time than deformation degrees of freedom.

Thus we made an estimation of the influence of the charge variation on various observables. In our previous paper [62] the study of the reactions: ^{84}Kr+^{27}Al at 5.9 and 10.6 MeV/nucleus provided good description of the isobaric distribution of the evaporation residues [219] but the theoretical isotopic distributions of the fission fragments have been too narrow in comparison to the experimental data [198]. The variables important for the noticeable changes of the isotopic distribution is the charge variation. Thus variance of the charge distribution of the fission fragments affects various observables calculated by solving the Langevin equations in the four dimensional collective coordinate space. The newly published data [177] are perfect for such an investigation as they comprise complete and wide range of isotopic species, measured with good accuracy, producing in our favorable conditions.

The correct method to obtain the charge division between the nascent fragments requires calculations of the charge density distribution in the fissioning nucleus. The alternative idea was proposed in [102–104]. The variance of the charge distribution was calculated as a function of the mean internal excitation energy at scission for one-body and two-body viscosities. They proposed to introduce the collective coordinates connected to the ratio of the fragment charges as a mimic of the charge density distributions. In place of the mass asymmetry parameter they introduced the charge asymmetry parameter. The energy term depends on this coordinate by the stiffness parameters and the friction parameter of the charge mode have been shown within one-body dissipation model. In this approach, the variance of the charge asymmetry parameters, obtained in the scission point, is directly translated into the variance of the charge distribution σ_Z^2. The main message was that the results obtained with constant charge variance well estimate the calculation done with charge-asymmetry coordinate. This statement is very significant for our model, because when we already calculate Langevin trajectories in four dimensions, we are legitimated to add the charge fluctuation in the scission point, instead of increasing the number degrees of freedom by another collective degree of freedom.

Once the scission point is reached, mass division is determined according to the volume of the nascent fragments. In any Langevin code, whenever the dynamics of the charge asymmetry degree of freedom is not treated by means of an explicit collective coordinate, an assumption has to be made about partitioning of protons between the fragments. A number of empirical hypotheses have been proposed by various authors [201,223]. Sharing of neutrons straightforwardly follows from mass and charge. In the code used in this work, proton partitioning is based on the Unchanged Charge Density (UCD) assumption, which is a reasonable approximation for the most probable charge at fixed mass at medium and high $E^\star$ [224]. It implies conservation of A/Z between the fissioning nucleus and the fragments at scission. For a specific mass split, the atomic number of the fragments is then unequivocally defined by

$$Z_{FFi}^{UCD} = \frac{A_{FFi} Z_{\rm fiss}}{A_{\rm fiss}}. \tag{40}$$

where A_{FFi} (Z_{FFi}) is the mass (charge) of the i^{th} fragment before post-scission evaporation, and $A_{\rm fiss}$ ($Z_{\rm fiss}$) is the mass (charge) of the fissioning nucleus. In such a "sharp" scheme, charge fluctuations are inexistent: the isobaric charge variance σ_Z —given by the width of the charge-dispersion curve at fixed mass [221]— is zero. To our knowledge, the absence of charge fluctuations is common to (nearly) all available Langevin codes, although the most probable charge may be derived from one or another hypotheses [21, 27, 52, 63, 185, 225–228].

The charge fluctuation in our model are taken into account in the scission moment. The random Gaussian distribution with fixed σ_Z widths is applied to differ the estimated Z_{FFi}^{UCD} by $\pm 1, \pm 2, \ldots$. This σ_Z widths has to be fitted to existing data as there is no clear prescription what should be the correct values and the study are in progress. The dynamic calculation has been done for the fusion-fission reaction of ^{238}U on ^{12}C leading to a compound ^{250}Cf with excitation energy of 45 MeV. The experimental data are taken from [177, 220].

The experimental set-up allows to measure the mass and charge distributions with good resolution, it provides the isotopic identification of the fission fragments. The isotopic distribution has been obtained for $Z = 30$ up to

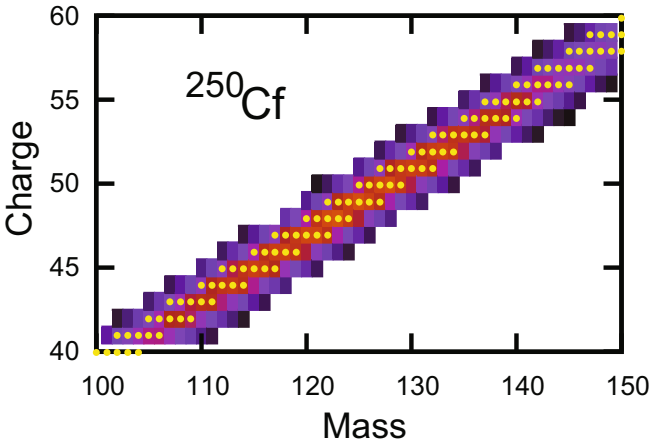

Fig. 20. (Color online) Calculated isotopic production for fission of ^{250}Cf at $E^\star = 45$ MeV and with $\sigma_Z = 0$ (yellow dots) and 0.8 (color boxes).

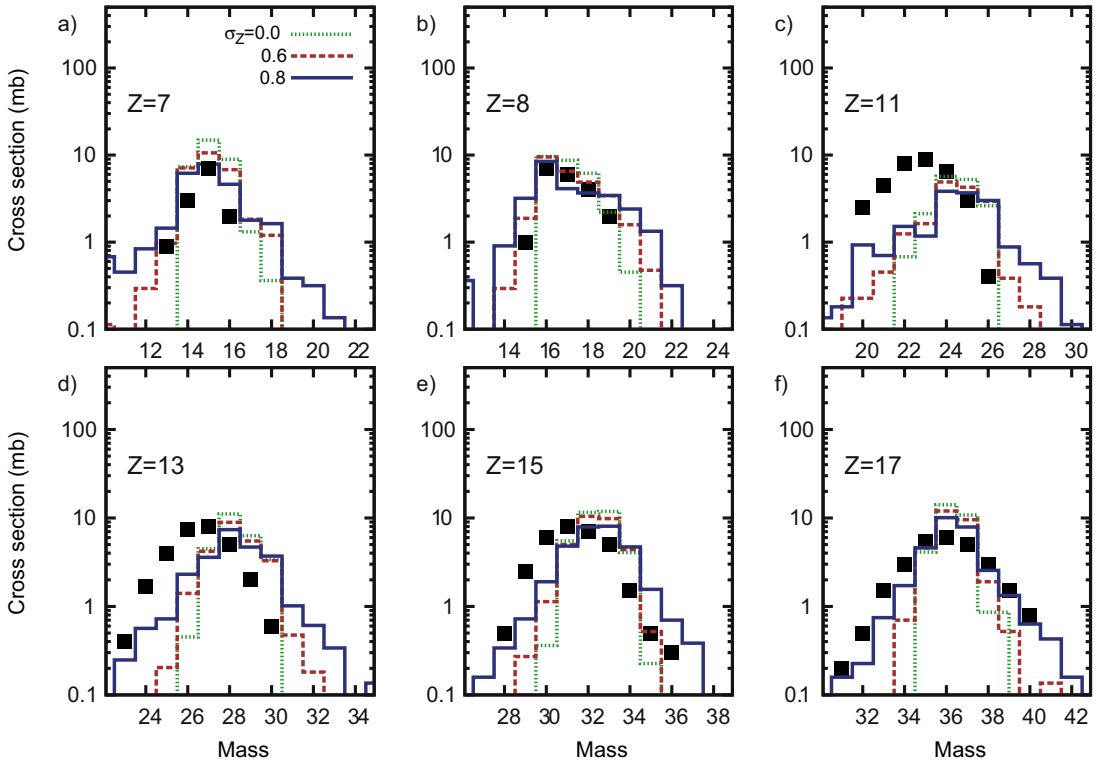

Fig. 21. (Color online) Isotopic cross-section distributions of fission fragments in the reaction ^{84}Kr + ^{27}Al → ^{111}In at 10.6 MeV/nucleon for elements of Z = 7, 8, 10, 13, 15, 19 from (a) to (f). The data [198] (gray histograms) are compared to predictions without (dotted green line) and with account of charge fluctuations with $\sigma_Z = 0.6$ (dashed red line) and 0.8 (full blue line).

64. Such data are unique in the literature for the medium excitation energies. The neutron excess for the experimental data on fusion-fission reaction shows nearly constant values about 1.46 while the $N_{\rm CN}/Z_{\rm CN}$ of ^{250}Cf is 1.55. The total neutron evaporation multiplicity is around 9 which is in good agreement with our results, where we have two prescission neutrons emitted and 6.7 postscission neutrons.

Figure 20 shows the influence of the charge variation on the isotopic distribution. The yellow dots are the isotopic distribution obtained with UCD assumption. The dispersion from the fixed $Z_{FF}/A_{FF} = Z_{\rm fiss}/A_{\rm fiss}$ is due to evaporated particles before and after scission. The color boxes allow to estimate the isotopic cross-section and give the impression how big change is done due to the implementation the charge variation in the scission process.

For the moderate mass of the compound nucleus (^{111}In), the experimental isotopic distribution is displayed in fig. 21 together with the theoretical estimations. The charge variation with $\sigma_Z = 0.6$ and 0.8 are verified. Almost for each element the better description of the measured data is done with $\sigma_Z = 0.8$. Similar investigation was done for a heavy system ^{250}Cf in [64] and complementary isotopic distributions are shown in fig. 22.

The reaction ^{22}Ne + ^{238}U → ^{260}No with beam energies: 6 AMeV ($E^\star$ = 120 MeV) and 7.4 AMeV ($E^\star$ = 149 MeV) [200] permits to check the isotopic distribution for higher excitation energies than in case of ^{250}Cf at $E^\star$ = 45 MeV. The experimental data are available only for samarium and cesium (Z = 37 and 55) isotopic chains and they are presented in fig. 23. The influence of the charge variation parameter is clearly visible and the best reproduction is obtained for $\sigma_Z = 0.8$. Further tests are necessary but this preliminary discussion for fission of the medium mass CN ^{111}In and heavy system ^{250}Cf allows to draw a conclusion that the width of the charge variation is independent of the size of the fissioning system. The reaction ^{22}Ne + ^{238}U → ^{260}No with different excitation energy (fig. 23) shows, however, that the $\sigma_Z = 0.8$ works slightly better for lower energy ($E^\star$ = 120 MeV) and the calculation with $\sigma_Z = 0.6$ are better for higher excitation energy ($E^\star$ = 149 MeV). As for ^{111}In reaction the $E^\star$ is around 216 MeV and better reproduction of the isotopic distribution was with lower $\sigma_Z = 0.6$, the direct connection between excitation energy and width of the charge fluctuation could not be drawn.

Moreover recent articles [79,229] show that the low energy fission described with the microscopic-like approaches also needs the charge variation but there fluctuation are implemented in less phenomenological way. The isotopic distribution for actinide nuclei has been discussed in [229] where the two-center shell model has been applied for the Langevin model. Apart of deformation-driven collective coordinates, also the charge variation is taken into account on this same footing. The calculation done for fissioning ^{236}U shows good agreement with experimental data basis for isotopic distribution of Z = 39, 52 and also isotonic distribution with A = 132. That paper confirms that also

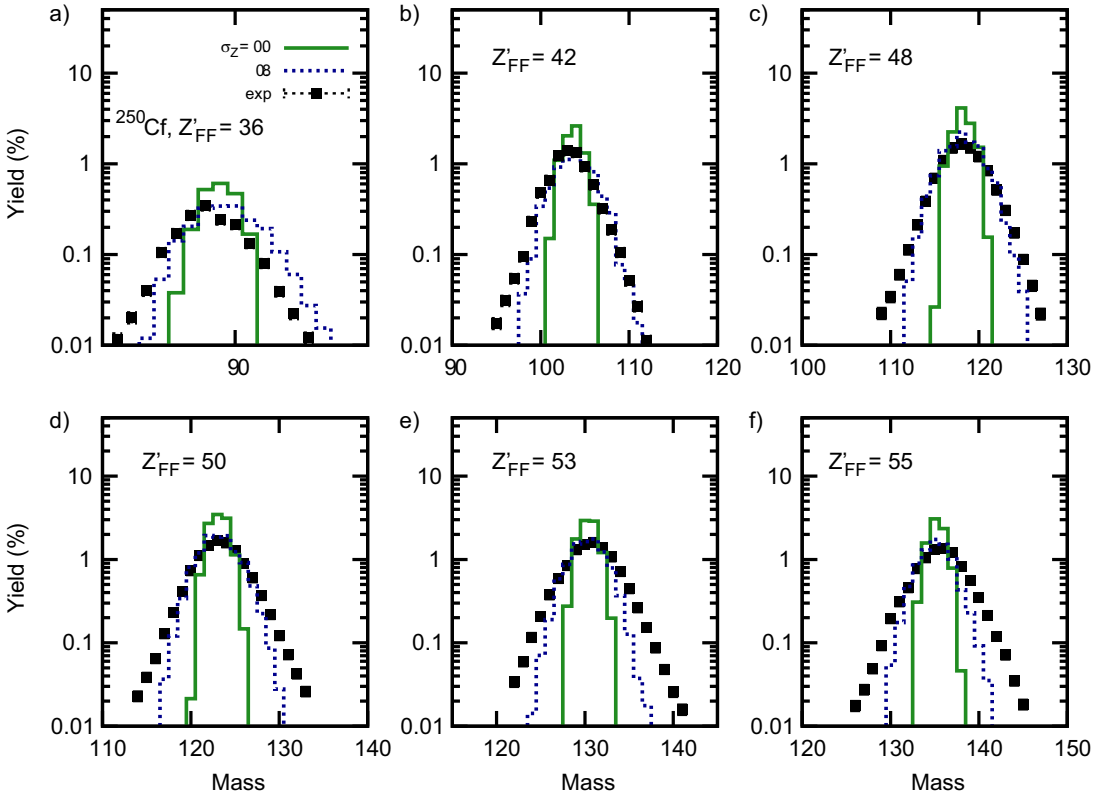

Fig. 22. (Color online) Fragment isotopic distribution for fission of ^{250}Cf at $E^\star = 45$ MeV for elements between Sr and Nd. Experimental data [177] (full squares) are compared to calculations obtained without (full green line) and with (dashed red line) account of charge fluctuations with $\sigma_Z = 0.8$. Other isotopes are presented in [64].

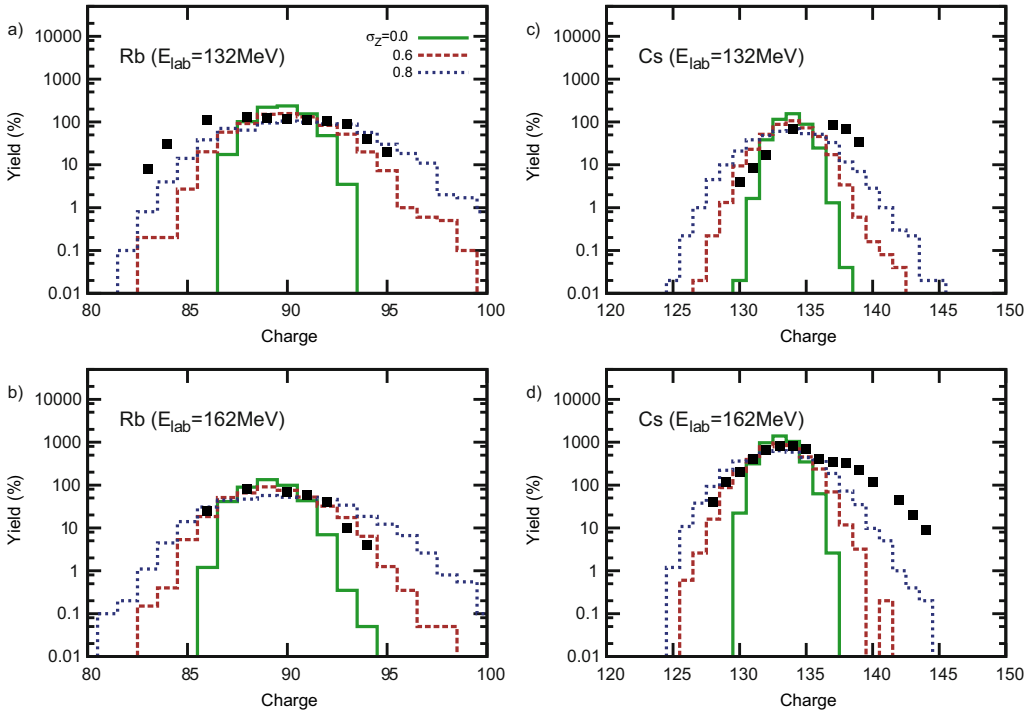

Fig. 23. Isotopic distribution for $Z = 37$ and 55 for reactions ^{22}Ne+^{238}U $\rightarrow$ ^{260}No with beam energies: 6 AMeV ($E^\star = 120$ MeV) and 7.4 AMeV ($E^\star = 149$ MeV) [200].

for low-energy fission description, the charge variation is crucial and should be applied.

The charge variation of the fission fragments was taken into account also by another group [79], which use the five-dimensional deformation space and Brownian-shape motion as the approximation of the Langevin transport equations. The model has been applied to actinide nuclei excited in neutron- or γ-induced reaction to no more than 11 MeV of excitation energy. The odd-even staggering in charge distribution has been well reproduced and the influence of the pairing constituents on the amelioration of the theoretical estimations is shown. The charge variation is governed microscopically by changing the pairing gap, which is partially responsible for the breaking the proton pairs and providing the odd-even staggering in the charge distribution of the fission fragments.

These two articles [79, 229] in addition to our previous [64] and present discussion show directly the importance of the charge variation in different mass regions and also the excitation energies. Even if the charge/mass distribution in medium mass nuclei at 100–200 MeV excitation energy is not sensitive to the implementation of the charge variation in the FF separation process, descriptions of the proton-, neutron-induced reaction with actinides are susceptible to the possibility of non-unified charge distribution in the nascent fragments.

6 Summary and perspectives

Different kinds of the fission fragment distributions are the most frequent observables studied and measured in various reactions. The dynamical approach shortly presented here is pinned by the stochastic theory. The differential Langevin equations describe the time evolution of the excited nucleus. The change of its shape governed by the interplay between potential energy and inertia and friction coefficients. The statistical consideration joint with dynamical modeling provide the description of the particles evaporation from the fissioning nucleus. Depending on the excitation energy and the mass of the compound nucleus, the calculated MED are more or less sensitive to various constituents of the transport equations. The deexcitation of medium mass compound nuclei is highly dependent on the PES model used to calculate the deformation and rotation energies, almost opposite to the heavy nuclei. The moderate mass of CN attenuates the dissipation effects thus differences between friction and mass tensor models used in calculations are more pronounced for heavy nuclei. The influence of viscosity on MED parameters depends also on the excitation energy of the system.

During the past two decades dynamical approach based on multidimensional Langevin equations has been widely used for describing the dynamics of heavy-ion-induced fission. In this review we showed potential of this approach with regard to description of the large number of different observables in fusion-fission reactions. In our opinion, the results obtained in recent years with the use of the multidimensional stochastic approach are impressive. In particular, calculations in the 3D Langevin dynamics naturally reproduce the variances of the MED distribution of fission fragments and also their significant growth with the compound nucleus fissility parameter. These characteristic pronounced features of the MED distributions cannot be explained within the framework of fission models conventionally used for the analysis of fragment distribution and the previously favored 2D Langevin calculations. Within 3D Langevin dynamics the angular momentum influence on the MED characteristics were thoroughly studied and well understood [48,49]. In addition, within the developed multidimensional approach it is possible [63, 213] to describe quantitatively fine correlation characteristics of the MED of fragments with evaporated prescission neutrons. Now there is evidently no doubt that a dynamical stochastic approach combined with evaporation of light prescission particles and gamma quanta provides the most adequate description of the investigated fusion-fission reactions. At the same time, the ingredients of dynamical equations are not well defined, and some ambiguity exists in determination of inertia and friction parameters. As before, it primarily concerns the choice of the coordinate and temperature dependencies of friction parameter (tensor).

It would also be desirable to emphasize that the systematic calculations of the MED distribution of fragments and prescission neutron multiplicities performed within 3D [19, 27, 49] and 4D [61, 63, 159, 213, 230] stochastic approach have made it possible to unambiguously choose, after a long discussion, which nuclear viscosity mechanism (two-body or one-body) is realized during nuclear fission. A simultaneous description of the fission fragment MED parameters and the mean prescission neutron multiplicities is attained for the one-body mechanism of viscosity in its modified variant [56, 57] with the reduction coefficient $k_s = 0.25$–0.5 for the contribution from the wall formula. The calculations performed in [63] have shown that deformation-dependent coefficient $k_s(q)$ found on the basis of "chaos-weighted" formula [137] yield almost the same results as those using constant k_s coefficient from the interval $0.2 < k_s < 0.5$ [63, 159, 213, 231]. The attenuation of the dissipation relative to the wall-formula predictions for a fissile nucleus with highly symmetric configuration (such as a sphere or weakly deformed ellipsoid) is now understood well both from use of quantum-mechanical calculations and from ideas of chaos theory. However, the abnormally sharp increase of the dissipation for strongly deformed configurations close to scission which was introduced in the calculations of Fröebrich and Gontchar has yet to receive a proper theoretical explanation despite the good agreement of their calculations with experimental data. Therefore, the character of the mechanism of dissipation realized in fission requires further both theoretical and experimental study.

One should note that the k_s value found in different theoretical studies should be compared with caution. The important feature of any theoretical model is the number of collective coordinates included for the dynamical consideration. As was found in refs. [63, 213] the inclusion of the K collective coordinate into the 3D model changes the prediction for the k_s value, which fits best the ex-

perimental data. The same is true in case of comparison of 3D model, and dynamical models with lower dimensionality. For example, the sharp increase of the dissipation for strongly deformed configurations close to scission was introduced in the 1D calculations of Fröebrich and Gontchar in order to get the good agreement of theoretical calculations with experimental data. In refs. [17, 28] it was also shown how the inclusion of mass-asymmetry collective coordinate to the 2D dynamical model will influence the parameters of fission fragment energy distribution. The influence of the dimensionality of the model on the fission width and different experimental observables is presented in refs. [232, 233]. Moreover, even details of some specific parametrization of nuclear shapes could influence the calculated results, as it is shown for example in ref. [234]. Another important point which influences the predicted k_s value is the number of observables taken for the analysis. In order to have a severe constraints on the predicted k_s values theoretical model should consider as many experimental observables as possible. Otherwise, theoretical model dealing only with limited number of observables and/or modeling only one or two collective coordinates could come to wrong conclusions about dissipation strength and its dependence on collective coordinates. Therefore, it is extremely difficult to compare predictions of dissipation strength found in various theoretical models, which use different parameterizations of nuclear shapes, different dimensionality and dealing with investigations of different observables.

The extensions of 3D Langevin dynamics by adding the tilting degree of freedom (K coordinate) [61, 63] and the collective coordinate of the charge asymmetry η_Z [64, 103, 104] to the three collective coordinates that describe the shape of the fissioning nuclei were successful. The 4D Langevin dynamics with K coordinate makes it possible to treat dynamically the angular distribution of fission fragments in addition to evaluation of the parameters MED of fragments and the mean prescission neutron multiplicities.

Different possibilities of the deformation-dependent dissipation coefficient (γ_K) for the K coordinate are investigated. The presented results [159, 213] demonstrate that impact of the k_s and γ_K parameters on the calculated observables characteristics can be selectively probed. The nuclear viscosity with respect to nuclear shape parameters influences $\langle n_{\rm pre}\rangle$, the fission fragment MED parameters, and the angular distribution of fission fragments. At the same time the dissipation coefficient γ_K affects the angular distribution of fission fragments only. It was found that it is possible to describe the experimental data on the angular distributions of fragments consistently with the deformation-dependent $\gamma_K(q)$ coefficient for shapes featuring a neck, which predicts quite small values of $\gamma_K = 0.077\,(\mathrm{MeV\,zs})^{-1/2}$ and constant $\gamma_K = 0.1$–$0.4\,(\mathrm{MeV\,zs})^{-1/2}$ for compact shapes featuring no neck.

The 4D Langevin dynamics with η_Z coordinate makes it possible to calculate the charge and the isotope distributions of fission fragments in addition to the observables evaluated in 3D Langevin dynamics. The dynamical approach to the formation of the charge distribution of fission fragments shows [102–104] that statistical equilibrium with respect to the charge mode can be established at each instant of time throughout the entire descent from the saddle point to scission except for its very last stage directly preceding the rupture of the neck. This explains the successful use of the statistical model for calculations of the fission fragment charge distribution. We mention especially that in the method of calculation of isotopic distribution of fission fragments suggested in [64] and described in this review in sect. 5 statistical estimation of the charge distribution variance is used as a key idea that allows not to consider η_Z as an additional collective coordinate. At the same time in the recent work [229] η_Z was considered as an independent collective coordinate in 4D Langevin dynamics with specific assumptions about inertia and friction coefficient of the charge mode. Both methods of calculation of the isotopic distribution provide a sufficient accuracy in description of the experimental data.

The isotopic/isobaric FF distributions are the most detailed observables, but they demand much more experimental and theoretical efforts. The iso-distribution contains already information about multiplicities and sort of emitted particles during full fission process and also about the mass/charge/total kinetic distributions as it is integral part. The isotopic distribution is sensitive to the potential energy models as well as to the dissipation mechanism. Thus, the experimental and theoretical studies of the iso-distributions can provide additional information about fission dynamics.

The theoretical description of the fission dynamics is a subject of deep studies and there are few ways to further developments. As it is done by [53, 72, 80] the investigation of the most optimal shape parametrization for the description of the fissioning nuclei is crucial because the more flexible and reach ensemble of nuclear deformations should help to reproduce in calculations the experimental fission fragment kinetic energy distributions.

Another important point is tackling shell effects in proper excitation energy range. The highly excited nucleus cools down quite fast by evaporation of prescission particles and also its angular momentum is decreasing. Thus, the shell effects in the last steps of evaporation chain are important and could influence the final observables.

Finally, the time evolution of the excited nucleus is substantially dependent on the initial condition used in dynamical calculations. The dynamical description of the movement of two nuclei toward each other and the emulation of the time evolution of the di-nuclear system after contact of colliding ions could provide the most complete description of the fusion-fission, quasi-fission and fast-fission process. The step in this direction has now been performed [72, 235, 236].

We would like to thank Drs. C. Schmitt, A.V. Karpov, D.O. Eremenko, E. Vardaci, A. Di Nitto, G. La Rana for their continued interest in this study, stimulating discussions and useful advice. We also thank two anonymous referees for their helpful comments and constructive suggestions that greatly

improved the first version of the manuscript. The work was partially supported by the National Science Centre under Contract No. 2013/08/M/ST2/00257 (LEA-COPIGAL) (Project No. 18) and IN2P3-COPIN (Project No. 12-145, 09-146), and by the Russian Foundation for Basic Research (Project No. 13-02-00168).

References

1. O. Hahn, F. Strassmann, Naturwissenschaften **27**, 11 (1939).
2. L. Meitner, O.R. Frisch, Nature (London) **143**, 239 (1939).
3. N. Bohr, J.A. Wheeler, Phys. Rev. **56**, 426 (1939).
4. P. Fong, *Statistical Theory of Nuclear Fisson* (Gordon and Breach, New York, 1969).
5. B.D. Wilkins, E.P. Steinberg, R.R. Chasman, Phys. Rev. C **14**, 1832 (1976).
6. H.A. Kramers, Physica **7**, 284 (1940).
7. V.V. Volkov, Phys. Rep. **44**, 93 (1978).
8. H. Feldmeier, Rep. Prog. Phys. **50**, 915 (1987).
9. P. Grangé, L. Jun-Qing, H.A. Weidenmüller, Phys. Rev. C **27**, 2063 (1983).
10. Z. Jing-Shang, H.A. Weidenmüller, Phys. Rev. C **28**, 2190 (1983).
11. G.D. Adeev, I.I. Gonchar, V.V. Pashkevich, N.I. Pischasov, O.I. Serdyuk, Sov. J. Part. Nucl. **19**, 529 (1988).
12. G. Adeev, V. Pashkevich, Nucl. Phys. A **502**, 405c (1989).
13. H. Delagrange, C. Grégoire, F. Scheuter, Y. Abe, Z. Phys. A **323**, 437 (1986).
14. E. Strumberger, K. Dietrich, K. Pomorski, Nucl. Phys. A **529**, 522 (1991).
15. Y. Abe, C. Grégoire, H. Delagrange, J. Phys. Colloq. **47**, C4 (1986).
16. P. Fröbrich, S. Xu, Nucl. Phys. A **477**, 143 (1988).
17. T. Wada, in *Proceedings of the 2nd Tours Symposium on Nuclear Physics, Tours, 1994*, Vol. **2** (World Scientific, Singapore, 1995) p. 470.
18. J. Blocki, O. Mazonka, J. Wilczynski, Z. Sosin, A. Wieloch, Acta Phys. Pol. **31**, 1513 (2000).
19. A.V. Karpov, P.N. Nadtochy, D.V. Vanin, G.D. Adeev, Phys. Rev. C **63**, 054610 (2001).
20. P.N. Nadtochy, G.D. Adeev, A.V. Karpov, Phys. Rev. C **65**, 064615 (2002).
21. C. Schmitt, J. Bartel, K. Pomorski, A. Surowiec, Acta Phys. Pol. B **34**, 1651 (2003).
22. C. Schmitt, J. Bartel, A. Surowiec, K. Pomorski, Acta Phys. Pol. B **34**, 2135 (2003).
23. Y. Aritomo, J. Nucl. Radiochem. Sci. **3**, 17 (2002).
24. T. Ichikawa, T. Asano, T. Wada, M. Ohta, J. Nucl. Radiochem. Sci. **3**, 67 (2002).
25. G.I. Kosenko, F.A. Ivanyuk, V.V. Pashkevich, J. Nucl. Radiochem. Sci. **3**, 71 (2002).
26. C. Shen, G.I. Kosenko, Y. Abe, Phys. Rev. C **66**, 061602(R) (2002).
27. G.D. Adeev, A.V. Karpov, P.N. Nadtochy, D.V. Vanin, Phys. Part. Nucl. **36**, 378 (2005).
28. Y. Abe, S. Ayik, P.G. Reinhard, E. Suraud, Phys. Rep. **275**, 49 (1996).
29. P. Fröbrich, I.I. Gontchar, Phys. Rep. **292**, 131 (1998).
30. P. Fröebrich, R. Lipperheide, *Theory of Nuclear Reactions. Studies in Nuclear Physics*, Vol. **18** (Oxford Univ. Press, Oxford, 1996).
31. H.J. Krappe, K. Pomorski, *Theory of Nuclear Fission*, Lect. Notes Phys. Vol. **838** (Berlin, Heidelberg, Springer Verlag, 2012).
32. S.A. Kalandarov, G.G. Adamian, N.V. Antonenko, W. Scheid, Phys. Rev. C **82**, 044603 (2010).
33. S.A. Kalandarov, G.G. Adamian, N.V. Antonenko, W. Scheid, J.P. Wieleczko, Phys. Rev. C **84**, 064601 (2011).
34. S.A. Kalandarov, G.G. Adamian, N.V. Antonenko, W. Scheid, Phys. Rev. C **83**, 054611 (2011).
35. S.A. Kalandarov, G.G. Adamian, N.V. Antonenko, J.P. Wieleczko, Phys. Rev. C **90**, 024609 (2014).
36. G.G. Adamian, N.V. Antonenko, H. Lenske, Phys. Rev. C **91**, 054602 (2015).
37. S.A. Kalandarov, G.G. Adamian, N.V. Antonenko, J.P. Wieleczko, Phys. Rev. C **93**, 054607 (2016).
38. A.V. Andreev, G.G. Adamian, N.V. Antonenko, A.N. Andreyev, Phys. Rev. C **88**, 047604 (2013).
39. S.N. Kuklin, G.G. Adamian, N.V. Antonenko, Phys. Part. Nucl. **47**, 206 (2016).
40. H. Pasca, A.V. Andreev, G.G. Adamian, N.V. Antonenko, Y. Kim, Phys. Rev. C **93**, 054602 (2016).
41. G.G. Adamian, N.V. Antonenko, S.A. Kalandarov, Phys. Part. Nucl. **47**, 1 (2016).
42. K.H. Schmidt, B. Jurado, C. Amouroux, C. Schmitt, Nucl. Data Sheets **131**, 107 (2016).
43. R. Charity, M. McMahan, G. Wozniak, R. McDonald, L. Moretto, D. Sarantites, L. Sobotka, G. Guarino, A. Pantaleo, L. Fiore, A. Gobbi, K. Hildenbrand, Nucl. Phys. A **483**, 371 (1988).
44. A.J. Sierk, Phys. Rev. C **33**, 2039 (1986).
45. R.J. Charity, Phys. Rev. C **82**, 014610 (2010).
46. M. Ciemala, M. Kmiecik, M. Krzysiek, A. Maj, K. Mazurek, R. Charity, D. Mancusi, Acta Phys. Pol. B **44**, 611 (2013).
47. D. Mancusi, A. Boudard, J. Carbonell, J. Cugnon, J.C. David, S. Leray, Phys. Rev. C **91**, 034602 (2015).
48. E. Ryabov, A. Karpov, G. Adeev, Nucl. Phys. A **765**, 39 (2006).
49. E.G. Ryabov, A.V. Karpov, P.N. Nadtochy, G.D. Adeev, Phys. Rev. C **78**, 044614 (2008).
50. H. Eslamizadeh, Eur. Phys. J. A **47**, 134 (2011).
51. R.M. Hiryanov, A.V. Karpov, G.D. Adeev, Phys. At. Nucl. **71**, 1361 (2008).
52. Y. Aritomo, Phys. Rev. C **88**, 044614 (2013).
53. F.A. Ivanyuk, S. Chiba, Y. Aritomo, Phys. Rev. C **90**, 054607 (2014).
54. Y. Aritomo, S. Chiba, F. Ivanyuk, Phys. Rev. C **90**, 054609 (2014).
55. J. Blocki, Y. Boneh, J.R. Nix, J. Randrup, M. Robel, A.J. Sierk, W.J. Swiatecki, Ann. Phys. (N.Y.) **113**, 330 (1978).
56. J.R. Nix, A.J. Sierk, in *Proceedings of the International School-Seminar on Heavy Ion Physics, Dubna, USSR, 1986*, edited by M.I. Zarubina, E.V. Ivashkevich (JINR, Dubna, 1987) pp. 453–464.

57. J.R. Nix, A.J. Sierk, in *Proceedings of the 6th Adriatic Conference on Nuclear Physics: Frontiers of Heavy Ion Physics, Dubrovnik, Yugoslavia, 1987*, edited by N. Cindro, R. Caplar, W. Greiner (World Scientific, Singapore, 1990) pp. 333–340.
58. H. Feldmeier, H. Spangenberger, Nucl. Phys. A **435**, 229 (1985).
59. M.R. Pahlavani, S.M. Mirfathi, Phys. Rev. C **92**, 024622 (2015).
60. M.R. Pahlavani, S.M. Mirfathi, Phys. Rev. C **93**, 044617 (2016).
61. P.N. Nadtochy, E.G. Ryabov, A.E. Gegechkori, Y.A. Anischenko, G.D. Adeev, Phys. Rev. C **85**, 064619 (2012).
62. K. Mazurek, C. Schmitt, P.N. Nadtochy, M. Kmiecik, A. Maj, P. Wasiak, J.P. Wieleczko, Phys. Rev. C **88**, 054614 (2013).
63. P.N. Nadtochy, E.G. Ryabov, A.E. Gegechkori, Y.A. Anischenko, G.D. Adeev, Phys. Rev. C **89**, 014616 (2014).
64. K. Mazurek, C. Schmitt, P.N. Nadtochy, Phys. Rev. C **91**, 041603 (2015).
65. H. Eslamizadeh, Eur. Phys. J. A **50**, 186 (2014).
66. H. Eslamizadeh, J. Phys. G: Nucl. Part. Phys. **44**, 025102 (2017).
67. A. Karpov, V. Zagrebaev, W. Greiner, EPJ Web of Conferences **17**, 10002 (2011).
68. V.I. Zagrebaev, A.V. Karpov, W. Greiner, Phys. Rev. C **85**, 014608 (2012).
69. A.V. Karpov, Phys. Rev. C **94**, 064615 (2016).
70. V.L. Litnevsky, G.I. Kosenko, F.A. Ivanyuk, V.V. Pashkevich, Phys. At. Nucl. **74**, 1001 (2011).
71. V.L. Litnevsky, G.I. Kosenko, F.A. Ivanyuk, V.V. Pashkevich, Phys. At. Nucl. **75**, 37 (2012).
72. V.L. Litnevsky, G.I. Kosenko, F.A. Ivanyuk, Phys. Rev. C **93**, 064606 (2016).
73. J. Randrup, P. Möller, Phys. Rev. Lett. **106**, 132503 (2011).
74. J. Randrup, P. Möller, A.J. Sierk, Phys. Rev. C **84**, 034613 (2011).
75. P. Möller, J. Randrup, A.J. Sierk, Phys. Rev. C **85**, 024306 (2012).
76. J. Randrup, P. Moller, Phys. Scr. **T150**, 014033 (2012).
77. J. Randrup, P. Möller, Phys. Rev. C **88**, 064606 (2013).
78. P. Möller, J. Randrup, A. Iwamoto, T. Ichikawa, Phys. Rev. C **90**, 014601 (2014).
79. P. Möller, J. Randrup, Phys. Rev. C **91**, 044316 (2015).
80. P. Möller, T. Ichikawa, Eur. Phys. J. A **51**, 173 (2015).
81. P. Möller, A.J. Sierk, A. Iwamoto, Phys. Rev. Lett. **92**, 072501 (2004).
82. H.J. Lipkin, Ann. Phys. (N.Y.) **9**, 272 (1960).
83. Y. Nogami, Phys. Rev. **134**, B313 (1964).
84. H. Pradhan, Y. Nogami, J. Law, Nucl. Phys. A **201**, 357 (1973).
85. K. Washiyama, S. Ayik, D. Lacroix, Phys. Rev. C **80**, 031602 (2009).
86. G. Scamps, C. Simenel, D. Lacroix, Phys. Rev. C **92**, 011602 (2015).
87. G.G. Adamian, N.V. Antonenko, L.A. Malov, G. Scamps, D. Lacroix, Phys. Rev. C **90**, 034322 (2014).
88. J. Sadhukhan, W. Nazarewicz, N. Schunck, Phys. Rev. C **93**, 011304 (2016).
89. A. Bulgac, P. Magierski, K.J. Roche, I. Stetcu, Phys. Rev. Lett. **116**, 122504 (2016).
90. E. Vardaci, A. Di Nitto, A. Brondi, G. La Rana, R. Moro, P.N. Nadotchy, M. Trotta, A. Ordine, A. Boiano, M. Cinausero, E. Fioretto, G. Prete, V. Rizzi, D. Shetty, M. Barbui, D. Fabris, M. Lunardon, G. Montagnoli, S. Moretto, G. Viesti, N. Gelli, F. Lucarelli, G.N. Knyazheva, E.M. Kozulin, Eur. Phys. J. A **43**, 127 (2010).
91. A. Di Nitto, E. Vardaci, A. Brondi, G. La Rana, R. Moro, P.N. Nadtochy, M. Trotta, A. Ordine, A. Boiano, M. Cinausero, E. Fioretto, G. Prete, V. Rizzi, D.V. Shetty, M. Barbui, D. Fabris, M. Lunardon, G. Montagnoli, S. Moretto, G. Viesti, N. Gelli, F. Lucarelli, G.N. Knyazheva, E.M. Kozulin, Eur. Phys. J. A **47**, 83 (2011).
92. M. Brack, J. Damgaard, A.S. Jensen, H.C. Pauli, V.M. Strutinsky, C.Y. Wong, Rev. Mod. Phys. **44**, 320 (1972).
93. J.R. Nix, Nucl. Phys. A **130**, 241 (1969).
94. S. Trentalange, S.E. Koonin, A.J. Sierk, Phys. Rev. C **22**, 1159 (1980).
95. U. Brosa, S. Grossmann, A. Müller, Phys. Rep. **197**, 167 (1990).
96. V. Stavinsky, N. Rabotnov, A. Seregin, Yad. Fiz. **7**, 1051 (1968).
97. V. Pashkevich, Nucl. Phys. A **169**, 275 (1971).
98. D.V. Vanin, G.I. Kosenko, G.D. Adeev, Phys. Rev. C **59**, 2114 (1999).
99. J. Maruhn, W. Greiner, Z. Phys. A **251**, 431 (1972).
100. K. Sato, K. Iwamoto, K. Harada, S. Yamaji, S. Yoshida, Z. Phys. A **288**, 383 (1978).
101. R.W. Hasse, W.D. Myers, *Geometrical Relationships of Macroscopic Nuclear Physics* (Springer-Verlag, Heidelberg, 1988).
102. G.D. Adeev, Sov. J. Part. Nucl. **23**, 684 (1992).
103. A.V. Karpov, G.D. Adeev, Eur. Phys. J. A **14**, 169 (2002).
104. A.V. Karpov, G.D. Adeev, Phys. At. Nucl. **65**, 1596 (2002).
105. H.C. Pauli, Phys. Rep. **7**, 35 (1973).
106. V.M. Strutinsky, N.Y. Lyashchenko, N.A. Popov, Nucl. Phys. **46**, 639 (1963).
107. J. Bao, Y. Zhuo, X. Wu, Z. Phys. A **352**, 321 (1995).
108. G.I. Kosenko, D.V. Vanin, G.D. Adeev, Phys. At. Nucl. **61**, 2031 (1998).
109. G.I. Kosenko, D.V. Vanin, G.D. Adeev, Phys. At. Nucl. **61**, 356 (1998).
110. A. Mamdouh, J.M. Pearson, M. Rayet, F. Tondeur, Nucl. Phys. A **644**, 389 (1998).
111. A. Ignatyuk, M.G. Itkis, V. Okolovich, G. Smirenkin, Yad. Fiz. **21**, 1185 (1975).
112. H.J. Krappe, J.R. Nix, A.J. Sierk, Phys. Rev. C **20**, 992 (1979).
113. J.P. Lestone, Phys. Rev. C **59**, 1540 (1999).
114. S.G. McCalla, J.P. Lestone, Phys. Rev. Lett. **101**, 032702 (2008).
115. J.P. Lestone, S.G. McCalla, Phys. Rev. C **79**, 044611 (2009).
116. D.O. Eremenko, V.A. Drozdov, M.H. Eslamizadeh, O.V. Fotina, S.Y. Platonov, O.A. Yuminov, Phys. At. Nucl. **69**, 1423 (2006).
117. V.A. Drozdov, D.O. Eremenko, O.V. Fotina, S.Y. Platonov, O.A. Yuminov, in *Tours Symposium on Nuclear Physics V, Tours 2003*, edited by M. Arnold, M. Lewitowicz, G. Münzenberg, H. Akimune, M. Ohta, H. Utsunomiya, T. Wada, T. Yamagata, Vol. **704**, AIP Conf. Proc. (Melville, New York, 2004) pp. 130–138.

118. A.V. Karpov, R.M. Hiryanov, A.V. Sagdeev, G.D. Adeev, J. Phys. G: Nucl. Part. Phys. **34**, 255 (2007).
119. J. Marten, P. Fröbrich, Nucl. Phys. A **545**, 854 (1992).
120. D.O. Eremenko, V.A. Drozdov, O.V. Fotina, S.Y. Platonov, O.A. Yuminov, Phys. Rev. C **94**, 014602 (2016).
121. M.V. Borunov, P.N. Nadtochy, G.D. Adeev, Nucl. Phys. A **799**, 56 (2008).
122. K.T.R. Davies, A.J. Sierk, J.R. Nix, Phys. Rev. C **13**, 2385 (1976).
123. I. Kelson, Phys. Rev. **136**, B1667 (1964).
124. J.N.P. Lawrence, Phys. Rev. **139**, B1227 (1965).
125. F.A. Ivanyuk, V.M. Kolomietz, A.G. Magner, Phys. Rev. C **52**, 678 (1995).
126. H. Jeffreys, B. Swirles, *Methods of Mathematical Physics, 3rd edition* (Cambridge University Press, Cambridge, 1966; Mir, Moscow, 1970).
127. J. Randrup, W.J. Swiatecki, Ann. Phys. (N.Y.) **125**, 193 (1980).
128. A.J. Sierk, J.R. Nix, Phys. Rev. C **21**, 982 (1980).
129. J.J. Griffin, M. Dworzecka, Nucl. Phys. A **455**, 61 (1986).
130. A.J. Sierk, J.R. Nix, Phys. Rev. C **21**, 982 (1980).
131. G. Abal, R. Donangelo, C.O. Dorso, Phys. Rev. C **46**, 380 (1992).
132. J. Töke, W.J. Swiatecki, Nucl. Phys. A **372**, 141 (1981).
133. R. Donangelo, L.F. Canto, Nucl. Phys. A **451**, 349 (1986).
134. S.E. Koonin, R.L. Hatch, J. Randrup, Nucl. Phys. A **283**, 87 (1977).
135. S.E. Koonin, J. Randrup, Nucl. Phys. A **289**, 475 (1977).
136. J. Blocki, J.J. Shi, W. Swiatecki, Nucl. Phys. A **554**, 387 (1993).
137. S. Pal, T. Mukhopadhyay, Phys. Rev. C **57**, 210 (1998).
138. G.I. Kosenko, F.A. Ivanyuk, V.V. Pashkevich, Phys. At. Nucl. **65**, 1588 (2002).
139. G. Chaudhuri, S. Pal, Eur. Phys. J. A **18**, 9 (2003).
140. J. Blocki, R. Planeta, J. Brzychczyk, K. Grotowski, Z. Phys. A **341**, 307 (1992).
141. P. Fröbrich, I.I. Gontchar, N.D. Mavlitov, Nucl. Phys. A **556**, 281 (1993).
142. D. Hilscher, H. Rossner, Ann. Phys. (France) **17**, 471 (1992).
143. E. Vardaci, P.N. Nadtochy, A. Di Nitto, A. Brondi, G. La Rana, R. Moro, P.K. Rath, M. Ashaduzzaman, E.M. Kozulin, G.N. Knyazheva, I.M. Itkis, M. Cinausero, G. Prete, D. Fabris, G. Montagnoli, N. Gelli, Phys. Rev. C **92**, 034610 (2015).
144. P. Nadtochy, A. Brondi, A. Di Nitto, G. La Rana, R. Moro, E. Vardaci, A. Ordine, A. Boiano, M. Cinausero, G. Prete, V. Rizzi, N. Gelli, F. Lucarelli, EPJ Web of Conferensces **2**, 08003 (2010).
145. T. Wada, Y. Abe, N. Carjan, Phys. Rev. Lett. **70**, 3538 (1993).
146. P. Fröbrich, Nucl. Phys. A **545**, 87c (1992).
147. E. Vardaci, A. Di Nitto, P. Nadtochy, A. Brondi, G. La Rana, R. Moro, M. Cinausero, G. Prete, N. Gelli, E.M. Kozulin, G. Knyazheva, EPJ Web of Conferences **62**, 07004 (2013).
148. G. Wegmann, Phys. Lett. B **50**, 327 (1974).
149. P. Paul, M. Thoennessen, Annu. Rev. Nucl. Part. Sci. **44**, 65 (1994).
150. D.J. Hofman, B.B. Back, I. Diószegi, C.P. Montoya, S. Schadmand, R. Varma, P. Paul, Phys. Rev. Lett. **72**, 470 (1994).
151. G. Rudolf, A. Kelić, Nucl. Phys. A **679**, 251 (2001).
152. V.A. Rubchenya, A.V. Kuznetsov, W.H. Trzaska, D.N. Vakhtin, A.A. Alexandrov, I.D. Alkhazov, J. Äystö, S.V. Khlebnikov, V.G. Lyapin, O.I. Osetrov, Y.E. Penionzhkevich, Y.V. Pyatkov, G.P. Tiourin, Phys. Rev. C **58**, 1587 (1998).
153. A.K. Dhara, K. Krishan, C. Bhattacharya, S. Bhattacharya, Phys. Rev. C **57**, 2453 (1998).
154. S. Yamaji, H. Hofmann, R. Samhammer, Nucl. Phys. A **475**, 487 (1987).
155. H. Hofmann, S. Yamaji, A.S. Jensen, Phys. Lett. B **286**, 1 (1992).
156. M.D. Usang, F.A. Ivanyuk, C. Ishizuka, S. Chiba, Phys. Rev. C **94**, 044602 (2016).
157. T. Døssing, J. Randrup, Nucl. Phys. A **433**, 215 (1985).
158. J. Randrup, Nucl. Phys. A **383**, 468 (1982).
159. P.N. Nadtochy, E.G. Ryabov, A.V. Cheredov, G.D. Adeev, Eur. Phys. J. A **52**, 308 (2016).
160. N.D. Mavlitov, P. Fröbrich, I.I. Gontchar, Z. Phys. A **342**, 195 (1992).
161. A.S. Iljinov, M.V. Mebel, N. Bianchi, E.D. Sanctis, C. Guaraldo, V. Lucherini, V. Muccifora, E. Polli, A.R. Reolon, P. Rossi, Nucl. Phys. A **543**, 517 (1992).
162. A.R. Junghans, M. de Jong, H.G. Clerc, A.V. Ignatyuk, G.A. Kudyaev, K.H. Schmidt, Nucl. Phys. A **629**, 635 (1998).
163. S. Björnholm, A. Bohr, B.R. Mottelson, in *Proceedings of the Third IAEA Symposium on Physics and Chemistry of Fission, Rochester, 1973*, Vol. **1** (IAEA, Vienna, 1974) pp. 367–374.
164. G. Hansen, A.S. Jensen, Nucl. Phys. A **406**, 236 (1983).
165. A.V. Karpov, P.N. Nadtochy, E.G. Ryabov, G.D. Adeev, J. Phys. G: Nucl. Phys. **29**, 2365 (2003).
166. G. La Rana, D.J. Moses, W.E. Parker, M. Kaplan, D. Logan, R. Lacey, J.M. Alexander, R.J. Welberry, Phys. Rev. C **35**, 373 (1987).
167. I.I. Gontchar, P. Fröbrich, N.I. Pischasov, Phys. Rev. C **47**, 2228 (1993).
168. H. Hofmann, F.A. Ivanyuk, Phys. Rev. Lett. **90**, 132701 (2003).
169. J.D. Bao, Y. Jia, Phys. Rev. C **69**, 027602 (2004).
170. P. Hänggi, P. Talkner, M. Borkovec, Rev. Mod. Phys. **62**, 251 (1990).
171. J.R. Nix, W.J. Swiatecki, Nucl. Phys. A **71**, 1 (1965).
172. O.I. Serdyuk, G.D. Adeev, I.I. Gonchar, V.V. Pashkevich, N.I. Pischasov, Sov. J. Nucl. Phys. **46**, 399 (1987).
173. G.I. Kosenko, I.I. Gonchar, O.I. Serdyuk, N.I. Pischasov, Yad. Fiz. **55**, 920 (1992) Sov. J. Nucl. Phys. **55**, 514 (1992).
174. G.D. Adeev, P.N. Nadtochy, Phys. At. Nucl. **66**, 618 (2003).
175. U.L. Businaro, S. Gallone, Nuovo Cimento **5**, 315 (1957).
176. K. Mazurek, C. Schmitt, P.N. Nadtochy, A.V. Cheredov, Phys. Rev. C **94**, 064602 (2016).
177. M. Caamaño, O. Delaune, F. Farget, X. Derkx, K.H. Schmidt, L. Audouin, C.O. Bacri, G. Barreau, J. Benlliure, E. Casarejos, A. Chbihi, B. Fernández-Domínguez, L. Gaudefroy, C. Golabek, B. Jurado, A. Lemasson, A. Navin, M. Rejmund, T. Roger, A. Shrivastava, C. Schmitt, Phys. Rev. C **88**, 024605 (2013).
178. H. Goutte, J.F. Berger, P. Casoli, D. Gogny, Phys. Rev. C **71**, 024316 (2005).
179. N. Schunck, L.M. Robledo, Rep. Prog. Phys. **79**, 116301 (2016).

180. P. Möller, D.G. Madland, A.J. Sierk, A. Iwamoto, Nature **409**, 785 (2001).
181. Y. Aritomo, K. Hagino, K. Nishio, S. Chiba, Phys. Rev. C **85**, 044614 (2012).
182. M.G. Itkis, A.Y. Rusanov, Phys. Part. Nucl. **29**, 160 (1998).
183. M.G. Itkis, S.M. Lukyanov, V.N. Okolovich, Y.E. Penionzkevich, A.Y. Rusanov, V.S. Salamatin, G.N. Smirenkin, G.G. Chubaryan, Phys. At. Nucl. **52**, 15 (1990).
184. M.G. Itkis, V.N. Okolovich, G.N. Smirenkin, Nucl. Phys. A **502**, 243 (1989).
185. G.R. Tillack, Phys. Lett. B **278**, 403 (1992).
186. T. Wada, N. Carjan, Y. Abe, Nucl. Phys. A **538**, 283c (1992).
187. V.E. Viola, K. Kwiatkowski, M. Walker, Phys. Rev. C **31**, 1550 (1985).
188. P.N. Nadtochy, A.V. Karpov, D.V. Vanin, G.D. Adeev, Phys. At. Nucl. **66**, 1203 (2003).
189. P.N. Nadtochy, G.D. Adeev, Phys. Rev. C **72**, 054608 (2005).
190. P. Möller, A.J. Sierk, T. Ichikawa, A. Iwamoto, R. Bengtsson, H. Uhrenholt, S. Åberg, Phys. Rev. C **79**, 064304 (2009).
191. V. Pashkevich, A. Rusanov, Nucl. Phys. A **810**, 77 (2008).
192. K. Mazurek, C. Schmitt, J.P. Wieleczko, P.N. Nadtochy, G. Ademard, Phys. Rev. C **84**, 014610 (2011).
193. K. Pomorski, J. Dudek, Phys. Rev. C **67**, 044316 (2003).
194. J. Dudek, K. Pomorski, N. Schunck, N. Dubray, Eur. Phys. J. A **20**, 165 (2004).
195. P. Moller, J. Nix, W. Myers, W. Swiatecki, At. Data Nucl. Data Tables **59**, 185 (1995).
196. K. Mazurek, C. Schmitt, P. Nadtochy, A. Maj, P. Wasiak, M. Kmiecik, B. Wasilewska, Acta Phys. Pol. A **44**, 293 (2013).
197. K. Mazurek, P. Nadtochy, C. Schmitt, P. Wasiak, M. Kmiecik, A. Maj, E. Bonnet, A. Chbihi, J. Frankland, D. Gruyer, J.-P. Wieleczko, EPJ Web of Conferences **62**, 02002 (2013).
198. Y. Futami, K. Yuasa-Nakagawa, T. Nakagawa, S. Lee, K. Furutaka, K. Matsuda, K. Yoshida, S. Jeong, H. Fujiwara, T. Mizota, Y. Honjo, S. Tomita, B. Heusch, K. Ieki, J. Kasagi, W. Shen, T. Matsuse, Nucl. Phys. A **607**, 85 (1996).
199. D.J. Hinde, D. Hilscher, H. Rossner, B. Gebauer, M. Lehmann, M. Wilpert, Phys. Rev. C **45**, 1229 (1992).
200. M. de Saint-Simon, L. Lessard, W. Reisdorf, L. Remsberg, C. Thibault, E. Roeckl, R. Klapisch, I.V. Kuznetsov, Y.T. Oganessian, Y.E. Penionshkevitch, Phys. Rev. C **14**, 2185 (1976).
201. R. Vandenbosch, J.R. Huizenga, *Nuclear Fission* (Academic Press, New York, 1973).
202. A. Bohr, B.R. Mottelson, *Nuclear structure*, Vol. **2** (World Scientific, Singapore, 1998).
203. I. Halpern, V.M. Strutinsky, in *Proceedings Of the Second United Nations International Conference on the Peaceful Uses of Atomic Energy, Geneva, Switzerland, 1957*, Vol. **15** (United Nations, Geneva, Switzerland, 1958) pp. 408–418.
204. P. Fröbrich, H. Rossner, Z. Phys. A **349**, 99 (1994).
205. V.A. Drozdov, D.O. Eremenko, S.Y. Platonov, O.V. Fotina, O.A. Yuminov, Phys. At. Nucl. **64**, 179 (2001).
206. Y. Jia, J.D. Bao, Phys. Rev. C **75**, 034601 (2007).
207. B.B. Back, R.R. Betts, J.E. Gindler, B.D. Wilkins, S. Saini, M.B. Tsang, C.K. Gelbke, W.G. Lynch, M.A. McMahan, P.A. Baisden, Phys. Rev. C **32**, 195 (1985).
208. L.C. Vaz, J.M. Alexander, Phys. Rep. **97**, 1 (1983).
209. J.O. Newton, Fiz. Elem. Chast. At. Yadra **21**, 821 (1990).
210. T. Døssing, J. Randrup, Nucl. Phys. A **433**, 280 (1985).
211. J. Randrup, Nucl. Phys. A **327**, 490 (1979).
212. P. Nadtochy, E. Ryabov, A. Gegechkori, Y. Anischenko, G. Adeev, EPJ Web of Conferences **62**, 07001 (2013)
213. P.N. Nadtochy, E.G. Ryabov, G.D. Adeev, J. Phys. G: Nucl. Part. Phys. **42**, 045107 (2015).
214. E.G. Ryabov, P.N. Nadtochy, G.D. Adeev, Acta Phys. Pol. B **46**, 579 (2015).
215. L. Nikkinen, B.P. Pathak, L. Lessard, I.S. Grant, Phys. Rev. C **22**, 617 (1980).
216. B.P. Pathak, L. Lessard, L. Nikkinen, J.K.P. Lee, Phys. Rev. C **25**, 2534 (1982).
217. W. Krlas, R. Broda, B. Fornal, T. Pawat, H. Grawe, K. Maier, M. Schramm, R. Schubart, Nucl. Phys. A **724**, 289 (2003).
218. M.B. Tsang, R. Shomin, O. Bjarki, C.K. Gelbke, G.J. Kunde, R.C. Lemmon, W.G. Lynch, D. Magestro, R. Popescu, A.M. Vandermolen, G. Verde, G.D. Westfall, H.F. Xi, W.A. Friedman, G. Imme, V. Maddalena, C. Nociforo, G. Raciti, G. Riccobene, F.P. Romano, A. Saija, C. Sfienti, S. Fritz, C. Groß, T. Odeh, C. Schwarz, A. Nadasen, D. Sisan, K.A.G. Rao, Phys. Rev. C **66**, 044618 (2002).
219. W. Schneider, R. Pühlhoferand, F. Chestnut, C. Volant, H. Freiesleben, W. Pfeffer, B. Kohlmeyer, Nucl. Phys. A **371**, 493 (1981).
220. O. Delaune, EPJ Web of Conferences **31**, 00025 (2012).
221. A.C. Wahl, R.L. Ferguson, D.R. Nethaway, D.E. Troutner, K. Wolfsberg, Phys. Rev. **126**, 1112 (1962).
222. P. Armbruster, Nucl. Phys. A **140**, 385 (1970).
223. J.A. McHugh, M.C. Michel, Phys. Rev. **172**, 1160 (1968).
224. Y.L. Zhao, Y. Nagame, I. Nishinaka, K. Sueki, H. Nakahara, Phys. Rev. C **62**, 014612 (2000).
225. S. Pal, G. Chaudhuri, J. Sadhukhan, Nucl. Phys. A **808**, 1 (2008).
226. G. Chaudhuri, S. Pal, Phys. Rev. C **65**, 054612 (2002).
227. W. Ye, N. Wang, J. Tian, Phys. Rev. C **90**, 041604 (2014).
228. D. Naderi, Phys. Rev. C **90**, 024614 (2014).
229. C. Ishizuka, S. Chiba, A. Karpov, Y. Aritomo, EPJ Web of Conferences **122**, 01003 (2016).
230. P. Nadtochy, D.V. Vanin, A.V. Cheredov, S.V. Fedorov, E. Ryabov, G. Adeev, EPJ Web of Conferences **117**, 08015 (2016).
231. Y.A. Anischenko, G.D. Adeev, Phys. At. Nucl. **75**, 933 (2012).
232. P.N. Nadtochy, A. Kelić, K.H. Schmidt, Phys. Rev. C **75**, 064614 (2007).
233. P.N. Nadtochy, E. Vardaci, A. Di Nitto, A. Brondi, G. La Rana, R. Moro, M. Cinausero, G. Prete, N. Gelli, F. Lucarelli, Phys. Lett. B **685**, 258 (2010).
234. P. Nadtochy, C. Schmitt, K. Mazurek, Phys. Scr. T **154**, 014004 (2013).
235. V.L. Litnevsky, V.V. Pashkevich, G.I. Kosenko, F.A. Ivanyuk, Phys. Rev. C **85**, 034602 (2012).
236. V.L. Litnevsky, V.V. Pashkevich, G.I. Kosenko, F.A. Ivanyuk, Phys. Rev. C **89**, 034626 (2014).

Katarzyna Mazurek is a theoretical nuclear physicist. She received the doctoral degree from Maria Curie-Sklodowska University in Lublin, Poland in 2004 and works as a researcher at the Institute of Nuclear Physics, Polish Academy of Science in Krakow. Her participation in many experiments allows her to develop a phenomenological method to study the Giant Dipole Resonances emitted from hot, rotating nuclei. When she was a postdoc in GANIL, she started a collaboration with the Omsk group of P.N. Nadtochy and G.D. Adeev; thus since 2009 she has been working on the description of fission dynamics. She received her habilitation degree in 2012.

Ryabov Eugeny is a theoretical nuclear physicist. He received the PhD Russian degree in 2006 from Tomsk Technical University in Tomsk and has been working at the Physical Department of the Omsk State University as a senior teacher since 2007. His main works are devoted to the application of the stochastic methods to nuclear fission dynamics and parallel programming.

Pavel Nadtochy took his doctorate in theoretical nuclear physics from Omsk State University in 2002 and worked as a researcher. In 2005 he was awarded the Humboldt PostDoctoral Fellowship and worked at GSI Helmholtzzentrum für Schwerionenforschung, Darmstadt. After a period spent in Germany he moved to the Istituto Nazionale di Fisica Nucleare, Naples Section (Italy) as a postdoc and worked there in 2007–2009. Now he is working as a Professor at the Omsk State Technical University. His main research interests are the theoretical nuclear physics, dynamics of fission reactions and multifragmentation process.

Adeev Gennady is a theoretical nuclear physicist. He received the PhD Russian degree in 1973 from Tomsk Technical University in Tomsk and worked as researcher at the Institute for Nuclear Physics of the Tomsk Technical University. In 1976–1977 he was a postdoc at the Niels Bohr Institute in Copenhagen. In 1978 he started his work at the Physical Department of the Omsk State University as an associate Professor and since 1990 as a full Professor. In 1989 he was awarded Doctor of Sciences Russian degree by the Laboratory of Theoretical Physics of the Joint Institute for Nuclear Research in Dubna. His main works are devoted to the application of the stochastic methods to nuclear fission dynamics.